

30745



National Library  
of Canada

Bibliothèque nationale  
du Canada

CANADIAN THESES  
ON MICROFICHE

THÈSES CANADIENNES  
SUR MICROFICHE

NAME OF AUTHOR/NOM DE L'AUTEUR A WILLIAM LIPSETT

TITLE OF THESIS/TITRE DE LA THÈSE JET IMPINGEMENT HEAT TRANSFER  
INCLUDING EFFECT OF MELTING

UNIVERSITY/UNIVERSITÉ UNIVERSITY OF ALBERTA

DEGREE FOR WHICH THESIS WAS PRESENTED/  
GRADE POUR LEQUEL CETTE THÈSE FUT PRÉSENTÉE M. SC.

YEAR THIS DEGREE CONFERRED/ANNÉE D'OBTENTION DE CE GRADE 1976 FALL

NAME OF SUPERVISOR/NOM DU DIRECTEUR DE THÈSE DR. R. R. GILPIN

Permission is hereby granted to the NATIONAL LIBRARY OF  
CANADA to microfilm this thesis and to lend or sell copies  
of the film.

*L'autorisation est, par la présente, accordée à la BIBLIOTHÈ-  
QUE NATIONALE DU CANADA de microfilmer cette thèse et  
de prêter ou de vendre des exemplaires du film.*

The author reserves other publication rights, and neither the  
thesis nor extensive extracts from it may be printed or other-  
wise reproduced without the author's written permission.

*L'auteur se réserve les autres droits de publication; ni la  
thèse ni de longs extraits de celle-ci ne doivent être imprimés  
ou autrement reproduits sans l'autorisation écrite de l'auteur.*

DATED/DATÉ Oct 14, 1976 SIGNED/SIGNÉ A. William Lipsett

PERMANENT ADDRESS/RÉSIDENCE FIXE 164 Oakcliff Place S.W.  
Calgary, Alberta  
T2V 0J8

INFORMATION TO USERS

THIS DISSERTATION HAS BEEN  
MICROFILMED EXACTLY AS RECEIVED.

This copy was produced from a microfiche copy of the original document. The quality of the copy is heavily dependent upon the quality of the original thesis submitted for microfilming. Every effort has been made to ensure the highest quality of reproduction possible.

PLEASE NOTE: Some pages may have indistinct print. Filmed as received.

Canadian Theses Division  
Cataloguing Branch  
National Library of Canada  
Ottawa, Canada K1A 0N4

AVIS AUX USAGERS

LA THESE A ETE MICROFILMEE  
TELLE QUE NOUS L'AVONS RECUE

Cette copie a été faite à partir d'une microfiche du document original. La qualité de la copie dépend grandement de la qualité de la thèse soumise pour le microfilmage. Nous avons tout fait pour assurer une qualité supérieure de reproduction.

NOTA BENE: La qualité d'impression de certaines pages peut laisser à désirer. Microfilmée telle que nous l'avons reçue.

Division des thèses canadiennes  
Direction du catalogage  
Bibliothèque nationale du Canada  
Canada. K1A 0N4

THE UNIVERSITY OF ALBERTA

JET IMPINGEMENT HEAT TRANSFER INCLUDING  
EFFECT OF MELTING

by

(C)

A. WILLIAM LIPSETT

A THESIS

SUBMITTED TO THE FACULTY OF GRADUATE STUDIES AND RESEARCH  
IN PARTIAL FULFILMENT OF THE REQUIREMENTS FOR THE DEGREE  
OF MASTER OF SCIENCE

DEPARTMENT OF MECHANICAL ENGINEERING

EDMONTON, ALBERTA

FALL, 1976

THE UNIVERSITY OF ALBERTA

FACULTY OF GRADUATE STUDIES AND RESEARCH

The undersigned certify that they have read, and recommend to the Faculty of Graduate Studies and Research, for acceptance, a thesis entitled "JET IMPINGEMENT HEAT TRANSFER INCLUDING EFFECT OF MELTING" submitted by A. William Lipsett in partial fulfilment of the requirements for the degree of Master of Science

*Robert G. J.*  
.....  
Supervisor

*R. W. Murray*  
.....

*K. C. Cheng*  
.....

*Gordon W. ...*  
.....

Date *October 5, 1976* .....

## ABSTRACT

The problem of a laminar water jet impinging on an ice surface is studied analytically. The jet flow is divided into two parts, a potential flow solution and a boundary layer solution. The potential flow problem is formulated as a variational statement and is solved by the finite element method. From the potential flow solution, the velocity distribution on the impingement surface is used as the free stream velocity in the boundary layer analysis. The boundary layer is solved by a Karman-Pohlhausen integral technique.

To verify the solution method the results for a two-dimensional jet impinging on a flat surface without melting are compared with exact solutions for the potential flow and a numerical calculation of the boundary layer.

Solution of the problem of an axisymmetric jet impinging on a surface is discussed with respect to the distance from the nozzle to the impingement surface, impingement surface shape, shear stress on the surface and melting effects. Simulation of a block of ice being melted by a water jet is considered. The jet impinges on the ice surface, the heat transfer calculated, the change in ice surface shape due to melting is found and a new ice surface shape is generated. The procedure is then repeated. To

obtain a qualitative view of the melting process, photographs of a block of ice were taken at various intervals during the melting process. Finally the combined effect of melting heat transfer and erosion caused by shear stress are discussed with respect to axisymmetric jet impingement.

## ACKNOWLEDGEMENTS

The author wishes to express his sincere appreciation to the following persons and organizations.

Dr. R.R. Gilpin for his supervision and assistance in all stages of this investigation.

The National Research Council of Canada and The Department of Mechanical Engineering for financial assistance in the form of scholarship and teaching assistantship.

Miss Susan Schultz for her excellent typing of this thesis.

Fellow graduate students for their discussions on various aspects of this thesis.

## TABLE OF CONTENTS

CHAPTER		Page
I	INTRODUCTION.....	1
II	POTENTIAL FLOW ANALYSIS.....	8
	2.1 Governing Equations.....	9
	2.2 Boundary Conditions.....	16
	2.3 Variational Formulation.....	22
III	THE FINITE ELEMENT METHOD.....	29
	3.1 Background.....	29
	3.2 The Finite Element Method Applied to Jet Impingement.....	31
	(a) Finite Element Formulation.....	31
	(b) Boundary Conditions.....	41
	(c) Finding the Free Surface.....	44
IV	BOUNDARY LAYER SOLUTION.....	48
	4.1 Governing Equations.....	48
	4.2 Integration of the Boundary Layer Equations.....	53
	4.3 Velocity and Temperature Distribu- tions.....	57
	4.4 Solution of the Integral Equations....	70
V	TWO-DIMENSIONAL JET IMPINGEMENT ON A FLAT SURFACE.....	83
	5.1 Exact Solution of the Potential Flow Field.....	83
	5.2 Heat Transfer.....	92



CHAPTER	Page
VI	AXISYMMETRIC JET IMPINGEMENT..... 103
	6.1 Previous Work..... 106
	6.2 Flow Field of Axisymmetric Jet Impingement..... 107
	6.3 Heat Transfer..... 114
VII	MELTING AND EROSION CAUSED BY AXI- SYMMETRIC JET IMPINGEMENT..... 123
	7.1 Previous Work..... 123
	7.2 Melting Ice with a Water Jet..... 125
VIII	CONCLUSIONS AND RECOMMENDATIONS..... 144
	REFERENCES..... 149
	APPENDIX 1 - FINITE ELEMENT MATRIX FORMULATION..... 154
	APPENDIX 2 - COMPUTER PROGRAM AND CUBIC SPLINE INTERPOLATION..... 166

# LIST OF TABLES

TABLE		Page
1	Exact solution of a two-dimensional jet impinging on a flat plate.....	98
2	Radii of curvature at the stagnation point for a family of paraboloids given by the equation, $w = ar^2$ .....	113
3	Axisymmetric jet impingement heat transfer on a flat surface.....	117

## LIST OF FIGURES

FIGURE		Page
2.1	Direction cosines of $\bar{n}$ , $\bar{s}$ .....	17
3.1	Axisymmetric jet impinging on a flat surface.....	32
3.2	Finite element mesh and numbering system.....	34
3.3	Area coordinates and element numbering system.....	36
3.4	Movement of a node on the free surface.....	46
4.1	Boundary layer on an ice surface.....	49
4.2	Velocity and temperature profile functions.....	61
4.3	Velocity profiles, $Ste = 0$ , effect of pressure gradient.....	62
4.4	Velocity profiles, $\Lambda = 6$ , effect of melting.....	63
4.5	Temperature profiles, effect of melting....	67
4.6	Two-dimensional starting values.....	77
4.7	Axisymmetric starting values.....	78
5.1	Two-dimensional jet impinging on a flat surface.....	85
5.2	Velocity distributions, two-dimensional jet impinging on a flat surface.....	87
5.3	Position of the free surface, two-dimensional jet impinging on a flat surface, $H \rightarrow \infty$ .....	88
5.4	Velocity gradient distributions, two-dimensional jet impinging on a flat surface.....	90

FIGURE		Page
5.5	Heat transfer near the stagnation point of a two-dimensional jet impinging on a flat surface.....	93
6.1	Flow regions of an impinging jet.....	105
6.2	Velocity distributions, axisymmetric jet impinging on a flat surface.....	109
6.3	Velocity gradient distributions, axisymmetric jet impinging on a flat surface..	110
6.4	Velocity distributions, axisymmetric jet impinging on curved surfaces.....	112
6.5	Heat transfer near the stagnation point of an axisymmetric jet impinging on a flat surface.....	119
6.6	Shear stress on a flat surface due to axisymmetric jet impingement.....	121
7.1	Heat transfer from an axisymmetric jet to a flat surface, effect of melting.....	126
7.2	Adjustment of the melted surface.....	129
7.3	Typical profiles of the ice interface.....	131
7.4	Steady state heat transfer due to axisymmetric jet impingement.....	134
7.5	Effect of reference temperature for calculating physical properties.....	136
7.6	Experimental apparatus.....	137
7.7	Profiles of a melted surface, with and without erosion.....	143
A.1	Computer Program Flow Chart.....	167

LIST OF PLATES

PLATE

Page

- 1 Time history of a block of ice melted  
by a water jet  $D = 1.27$  cm,  $V = 0.76$   
m/sec,  $Re_D = 5.4 \times 10^3$ ,  $Ste = 0.31$ ..... 139

## NOMENCLATURE

### Notation

u, v	velocity components
x, y, r, z	coordinate directions
V	reference velocity
D	jet diameter or slot width
n	normal component; n = 1 axisymmetric flow n = 0 two-dimensional flow
s	tangential component
I	variational integral
F, G, H	a function
A	area
l	length of an element side
T	element velocity function, equation 3.2.9
R	radius of curvature
U	mainstream velocity
L	latent heat of fusion - 80 cal/gm of ice
k	thermal conductivity
Re <sub>D</sub>	Reynolds number $\frac{VD}{\nu}$

Ste	Stefan number	$\frac{c_p (T_\infty - T_0)}{L}$
$c_p$	specific heat of water	$-\frac{1 \text{ cal}}{\text{gm}^\circ\text{C}}$
Pr	Prandtl number	$\frac{\nu}{\alpha}$
z	defined by equation	4.4.3
k	defined by equation	4.4.4, curvature
W	defined by equation	4.4.11
$\tilde{L}$	defined by equation	4.4.12
m	boundary layer thickness ratio	$\frac{\delta_t}{\delta_u}$
H	non-dimensional distance from nozzle exit to impingement surface	
h	heat transfer coefficient	
$Nu_D$	Nusseld number	$= \frac{hD}{k}$
$c_\tau$	shear stress coefficient	$= \frac{\mu}{\frac{1}{2} \rho V^2} \left. \frac{\partial u'}{\partial y'} \right _{y'=0}$
t	time	

#### Greek Symbols

$\phi$	velocity potential
$\psi$	stream function
$\epsilon$	a small parameter
$\rho$	density

$\eta$	arbitrary function, boundary layer distance
$\xi$	area coordinate
$\chi$	element interpolation function equation 3.2
$\lambda$	a relaxation parameter, melting parameter
$\delta$	boundary layer thickness
$\nu$	kinematic viscosity
$\theta$	non-dimensional temperature $\frac{T - T_0}{T_\infty - T_0}$
$\alpha$	thermal diffusivity
$\Lambda$	pressure gradient parameter, equation 4.3.5
$\gamma$	a parameter, equation 5.1.2
$\beta$	gradient of velocity at stagnation point, equation 5.2.6
$\mu$	absolute viscosity

#### Subscripts

$x, y, r, z$	a component in the coordinate direction
$B$	boundary
$m$	of the $m^{\text{th}}$ element
$i, j, k$	$i = (1, 2, 3)$ , $j = (2, 3, 1)$ , $k = (3, 1, 2)$ in cyclic permutation
$0$	on the melting surface



$\infty$  free stream  
u velocity  
t thermal  
f free surface  
s impingement surface

Superscripts

' dimensional variable  
— vector quantity  
\* specified quantity, transformed variable  
m of the  $m^{\text{th}}$  element

## CHAPTER I

### INTRODUCTION

Impinging jets used as heat transfer devices, in general, have a great practical importance for many industrial applications. A few industrial uses are the annealing of non-ferrous sheet metals, the tempering of glass, drying of textiles and paper, and turbine blade cooling. In fact, in any situation requiring local heating or cooling of industrial equipment, impinging jets may have applications.

Another possible use of impinging jets might be in the melting of ice. Mellor [42] gives some potential applications of ice cutting by water jets. Some of these are the aiding of river and lake icebreakers, deicing of road and runway pavements, as a cutter for the laying of an arctic pipeline, and as a protective cutter to prevent the icing of piers and pillings in harbours during winter. The cutting of frozen ground may be another potential application of impingement jet cutting. Here, both the mechanical action of the jet and the jet heat transfer properties will influence the cutting process.

There are two general cases of jet impingement. In the first case, a fluid jet issues into an ambient medium of a similar fluid, liquid into liquid or gas into gas.

The entrainment of the ambient fluid by the jet determines the flow field and consequently the heat transfer characteristics on the impingement surface. Many authors [24, 29-38] have studied the impingement heat transfer characteristics of these jets. Some of the important effects are the distance from the nozzle exit to the impingement surface, jet Reynolds number, Prandtl number, turbulence intensity and scale, and the impingement surface geometry.

Because of the complex nature of the interactions between the jet, ambient fluid and impingement surface, especially in the region of the stagnation point, these investigations have been experimental in nature.

The second case of jet impingement occurs when a liquid jet issues into a gaseous medium. The jet forms a free surface between it and the ambient medium. A difficulty in this problem is that the position of the free surface is unknown and its location must be found as part of the solution. It is easier to analyze this case of jet flow analytically. As stagnation point fluid flow and heat transfer can be analyzed by boundary layer methods, the division of the problem into a potential flow region and a boundary layer is appropriate.

The potential flow problem can be formulated as an elliptic boundary value problem or as a variational statement minimizing a functional. When the potential flow is stated as a boundary value problem the usual methods of solution are separation of variables and finite difference.

numerical solutions. The methods of complex variables and conformal mapping may be used as a solution technique for two-dimensional potential flows only. As a variational statement, the solution may be obtained by using the finite element method. Solutions for the potential flow field may also be found experimentally. The electrical analogy, and the measurement of the pressure distribution in the flow field are two experimental methods.

An exact solution for the potential flow of a two-dimensional jet issuing from a nozzle of a finite height and impinging on a flat surface is presented by Miyazaki and Silberman [23]. The solution method is a conformal mapping of the flow field. The velocity distribution on the impingement surface, important for boundary layer analysis, is found directly from the complex variable analysis. Separation of variables has been used by Scholtz and Trass [28] to solve the potential flow of a non-uniform axisymmetric jet impinging on a flat surface and by Sparrow and Lee [47] for a non-uniform two-dimensional jet. Non-uniformity exists because of the assumption of a fully developed jet velocity profile in the nozzle. The location of the free surface is found by a method of successive approximations. Sarpkaya and Hiriart [16] have used the finite element formulation of Chan and Larock [15] to find the potential flow field of axisymmetric jets impinging on curved target type thrust reversers. Potential flow of jets impinging on curved deflectors was

solved by a finite difference relaxation technique by Schnurr, Williamson and Tatom [49]. Curved deflectors and thrust reversers are important in connection with STOL and conventional aircraft. Experimentally, Leclerc [26] has used the electrical analogy and Brady and Ludwig [27] have measured the pressure distribution in the flow field of an axisymmetric jet impinging on a flat surface. Once the pressure distribution is known, the velocity distribution is calculated by Bernoulli's equation.

Of the methods mentioned above, the finite element method seems to offer the most flexibility in solving these jet impingement problems. Finite elements are well suited to both axisymmetric and two-dimensional flows as well as arbitrarily shaped boundaries. The method of complex variables is only useful for two-dimensional potential flow and not applicable to axisymmetric flow. Separation of variables requires simple boundary conditions and simple boundary geometry for calculations to be possible. The finite difference method requires many more nodes than the finite element method to adequately describe a curved boundary shape such as the shape of the free surface. Therefore, because of the flexibility of the finite element method, the potential flow jet impingement considered in this thesis was solved by the finite element method.

Boundary layer analysis is used to calculate the skin friction and heat transfer coefficients associated with a

particular flow. Miyazaki and Silberman [23] used the exact solution for the potential flow of a two-dimensional jet and then employed a finite difference boundary layer numerical technique to find the heat transfer and skin friction coefficients on the impingement surface. Another analytical method is to calculate the boundary layer parameters associated with Hiemenz stagnation point flow as described in Schlichting [17]. This method requires knowledge of the potential flow in the region of the stagnation point and is only valid in the immediate neighbourhood of the stagnation point.

Experimentally, the heat transfer coefficients may be found basically by two methods. The first is by using a naphthalene sublimation mass transfer technique. Scholtz and Trass [28] used this technique for the non-uniform axisymmetric jet impinging on a flat surface. The heat-mass transfer analogy is then used to determine the heat transfer coefficients from the measurements of mass transfer. The second method is to use a hot wire or hot film heat sensing device. Baines and Keffer [48] have used this method to determine the heat transfer and shear stress at a stagnation point arising from the impingement of a fully developed turbulent jet.

Because of the extremely complex nature of a water jet impinging on an ice surface there has not been much analytical treatment of this subject. Yen [41] has experimentally studied a bubble-induced water jet impinging on

an ice surface. The effects of entrainment are important in this case. Yen and Zehnder [43] and Gilpin [44] have studied the melting of a block of ice by an impinging water jet. In [43] the melting effect was determined by the mass of ice removed by the impinging jet. In [44] two distinct modes of melting were noted, differentiated by the shape of the ice cavity the water jet produced. The first was a smooth cavity shape occurring at small jet Reynolds numbers and the second was a rough cavity shape occurring at larger jet Reynolds number and is characteristic of fully turbulent flow.

Melting ice under conditions of forced convection has been analyzed for the case of laminar flow on a flat ice surface by Pozvonkov, Shurgalskii and Akselrod [19]. Their solution was attained by utilizing the integral boundary layer equations. As no pressure gradient term appears in the flow over a flat plate, their solution is not applicable to the present case of jet impingement flow. Other analytical treatments of forced convection melting of ice [50-53] also involve the case where the pressure gradient term has been neglected.

In this thesis the analytical treatment of a laminar water jet impinging on an ice surface is discussed. Chapter II deals with the potential flow problem formulation, as a boundary value problem and as a variational statement. The equivalence between the boundary value problem and the variational statement is shown by the

7

methods of the calculus of variations. Chapter III presents the finite element method as a solution to the potential flow problem. Chapter IV derives the boundary layer solution. The Karman-Pohlhausen integral method is used with a fourth order polynomial to approximate the velocity and temperature distributions in the boundary layer. Both the momentum integral equation and energy integral equation are formulated and it is seen that they are coupled through the boundary condition at the melting interface. Chapter V presents calculations based on two-dimensional jet impingement in the absence of melting. Comparisons with exact solutions and other numerical calculations is given to show confidence in the present method. Chapter VI deals with axisymmetric jet impingement. The effects of nozzle-plate spacing and impingement surface shape on the surface velocity distribution are discussed. In addition, the shear stress on the surface resulting from the impinging jet is noted. Chapter VII deals with the melting and erosion of a frozen material. If the material is ice then heat transfer between the water jet and the ice surface is the primary ice removal mechanism. When the material is frozen gravel or sand, for example, both removal mechanisms, heat transfer and erosion will be important. The effect of melting on heat transfer is discussed and an attempt is made to model the melting of a block of ice. Finally the combined removal mechanisms, heat transfer and erosion are discussed with respect to an axisymmetric jet impinging on a flat surface.



## CHAPTER II

### POTENTIAL FLOW ANALYSIS

The classical approach for the solution of many forced convection momentum and heat transfer problems begins with the computation of the inviscid flow, ignoring any boundary layers which may be present. The boundary layer is then computed assuming the flow conditions at the outer edge of the boundary layer are equal to the conditions predicted at the surface of the body by the inviscid flow analysis. The parameters of interest, the skin friction and heat transfer coefficients can then be found from boundary layer considerations.

In this chapter, the steady, irrotational flow of an inviscid incompressible fluid is considered. The flow field problem is formulated as a boundary value problem and as a variational statement both involving the scalar velocity potential and the stream function. Both two-dimensional, using plane cartesian coordinates and axisymmetrical flow using cylindrical polar coordinates independent of the angular coordinate are considered. The cartesian coordinates used are  $x, y$  and the cylindrical polar coordinates used are  $r, z$ .

The science and mathematics of inviscid flow analysis is very well established and the details may be found in

many standard textbooks, for example, Milne-Thompson [1], Batchelor [2], Lamb [3] and Robertson [4]. The boundary value problem formulation is given here for completeness and future reference. The variational formulation follows that of Kantorovich and Krylov [5] and is included to show the equivalence between the boundary value problem and the variational statement, especially with respect to the boundary conditions.

## 2.1 Governing Equations

Consider the steady, irrotational flow of an inviscid incompressible fluid. Let prime (') denote a dimensional variable and unprimed variables as non-dimensional. The equation of continuity is

$$\nabla' \cdot \bar{v}' = 0 \quad 2.1.1$$

where  $\bar{v}'$  is the velocity vector. This reduces to

$$\frac{\partial v'_x}{\partial x'} + \frac{\partial v'_y}{\partial y'} = 0 \quad 2.1.2$$

for two-dimensional flow and to

$$\frac{\partial(r'v'_z)}{\partial z'} + \frac{\partial(r'v'_r)}{\partial r'} = 0 \quad 2.1.3$$

for cylindrical axisymmetrical flow. The condition of irrotationality is mathematically expressed by

$$\nabla' \times \bar{V}' = 0 \quad 2.1.4$$

which becomes

$$\frac{\partial v'_y}{\partial x'} - \frac{\partial v'_x}{\partial y'} = 0 \quad 2.1.5$$

and

$$\frac{\partial v'_r}{\partial z'} - \frac{\partial v'_z}{\partial r'} = 0 \quad 2.1.6$$

for two-dimensional and axisymmetrical flow respectively.

To satisfy the continuity equations, 2.1.2 and 2.1.3, a stream function  $\psi'$  is introduced and is defined by

$$v'_x = -\frac{\partial \psi'}{\partial y'} ; \quad v'_y = \frac{\partial \psi'}{\partial x'} \quad 2.1.7$$

for two-dimensional flow and for axisymmetrical flow by

$$v'_z = -\frac{1}{r'} \frac{\partial \psi'}{\partial r'} ; \quad v'_r = \frac{1}{r'} \frac{\partial \psi'}{\partial z'} \quad 2.1.8$$

From the condition of irrotationality, 2.1.4, the curl of the velocity vector is zero and from vector analysis the curl of the gradient of a scalar function is also zero. Therefore, for irrotational flow the velocity vector is the gradient of a scalar function. Define a scalar velocity potential function  $\phi'$  as

$$\vec{V}' = -\nabla'\phi' \quad 2.1.9$$

The velocity components in terms of the potential function are

$$v'_x = -\frac{\partial\phi'}{\partial x'} ; \quad v'_y = -\frac{\partial\phi'}{\partial y'} \quad 2.1.10$$

and

$$v'_z = -\frac{\partial\phi'}{\partial z'} ; \quad v'_r = -\frac{\partial\phi'}{\partial r'} \quad 2.1.11$$

for two-dimensional and axisymmetrical flows respectively. Letting  $V$  be a reference velocity and  $D$  a reference length, a set of non-dimensional variables may be defined.

$$x = \frac{x'}{D} ; \quad y = \frac{y'}{D} ; \quad z = \frac{z'}{D} ; \quad r = \frac{r'}{D}$$

$$v_x = \frac{v'_x}{V} ; \quad v_y = \frac{v'_y}{V} ; \quad v_z = \frac{v'_z}{V} ; \quad v_r = \frac{v'_r}{V}$$

$$\bar{V} = \frac{\bar{V}'}{V} ; \psi = \frac{\psi'}{VD} ; \phi = \frac{\phi'}{VD} ; \nabla = \nabla'D \quad 2.1.12$$

Using non-dimensionalizations 2.1.12 the continuity equations 2.1.1, 2.1.2, and 2.1.3 become

$$\nabla \cdot \bar{V} = 0 \quad 2.1.13$$

in general and

$$\frac{\partial v_x}{\partial x} + \frac{\partial v_y}{\partial y} = 0 \quad 2.1.14$$

for two-dimensional flow and

$$\frac{\partial(rv_z)}{\partial z} + \frac{\partial(rv_r)}{\partial z} = 0 \quad 2.1.15$$

for axisymetrical flow. Using 2.1.12 the conditions of irrotationality, equations 2.1.4, 2.1.5 and 2.1.6 become

$$\nabla \times \bar{V} = 0 \quad 2.1.16$$

in general and

$$\frac{\partial v_y}{\partial x} - \frac{\partial v_x}{\partial y} = 0 \quad 2.1.17$$

for two-dimensional flow and

$$\frac{\partial v_r}{\partial z} - \frac{\partial w_z}{\partial r} = 0 \quad 2.1.18$$

for axisymmetrical flow. The velocity components in terms of the non-dimensional stream function  $\psi$  and the non-dimensional potential function  $\phi$  are found by substituting 2.1.12 into equations 2.1.7 through 2.1.11. Therefore

$$v_x = -\frac{\partial \psi}{\partial y}; \quad v_y = \frac{\partial \psi}{\partial x} \quad 2.1.19$$

$$v_x = -\frac{\partial \phi}{\partial x}; \quad v_y = -\frac{\partial \phi}{\partial y}$$

for two-dimensional flow and

$$v_z = -\frac{1}{r} \frac{\partial \psi}{\partial r}; \quad v_r = \frac{1}{r} \frac{\partial \psi}{\partial z} \quad 2.1.20$$

$$v_z = -\frac{\partial \phi}{\partial z}; \quad v_r = -\frac{\partial \phi}{\partial r}$$

for axisymmetrical flow and

$$\bar{V} = -\nabla \phi \quad 2.1.21$$

in general for irrotational flows. Substitution of equation 2.1.21 into the continuity equation 2.1.13 yields

$$\nabla^2 \phi = 0 \quad 2.1.22$$

This is Laplace's equation which reduces to

$$\frac{\partial^2 \phi}{\partial x^2} + \frac{\partial^2 \phi}{\partial y^2} = 0. \quad 2.1.23$$

for two-dimensional flow and to

$$\frac{\partial^2 \phi}{\partial r^2} + \frac{1}{r} \frac{\partial \phi}{\partial r} + \frac{\partial^2 \phi}{\partial z^2} = 0 \quad 2.1.24$$

for axisymmetrical flows. Substitution of the velocity components in terms of the stream function, 2.1.19 and 2.1.20 into equations 2.1.17 and 2.1.18 results in

$$\frac{\partial^2 \psi}{\partial x^2} + \frac{\partial^2 \psi}{\partial y^2} = 0 \quad 2.1.25$$

for two-dimensional flow and for axisymmetric flow

$$\frac{\partial^2 \psi}{\partial r^2} - \frac{1}{r} \frac{\partial \psi}{\partial r} + \frac{\partial^2 \psi}{\partial z^2} = 0 \quad 2.1.26$$

The three equations, 2.1.23, 2.1.24 and 2.1.25 are Laplace's equation but the equation for the axisymmetric stream function 2.1.26 is not. Consideration of equation 2.1.19 yields

$$\frac{\partial \phi}{\partial x} = \frac{\partial \psi}{\partial y} ; \quad \frac{\partial \phi}{\partial y} = - \frac{\partial \psi}{\partial x}$$

which are recognized as the Cauchy-Riemann conditions. The functions  $\phi$  and  $\psi$  are conjugate harmonic functions and two-dimensional problems can be solved by the methods of complex variables.

For the axisymmetric case, consideration of equations 2.1.20 result in

$$\frac{\partial \phi}{\partial z} = \frac{1}{r} \frac{\partial \psi}{\partial r} ; \quad \frac{\partial \phi}{\partial r} = - \frac{1}{r} \frac{\partial \psi}{\partial z}$$

The Cauchy-Riemann conditions are not satisfied and  $\phi$  and  $\psi$  are not conjugate harmonic functions. Although  $\phi$  satisfies Laplace's equation 2.1.24,  $\psi$  does not, equation 2.1.26.

The problem may be formulated either in terms of the velocity potential by equations 2.1.23 or 2.1.24 or in terms of the stream function by equations 2.1.25 or 2.1.26 depending if the flow is two-dimensional or axisymmetric. The velocity components are given by equations 2.1.19 and 2.1.20.



## 2.2 Boundary Conditions

For the derived governing equations 2.1.23 through 2.1.26 either Dirichlet or Neumann type boundary conditions apply. At a solid boundary the velocity component normal to the boundary must be the same as the velocity of the boundary in the normal direction. Therefore if  $\bar{n}$  is the normal unit vector

$$\bar{V} \cdot \bar{n} = \bar{V}_B \cdot \bar{n} \quad 2.2.1$$

In the two-dimensional case this results in

$$v_x n_x + v_y n_y = v_{Bx} n_x + v_{By} n_y \quad 2.2.2$$

When a solid boundary is stationary,  $V_B = 0$  and using equation 2.1.19

$$-\frac{\partial \psi}{\partial y} n_x + \frac{\partial \psi}{\partial x} n_y = 0$$

or

$$\frac{\partial \phi}{\partial x} n_x + \frac{\partial \phi}{\partial y} n_y = 0 \quad 2.2.3$$

Referring to Figure 2.1, the direction cosines of  $\bar{n}$  are

$$n_x = \frac{\partial x}{\partial n} = \frac{\partial y}{\partial s}$$

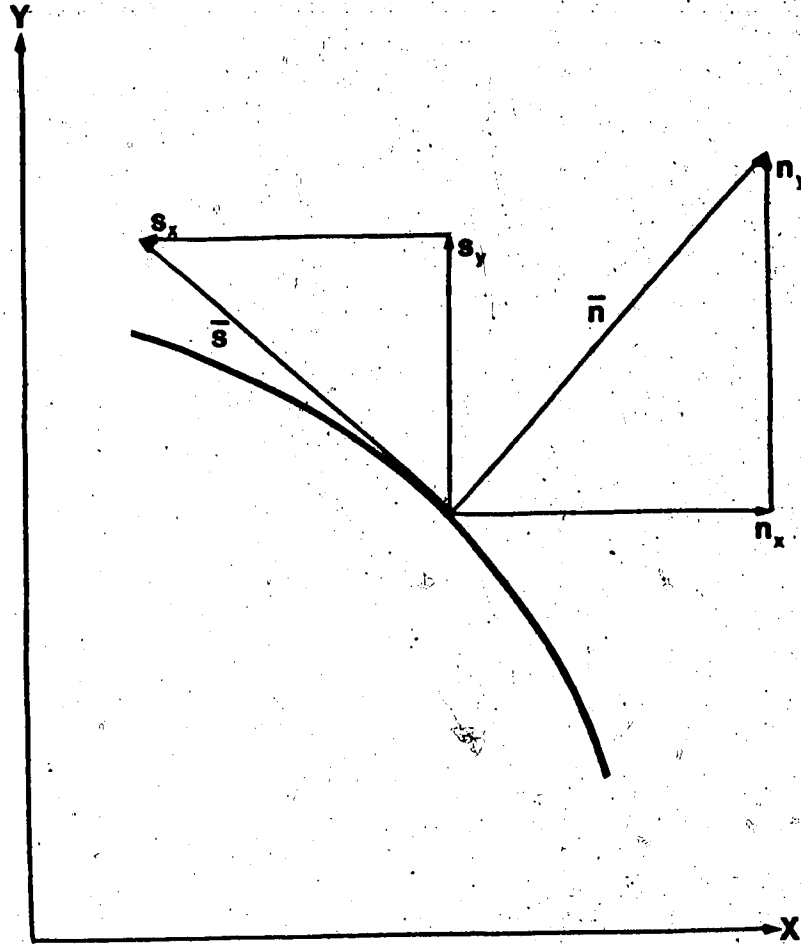


Figure 2.1 Direction cosines of  $\vec{n}$ ,  $\vec{s}$

and

$$n_y = \frac{\partial y}{\partial n} = - \frac{\partial x}{\partial s} \quad 2.2.4$$

Substituting equations 2.2.4 into 2.2.3 results in

$$\frac{\partial \psi}{\partial s} = \frac{\partial \psi}{\partial y} \frac{\partial y}{\partial s} + \frac{\partial \psi}{\partial x} \frac{\partial x}{\partial s} = 0$$

or

$$\frac{\partial \phi}{\partial n} = \frac{\partial \phi}{\partial x} \frac{\partial x}{\partial n} + \frac{\partial \phi}{\partial y} \frac{\partial y}{\partial n} = 0 \quad 2.2.5$$

Equations 2.2.5 state that the tangential derivative of the stream function along a stationary solid wall is zero, while the normal derivative of the potential function is zero.

That is, the velocity normal to the solid wall is zero.

The boundary condition of a constant specified velocity  $v^*$ , normal to a boundary segment is given by either

$$\frac{\partial \psi}{\partial s} = \bar{V} \cdot \bar{n} = v^*$$

or

$$\frac{\partial \phi}{\partial n} = \bar{V} \cdot \bar{n} = v^* \quad 2.2.6$$

If one of the boundaries is a streamline, the same arguments as for the solid wall boundary apply. The streamline is a

line through which there is no normal flow. Equations 2.2.5 and 2.2.6 are Neumann type boundary conditions.

Dirichlet conditions imply the stream function  $\psi$  or the potential function  $\phi$  being constant along a boundary segment. If the boundary is a streamline the stream function is constant along the boundary. If the potential function is constant along a boundary then the streamlines at the boundary are at right angles everywhere on the boundary.

The boundary value problem for the steady irrotational flow of an inviscid incompressible fluid may be formulated by a number of boundary value problems.

Given a flow region  $R$  bounded by a curve  $\Gamma$  the boundary value problem for two-dimensional flow is either

$$\frac{\partial^2 \phi}{\partial x^2} + \frac{\partial^2 \phi}{\partial y^2} = 0 \text{ in } R$$

subject to

2.2.7

$$\phi = \phi^* \text{ on } \Gamma_1$$

$$\frac{\partial \phi}{\partial n} = v^* \text{ on } \Gamma_2$$

or

$$\frac{\partial^2 \psi}{\partial x^2} + \frac{\partial^2 \psi}{\partial y^2} = 0 \text{ in } R$$

subject to

2.2.8

$$\psi = \psi^* \text{ on } \Gamma_1$$

$$\frac{\partial \psi}{\partial s} = v^* \text{ on } \Gamma_2$$

where  $\Gamma = \Gamma_1 + \Gamma_2$ . For axisymmetric flow the boundary value problem for flow region R and bounding curved  $\Gamma$  is either

$$\frac{\partial^2 \phi}{\partial r^2} + \frac{1}{r} \frac{\partial \phi}{\partial r} + \frac{\partial^2 \phi}{\partial z^2} = 0 \text{ in R}$$

subject to

2.2.9

$$\phi = \phi^* \text{ on } \Gamma_1$$

$$\frac{\partial \phi}{\partial n} = v^* \text{ on } \Gamma_2$$

or

$$\frac{\partial^2 \psi}{\partial r^2} - \frac{1}{r} \frac{\partial \psi}{\partial r} + \frac{\partial^2 \psi}{\partial z^2} = 0$$

subject to

2.2.10

$$\psi = \psi^* \text{ on } \Gamma_1$$

$$\frac{\partial \psi}{\partial s} = v^* \text{ on } \Gamma_2$$

and again  $\Gamma = \Gamma_1 + \Gamma_2$ .

The above formulations can usually be solved directly by an analytical or numerical method if the bounding curve  $\Gamma$  is known a priori. In free surface flow problems the position of the free surface is not known before hand and must be found as part of the solution. A free surface is a streamline on which the pressure is constant, for example, a jet of water issuing from a nozzle into air forms a free surface.

As the free surface is a streamline the velocity normal to the free surface is zero. In addition the condition of constant pressure along the free streamline must hold. That is

$$p = p^* \quad 2.2.11$$

on the free streamline.

Integration of the equations of motion along a streamline results in the well known Bernoulli equation

$$\frac{v'^2}{2} + \frac{p'}{\rho} + gh' = B^* \quad 2.2.12$$

where  $B^*$  is the Bernoulli constant for the streamline and  $v'^2$  is the square of the speed of fluid particles on the streamline;  $v'^2 = \bar{v}' \cdot \bar{v}'$ . If the gravity forces can be neglected, assumed valid for jet flows to be considered,

then the condition of constant pressure along the streamline implies a constant speed by Bernoulli's equation 2.2.12. So at the free surface two conditions must be satisfied

$$\frac{\partial \phi}{\partial n} = 0 \quad \text{or} \quad \frac{\partial \psi}{\partial s} = 0$$

2.2.13

$p = p^*$  on the streamline

and if gravity forces can be neglected the second condition reduces to

$$V = v^* \text{ on the streamline}$$

2.2.14

### 2.3 Variational Formulation

There are many methods available for the direct solution of the boundary value problems given by equations 2.2.7 through 2.2.10. Of these are the exact solutions of complex variables for two-dimensional flows and separation of variables methods for either two-dimensional or axisymmetric flows. Some approximate methods are the finite difference relaxation techniques and the electrical analogy graphical method.

Another method of solution would be to try and find an equivalent form of the boundary value problem. As is well known from structural and continuum mechanics, varia-

tional methods using the calculus of variations offer an alternative formulation for boundary value problems [6]. One method of solution of the variational method is the Finite Element Method [7,8,9]. Zienkiewicz and Cheung [10] first applied the Finite Element Method to the solution of field problems as an extension of its use in solving problems of structural and continuum mechanics. Since then the Finite Element Method has been used to solve many different problems of fluid mechanics including the flow of an ideal fluid, for example [11,12,13,14]. Reference [8] contains an extensive recent list of finite element solutions to fluid mechanics problems. It will be instructive to show the equivalence between one of the boundary value problems stated and its associated variational statement especially with respect to the boundary conditions. The derivation follows that of Kantorovich and Krylov [5].

Consider the two-dimensional boundary value problem formulated in terms of the potential function, equation 2.2.7. The variational formulation considers the integral

$$I = \frac{\rho}{2} \iint_R \left\{ \left( \frac{\partial \phi}{\partial x} \right)^2 + \left( \frac{\partial \phi}{\partial y} \right)^2 \right\} dx dy - \rho \int_{\Gamma_2} \phi v^* ds \quad 2.3.1$$

The boundary conditions are exactly the same as those used in the boundary value problem, i.e.,  $\phi = \phi^*$  on  $\Gamma_1$  and  $\frac{\partial \phi}{\partial n} = v^*$  on  $\Gamma_2$ . The object is to find the function  $\phi$  in competition with all the other admissible functions satisfying the



boundary conditions which make the integral  $I$  a minimum. Therefore  $I$  is a function of  $\phi$  or  $I = I(\phi)$ . Let  $\phi(x,y)$  be the function which minimizes the integral  $I$ . Now, let the set of all other admissible functions satisfying the boundary conditions,  $\hat{\phi}(x,y)$ , be defined by

$$\hat{\phi}(x,y) = \phi(x,y) + \epsilon \eta(x,y) \quad 2.3.2$$

where  $\epsilon$  is a parameter and  $\eta(x,y)$  is arbitrary. Consider the Dirichlet boundary condition,  $\phi = \phi^*$  on  $\Gamma_1$ . Since both  $\phi$  and  $\hat{\phi}$  must satisfy this boundary condition equation 2.3.2 results in

$$\eta(x,y) = 0 \text{ on } \Gamma_1 \quad 2.3.3$$

Evaluating  $I(\hat{\phi}) = I(\phi + \epsilon \eta)$

$$I(\phi + \epsilon \eta) = \frac{\rho}{2} \iint_R \left\{ \left( \frac{\partial \phi}{\partial x} + \epsilon \frac{\partial \eta}{\partial x} \right)^2 + \left( \frac{\partial \phi}{\partial y} + \epsilon \frac{\partial \eta}{\partial y} \right)^2 \right\} dx dy - \rho \int_{\Gamma_2} (\phi + \epsilon \eta) v^* ds \quad 2.3.4$$

For  $\hat{\phi}$  to approach the minimizing function  $\phi$ , the parameter  $\epsilon$  must go to zero. The minimum of the integral is

then obtained by evaluating

$$\left. \frac{\partial I(\phi + \epsilon \eta)}{\partial \epsilon} \right|_{\epsilon=0} = 0 \quad 2.3.5$$

Differentiating 2.3.4 and setting  $\epsilon = 0$

$$\left. \frac{\partial I}{\partial \epsilon} \right|_{\epsilon=0} = \iint_R \left( \frac{\partial \phi}{\partial x} \frac{\partial \eta}{\partial x} + \frac{\partial \phi}{\partial y} \frac{\partial \eta}{\partial y} \right) dx dy - \int_{\Gamma_2} n v^* ds = 0 \quad 2.3.6$$

Noting that

$$\frac{\partial \phi}{\partial x} \frac{\partial \eta}{\partial x} + \frac{\partial \phi}{\partial y} \frac{\partial \eta}{\partial y} = \frac{\partial}{\partial x} \left( \eta \frac{\partial \phi}{\partial x} \right) + \frac{\partial}{\partial y} \left( \eta \frac{\partial \phi}{\partial y} \right) - \eta \left( \frac{\partial^2 \phi}{\partial x^2} + \frac{\partial^2 \phi}{\partial y^2} \right)$$

and using Green's Theorem to change an area integral to a line integral, equation 2.3.6 becomes

$$\begin{aligned} \left. \frac{\partial I}{\partial \epsilon} \right|_{\epsilon=0} &= \int_{\Gamma} \frac{\partial \phi}{\partial x} \eta dy - \int_{\Gamma} \frac{\partial \phi}{\partial y} \eta dx - \iint_R \eta \left( \frac{\partial^2 \phi}{\partial x^2} + \frac{\partial^2 \phi}{\partial y^2} \right) dx dy \\ &\quad - \int_{\Gamma_2} n v^* ds = 0 \end{aligned} \quad 2.3.7$$

The first two line integrals vanish on the part  $\Gamma_1$  of  $\Gamma$  as  $\eta(x,y) = 0$  using equation 2.3.3. Therefore, the line integrals need only be evaluated over the part  $\Gamma_2$  and they

may be combined. So

$$\begin{aligned} \left. \frac{\partial I}{\partial \epsilon} \right|_{\epsilon=0} &= - \iint_R \eta \left( \frac{\partial^2 \phi}{\partial x^2} + \frac{\partial^2 \phi}{\partial y^2} \right) dx dy \\ &+ \int_{\Gamma_2} \eta \left( \frac{\partial \phi}{\partial x} \frac{\partial y}{\partial s} - \frac{\partial \phi}{\partial y} \frac{\partial x}{\partial s} - v^* \right) ds = 0 \end{aligned} \quad 2.3.8$$

As the area integral and line integral are independent and that  $\eta(x,y)$  is arbitrary, the result is

$$\frac{\partial^2 \phi}{\partial x^2} + \frac{\partial^2 \phi}{\partial y^2} = 0 \text{ in } R$$

and

$$\frac{\partial \phi}{\partial x} \frac{\partial y}{\partial s} - \frac{\partial \phi}{\partial y} \frac{\partial x}{\partial s} - v^* = 0 \text{ on } \Gamma_2$$

The condition  $\phi = \phi^*$  on  $\Gamma_1$  has already been used. With reference to Figure 2.1 and equations 2.2.4 the boundary conditions become

$$\frac{\partial \phi}{\partial n} = v^* \text{ on } \Gamma_2$$

$$\phi = \phi^* \text{ on } \Gamma_1$$

and the boundary value problem is recovered. A similar procedure can be used for the other cases. The integrals are listed below.

#### Two Dimensional-Stream Function

$$I(\psi) = \frac{\rho}{2} \iint_R \left\{ \left( \frac{\partial \psi}{\partial x} \right)^2 + \left( \frac{\partial \psi}{\partial y} \right)^2 \right\} dx dy - \rho \int_{\Gamma_2} \psi v^* ds \quad 2.3.9$$

where

$$\psi = \psi^* \text{ on } \Gamma_1$$

$$\frac{\partial \psi}{\partial n} = v^* \text{ on } \Gamma_2$$

#### Axisymmetric Potential Function

$$I(\phi) = \rho \pi \iint_R \left\{ \left( \frac{\partial \phi}{\partial z} \right)^2 + \left( \frac{\partial \phi}{\partial r} \right)^2 \right\} r dr dz = 2\rho \pi \int_{\Gamma_2} \phi v^* ds \quad 2.3.10$$

with the same boundary conditions as in the two-dimensional case.

#### Axisymmetric Stream Function

$$I(\psi) = \rho \pi \iint_R \left\{ \left( \frac{\partial \psi}{\partial z} \right)^2 + \left( \frac{\partial \psi}{\partial r} \right)^2 \right\} \frac{1}{r} dr dz - 2\rho \pi \int_{\Gamma_2} \psi v^* ds \quad 2.3.11$$

with boundary conditions

$$\psi = \psi^* \text{ on } \Gamma_1$$

$$\frac{1}{r} \frac{\partial \psi}{\partial n} = v^* \text{ on } \Gamma_2$$

Equations 2.3.1 and 2.3.9 are equally useful for two-dimensional flow and the choice of which one is most suited to a particular problem depends on the type of boundary conditions that are present. However, equation 2.3.11 is not as useful as 2.3.10 due to the presence of the radial coordinate  $r$  in the denominator of the first integral of the equation. To evaluate this integral it would be necessary to use numerical integration which is time consuming and susceptible to errors. Equation 2.3.10 will be used for all axisymmetric flow problems.

## CHAPTER III

### THE FINITE ELEMENT METHOD

#### 3.1 Background

The development of finite element techniques originated from classical approaches to structural analysis. The sciences of structural and continuum mechanics have used finite element techniques to solve many complex problems. Recently, the finite element method has been used to solve many field problems including those of potential flow in fluid mechanics [7-14].

The finite element method has been used extensively in recent years because it has, in general, several outstanding features. Listed by Chan [11] they are:

- Non-homogeneous and anisotropic problems are easily treated.
- Elements can be graded in size and shape to follow boundaries of arbitrary configuration.
- Once a computer program has been developed, problems of a similar nature can easily be solved by supplying the appropriate new input data.

The general method of solution of fluid flow problems using the finite element method is as follows:

- The entire flow region is divided into a set of elements, interconnected at various nodal points. A number-

ing system is chosen to assign values to the nodes and elements.

- An element interpolation function is chosen specifying the variation of the field variable within each element. In the cases considered the field variable is either the stream function or the potential function.

- The contributions of each element to the total flow pattern are assembled by a Ritz technique resulting in a system of symmetric, banded, linear simultaneous equations. The number of equations in the system equals the number of nodal points in the element mesh and the solution of the system gives the value of the field variable at each nodal point.

- All related physical properties are evaluated from the nodal values.

The Ritz technique is a procedure for changing a continuous medium problem into an approximate lumped parameter system. Consider the integral

$$I(u) = \int_R F(x, y, u, \frac{\partial u}{\partial x}, \frac{\partial u}{\partial y}) dR \quad 3.1.1$$

over the domain  $R$ . The object is to minimize  $I(u)$ ; that is find the function  $u$  from a set of admissible functions which makes the integral a minimum. This is accomplished by selecting an appropriate trial family of solutions  $u_n$ , where  $u_n$  is given by

$$u_n = \sum_{i=1}^N u_i \gamma_i(x,y) \quad 3.1.2$$

The  $u_i$  are the undetermined parameters and the  $\gamma_i$  are the coordinate functions or trial functions. The coordinate functions are known before hand but the  $u_i$  are to be determined so to make  $u_n$  the function which minimizes  $I(u)$ . The minimization is achieved by finding the quantity

$$\frac{\partial I(u)}{\partial u_i} = 0 \quad 3.1.3$$

The result is a set of linear equations which enables the best approximation to the true solution from the family of trial solutions to be found.

### 3.2 The Finite Element Method Applied to Jet Impingement

#### (a) Finite Element Formulation

The following is a description of the finite element method as applied to a jet impingement problem. The formulation follows that of Chan [11] and Chan and Larock [15]. Sarpkaya and Hiriart [16] have used this formulation to solve the jet flow associated with aerodynamic thrust reversers, a very similar problem.

Consider the flow of an axisymmetric jet impinging on a flat plate. The flow field is shown schematically in Figure 3.1. As the flow is axisymmetrical the potential



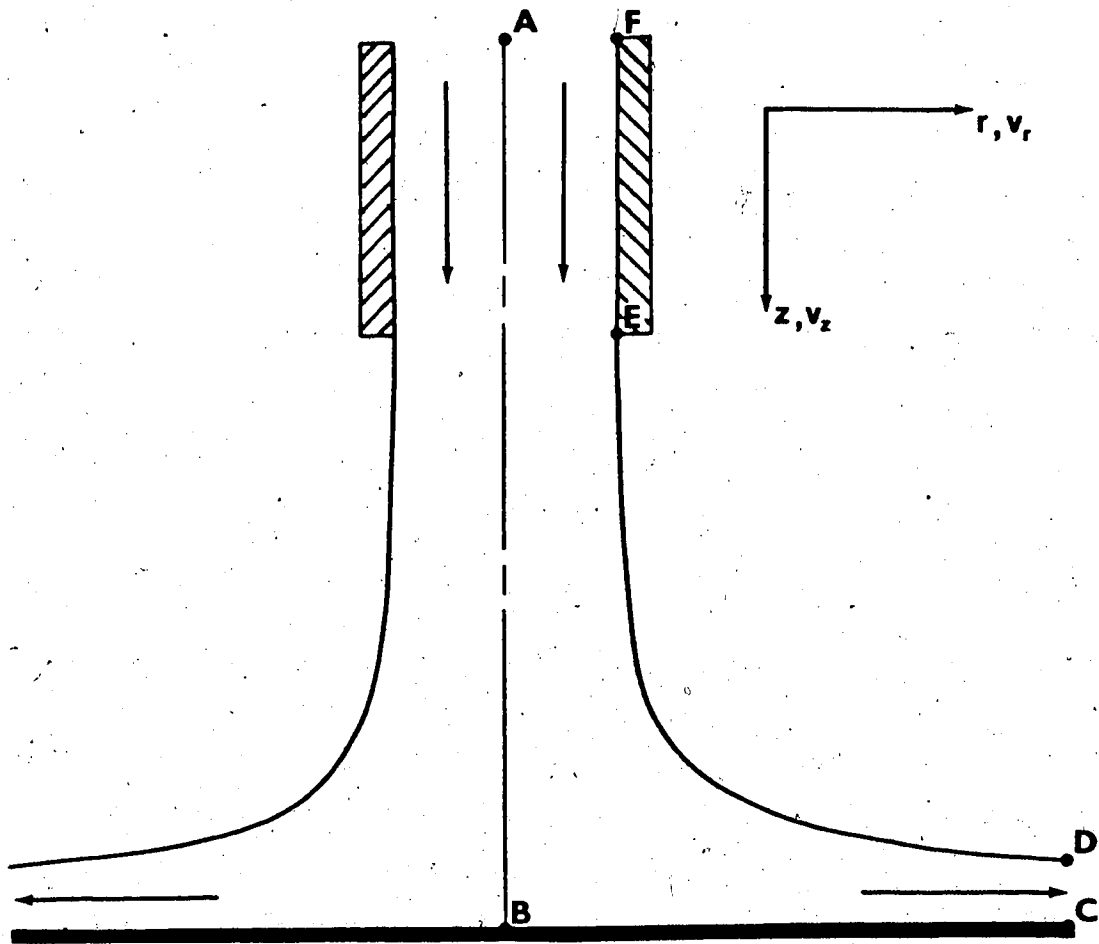


Figure 3.1 Axisymmetric jet impinging on a flat surface.

function formulation must be used and the appropriate integral is equation 2.3.10. The procedure followed here is identical with velocity potential and stream function formulations in two-dimensional flow. Since the flow is symmetrical about the stagnation streamline AB, only one-half of the flow region need be considered.

First the flow region is divided into a triangular element mesh, and a numbering system assigned to the nodes and elements. The pattern chosen is shown in Figure 3.2. There are a number of reasons for a pattern of this type. A sequence is established for the numbering of both the elements and the nodes. The elements shown in the figure are in blocks of six. All of the blocks of six elements are identical in the flow field. This enables the flow field to be modeled by as many elements as desired just by adding more blocks of six elements. The node numbering system also follows a distinct pattern. It is possible to generate the numbering system for the whole nodal field by starting with the node numbers of the first six elements. Therefore, a computer program may be written to generate the numbering system for the flow field just by inputting the numbering pattern for the first six elements and the number of blocks of six elements desired.

A six node triangular element is used as the basic element of the flow field. This enables a quadratic variation of the field variable, the potential function  $\phi$ , within the element. Introduction of triangular area or natural

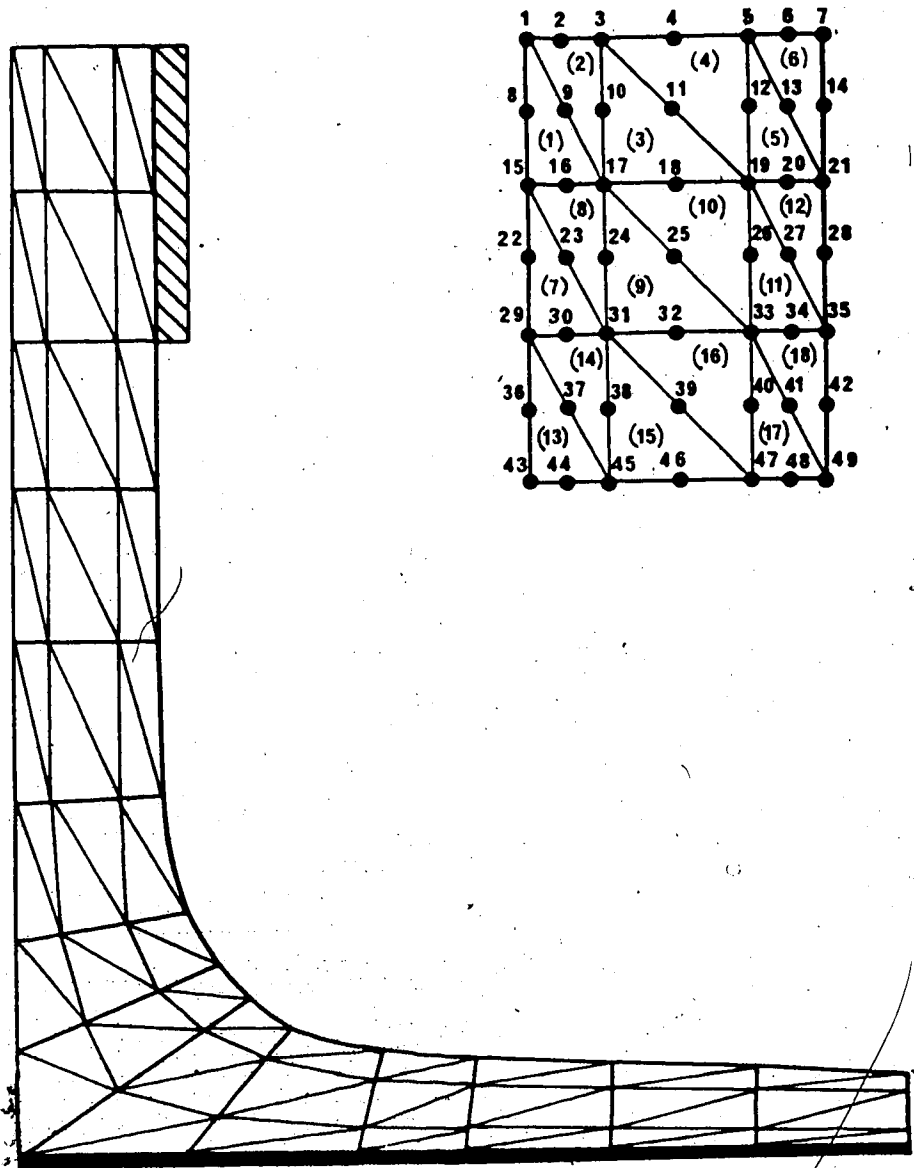


Figure 3.2 Finite element mesh and numbering system.

coordinates leads to simplification of the algebra involved. The area coordinates  $\xi_i$  are defined by

$$\xi_i = \frac{A_i}{A_m} \quad i=1,2,3 \quad 3.2.1$$

where  $A_m$  is the area of the triangular element and the  $A_i$  are the areas of the subtriangles as shown in Figure 3.3. Each element has three corner nodes (numbers 1, 2 and 3) and three mid-side nodes (numbers 4, 5 and 6). For example, the side connecting node 1 to node 2 is described by  $\xi_3 = 0$  with  $\xi_1$  varying from 1 to 0 and  $\xi_2$  varying from 0 to 1. Obviously, a constraint on the area coordinates defined by equation 3.2.1 is

$$\xi_1 + \xi_2 + \xi_3 = 1 \quad 3.2.2$$

The quadratic variation of the potential,  $\phi^m$ , in element  $m$  is given in terms of the potentials  $\phi_i^m$  at the node points.

$$\phi^m = \phi_i^m \chi_i \quad i = 1 \text{ to } 6 \quad 3.2.3$$

where

$$\chi_i = \{ \xi_1(2\xi_1-1), \xi_2(2\xi_2-1), \xi_3(2\xi_3-1), \\ 4\xi_1\xi_2, 4\xi_2\xi_3, 4\xi_3\xi_1 \} \quad 3.2.4$$

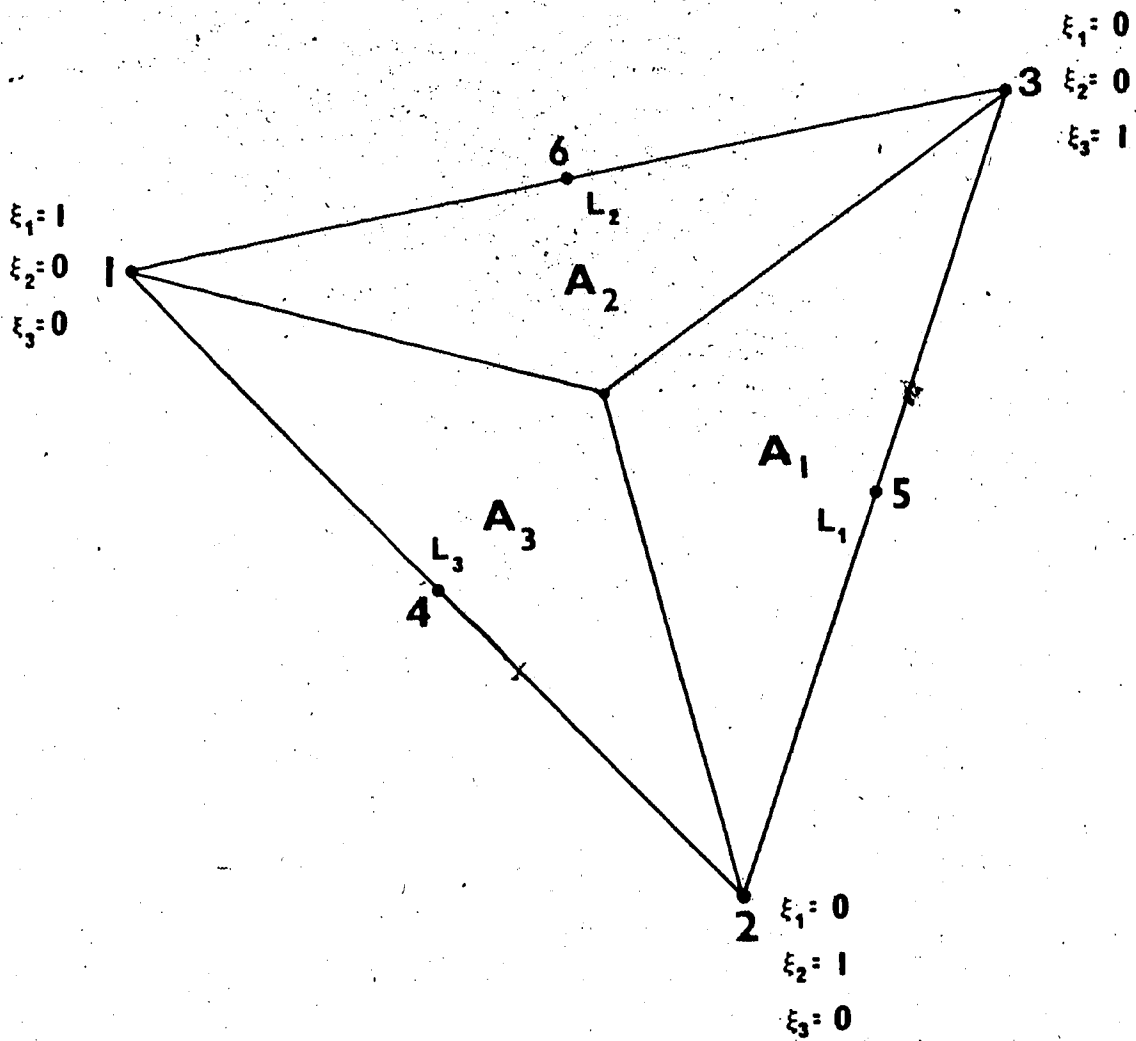


Figure 3.3 Area coordinates and element numbering system.

The derivation of the element interpolation function  $\chi_i$  is given by Huebner [8]. The original polar coordinates  $(r, z)$  of a point in the triangle are linearly related to the area coordinates  $(\xi_1, \xi_2, \xi_3)$  by the system of equations represented in matrix form by

$$\begin{bmatrix} z_1 & z_2 & z_3 \\ r_1 & r_2 & r_3 \\ 1 & 1 & 1 \end{bmatrix} \begin{bmatrix} \xi_1 \\ \xi_2 \\ \xi_3 \end{bmatrix} = \begin{bmatrix} z \\ r \\ 1 \end{bmatrix} \quad 3.2.5$$

where  $(r_i, z_i)$  are the coordinates of node  $i$  and  $i=(1,2,3)$ .

Solving equations 3.2.5 for  $(\xi_1, \xi_2, \xi_3)$  results in

$$\begin{bmatrix} \xi_1 \\ \xi_2 \\ \xi_3 \end{bmatrix} = \frac{1}{2A_m} \begin{bmatrix} b_1 & a_1 & c_1 \\ b_2 & a_2 & c_2 \\ b_3 & a_3 & c_3 \end{bmatrix} \begin{bmatrix} z \\ r \\ 1 \end{bmatrix} \quad 3.2.6$$

where  $2A_m = a_k b_j - a_j b_k$ ; twice the area of the triangle and  $b_k = r_i - r_j$ ;  $a_k = z_j - z_i$ ;  $c_k = z_i r_j - z_j r_i$  with  $i = (1,2,3)$ ;  $j = (2,3,1)$ ;  $k = (3,1,2)$ . In indicial notation equation 3.2.6 may be represented as

$$\xi_i = \frac{1}{2A_m} \{b_i z + a_i r + c_i\} \quad 3.2.7$$

As the variation of  $\phi^m$  is quadratic in the element, the variation of the velocity will be linear within the element. The velocity components are given by equation 2.1.20.

$$v_r^m = - \frac{\partial \phi^m}{\partial r} = - \frac{\partial \phi^m}{\partial \xi_i} \frac{\partial \xi_i}{\partial r}$$

$$i=(1,2,3)$$

$$v_z^m = - \frac{\partial \phi^m}{\partial z} = - \frac{\partial \phi^m}{\partial \xi_i} \frac{\partial \xi_i}{\partial z}$$

Differentiation of equations 3.2.3 and 3.2.7 yields

$$v_r^m = - \phi_i^m \hat{T}_i$$

3.2.8

$$v_z^m = - \phi_i^m T_i$$

where

$$T_i = \frac{1}{2A^m} \{ (4\xi_1 - 1)b_1; (4\xi_2 - 1)b_2; (4\xi_3 - 1)b_3; 4(\xi_2 b_1 + \xi_1 b_2);$$

$$4(\xi_3 b_2 + \xi_2 b_3); 4(\xi_1 b_3 + \xi_3 b_1) \} \quad 3.2.9$$

and  $\hat{T}_i$  is the same as 3.2.9 with  $a_i$  replacing  $b_i$ . Now the integral equation 2.3.10 can be evaluated for the  $m^{\text{th}}$  element. Substituting 3.2.8 and 3.2.3 into 2.3.10 yields

$$I^m(\phi^m) = \rho\pi \iint_R \left\{ (\phi_i^m T_i)^2 + (\phi_j \hat{T}_j)^2 \right\} r dr dz - 2\rho\pi \int_{\Gamma_2} \phi_i^m \chi_i v^* r ds \quad 3.2.10$$

The boundary conditions will be considered later. To minimize 3.2.10, differentiation with respect to the nodal values  $\phi_i^m$  as discussed in equation 3.1.3 is required.

$$\frac{\partial I^m(\phi^m)}{\partial \phi_i^m} = 2\rho\pi \iint_R \phi_j^m (T_i T_j + \hat{T}_i \hat{T}_j) r dr dz - 2\rho\pi \int_{\Gamma_2} \chi_i v^* r ds \quad 3.2.11$$

This expression gives the contribution of the  $m^{\text{th}}$  element to the overall flow field calculation. The integrals are evaluated in terms of area coordinates and transformations given by equation 3.2.5 are used. In short hand form

$$\frac{\partial I^m(\phi^m)}{\partial \phi_i^m} = SA_{ij}^m \phi_j^m - SLA_i^m \quad 3.2.12$$

where

$$SA_{ij}^m = 2\rho\pi \iint_R (T_i T_j + \hat{T}_i \hat{T}_j) r dr dz \quad 3.2.13$$

$$SLA_i^m = 2\rho\pi \int_{\Gamma_2} \chi_i v^* r ds$$



and  $i = 1$  to 6;  $j = 1$  to 6.

As the integration is carried out in area coordinates, which are the same for each element, the integrations need only be done once. The element matrices  $SA_{ij}^m$  and  $SLA_i^m$  for axisymmetrical elements and  $S_{ij}^m$  and  $SL_i^m$  for two-dimensional elements are listed in Appendix I. Also given is a sample integration.

Now, essentially a bookkeeping operation is required to add up the contributions of each element to form a global set of simultaneous equations. For the minimum by equation 3.1.3

$$\frac{\partial I(\phi)}{\partial \phi_i} = \sum_{m=1}^M \frac{\partial I^m(\phi^m)}{\partial \phi_i^m} = 0 \quad 3.2.14$$

Note that the factor  $2p\pi$  is common to all the terms and may be divided out. The resulting matrix equation is of the form

$$[SA]\{\phi\} - [SLA] = 0 \quad 3.2.15$$

In terms of structural analysis the matrix  $[SA]$  is the stiffness matrix and  $[SLA]$  the load matrix. This set of equations is symmetric, banded and linear and can be solved efficiently by a direct Gaussian elimination technique.

A saving is realized if the bandwidth is minimized. The half-bandwidth is determined by the node numbers of a given element. It is equal to one, plus the difference

between the largest and smallest node numbers in the element. As shown in Figure 3.2 the numbering of the nodes is such that the minimum bandwidth is realized. The half-bandwidth for those elements is seventeen. Because the matrix [SA] is banded and symmetric its size is [NN x NBW] where NN is the number of nodes and NBW is seventeen, the half-bandwidth.

(b) Boundary Conditions

The boundary conditions appear in the matrix [SLA]. Referring to Figure 3.1 they are as follows.

(1) Symmetry Line AB: This is the stagnation streamline and there is no flow normal to this line.

$$v_r = 0; \quad \frac{\partial \phi}{\partial r} = \frac{\partial \phi}{\partial n} = 0; \quad v^* = 0 \quad 3.2.16$$

(2) Impingement Surface BC: There is no flow normal to the solid wall.

$$v_z = 0; \quad \frac{\partial \phi}{\partial z} = \frac{\partial \phi}{\partial n} = 0; \quad v^* = 0 \quad 3.2.17$$

(3) Outlet Section CD: Assume that there is uniform flow at the outlet section. The velocity in the z direction is zero and the velocity in the r direction is assumed constant.

$$v_r = -\frac{\partial\phi}{\partial r} = \frac{\partial\phi}{\partial n} = c_1; \quad v^* = c_1 \quad 3.2.18$$

(4) Free Streamline DE: As this is a streamline there is no flow normal to it.

$$\frac{\partial\phi}{\partial n} = v^* = 0 \quad 3.2.19$$

The other condition of constant velocity on the free streamline is arrived at through an iterative procedure. An initial guess as to the position of the free streamline is made and the potential flow equations are solved. The velocities on the free streamline are then calculated and the position of the free streamline is adjusted to give a better approximation of the free surface which satisfies the constant velocity boundary condition. A more detailed discussion on the adjustment of the free surface is given in the next section.

(5) Nozzle Streamline EF: Again there is no flow normal to a solid wall and

$$v_r = -\frac{\partial\phi}{\partial r} = \frac{\partial\phi}{\partial n} = 0; \quad v^* = 0 \quad 3.2.20$$

(6) Inlet Section FA: Assume uniform flow at the inlet section. The velocity in the r direction is zero and the velocity in the z direction is constant.

$$v_z = - \frac{\partial \phi}{\partial z} = - \frac{\partial \phi}{\partial n} = c_2; \quad v^* = - c_2 \quad 3.2.21$$

The problem as formulated for jet impingement on a flat plate is

$$\nabla^2 \phi = 0 \text{ in } R$$

3.2.22

$$\frac{\partial \phi}{\partial n} = v^* \text{ on } \Gamma_2$$

Equations 3.2.22 constitute a Neumann boundary value problem which has a unique solution to within an arbitrary constant. To give a totally unique solution a value of the velocity potential  $\phi$  be specified at a point. Consider the boundary condition at the inlet section FA.

$$v_z = - \frac{\partial \phi}{\partial z} = c_2 \quad 3.2.23$$

$$v_r = - \frac{\partial \phi}{\partial r} = 0 \quad 3.2.24$$

Integrate 3.2.23 to get

$$\phi = - c_2 z + F(r)$$

where  $F(r)$  is some function of  $r$ . From 3.2.24,  $F(r)$  can only be a constant at most on the inlet section. At the

inlet section  $z$  is also a constant. Therefore an alternative boundary condition for uniform flow at the inlet is

$$\phi = c_3 \text{ on FA} \quad 3.2.25$$

As this is a Dirichlet boundary condition the inlet section of the boundary  $\Gamma$  becomes  $\Gamma_1$ . The only non-zero part of  $\Gamma_2$  is the outlet section CD. The constant  $c_3$  is arbitrary and may be set equal to zero.

#### (c) Finding the Free Surface

The position of the free surface is not known a priori and must be found as part of the solution. If gravity effects are neglected the condition of constant velocity is satisfied when the position of the free surface is found. An iterative technique, following that in [16] is used. An initial guess is made for the position of the free surface. The potential flow finite element equations are solved and the velocity at the nodes on the free surface determined. The velocity is compared with the velocity calculated for the node at the lip of the nozzle  $v_E$ . The lip of the nozzle is point E in Figure 3.1. The velocity on the streamline should be constant and equal to  $v_E$ . If the velocity calculated at a node on the free surface is larger than  $v_E$ , the node is moved in a direction normal to the streamline so as to decrease the velocity on the next iteration. If the calculated velocity is smaller than  $v_E$

then the node is moved in a direction so as to increase the velocity on the next iteration. Four cases of node movement are shown in Figure 3.4. In each case the node N is moved to the position N'. The movement is based on general continuity requirements. The distance moved normal to the streamlines is given by

$$\Delta n = \pm \lambda \left( \left( \frac{v_N}{v_E} \right)^2 - 1 \right) \quad 3.2.26$$

where  $\lambda$  is a parameter similar to a relaxation parameter. The square of the ratio of the calculated nodal velocity  $v_N$ , to the velocity at the lip of the nozzle  $v_E$  is used to accentuate the velocity difference.

This velocity comparison and subsequent movement of the free surface node is done for all nodes on the free surface. Once a new position of free surface is found, the finite element solution procedure is repeated, the velocity on the free surface again found and the velocities compared to  $v_E$ . The iteration is stopped when the calculated velocity agrees with the actual velocity to within a certain percentage. Usually the agreement limit was set between one and two percent.

As pointed out by Sarpkaya and Hiriart [16] convergence to the proper solution can be ensured with an appropriate choice of the parameter  $\lambda$ . They suggest a value of 0.015. This value was used and convergence always occurred.

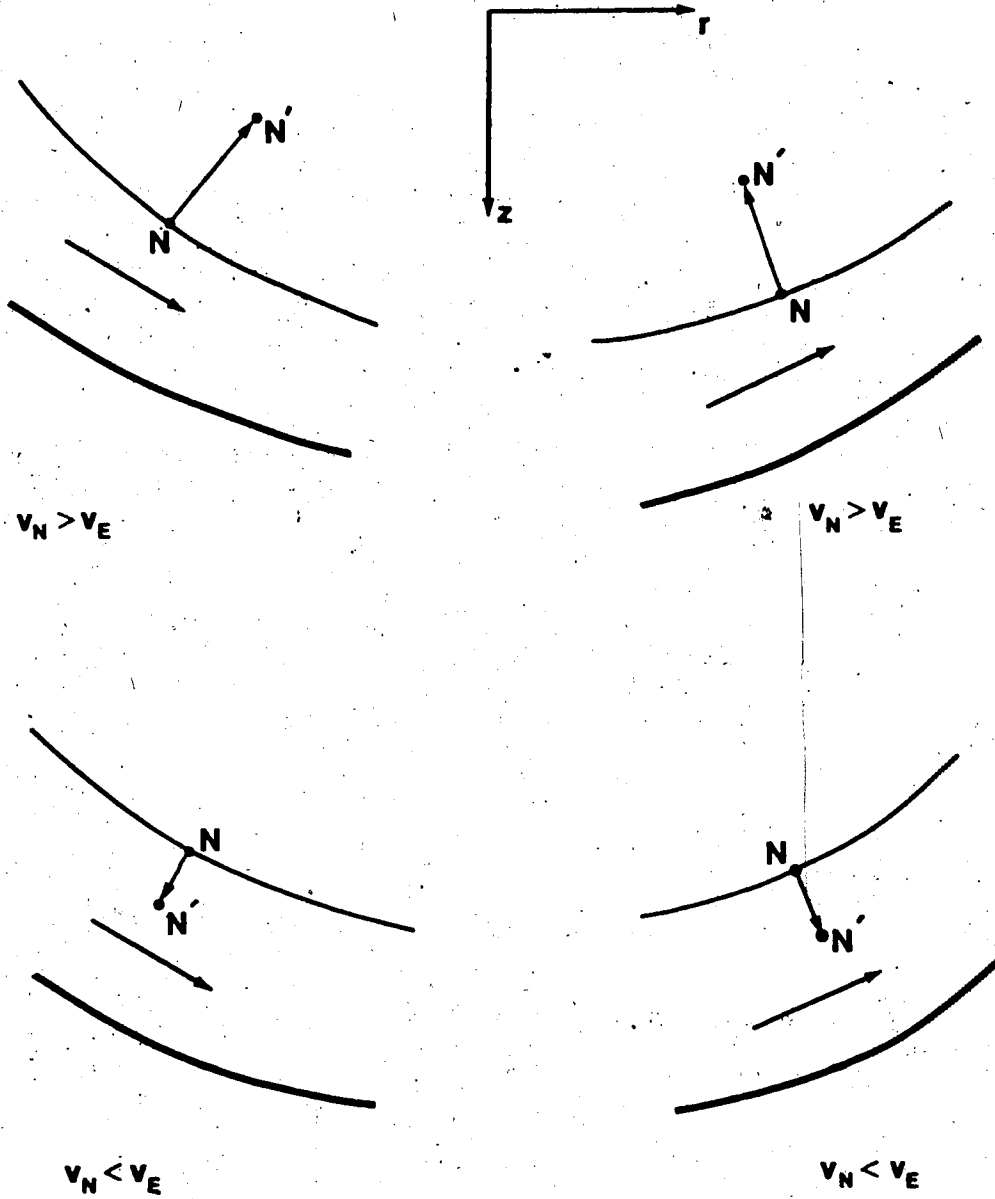


Figure 3.4 Movement of a node on the free surface.

The most important information derived from the potential flow analysis is the distribution of velocity along the solid wall, segment BC in Figure 3.1. This distribution is directly related to the pressure gradient in the boundary layer which grows from the stagnation point. The velocity distribution is required before the solution of the boundary layer may be considered.



## CHAPTER IV

### BOUNDARY LAYER SOLUTION

#### 4.1 Governing Equations

Consider the laminar boundary layer growing from a stagnation point of an incompressible warm water jet impinging on an ice surface. A schematic of the flow is shown in Figure 4.1. Because the position of the ice-water interface is not fixed but dependent on time and the rate of heat transfer, the problem is an unsteady one. This complication is removed by considering a coordinate system which moves with the melting ice front. The problem is now assumed to be a quasi-steady state problem.

Neglecting viscous dissipation and assuming that the radius of curvature  $R'$  of the ice surface is sufficiently large such that the condition  $\frac{\delta'_u}{R'} \ll 1$  is satisfied, [18] the boundary layer equations for two-dimensional flow ( $n = 0$ ) and axisymmetrical flow ( $n = 1$ ) of a constant property fluid are

CONTINUITY:

$$\frac{\partial(r^{n'} u')}{\partial x'} + \frac{\partial(r^{n'} v')}{\partial y'} = 0 \quad 4.1.1$$

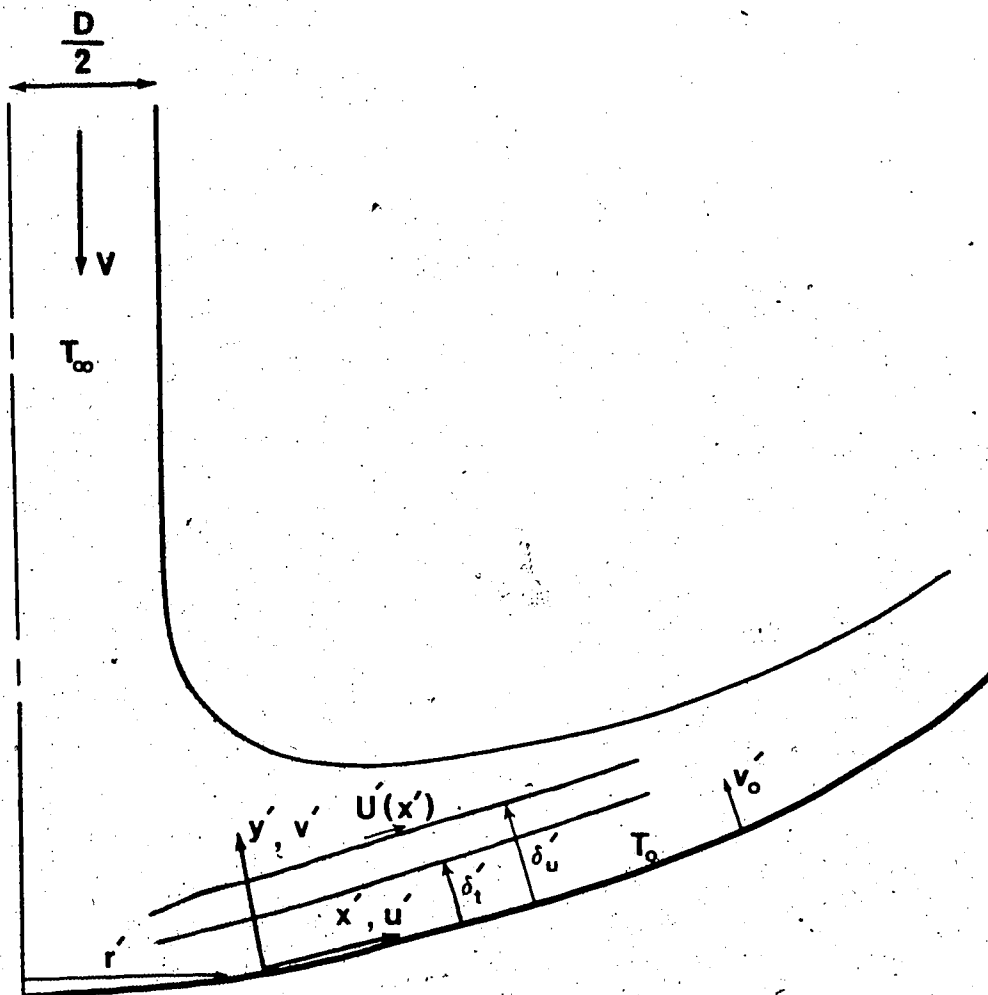


Figure 4.1 Boundary layer on an ice surface

## MOMENTUM:

$$u' \frac{\partial u'}{\partial x'} + v' \frac{\partial u'}{\partial y'} = U' \frac{dU'}{dx'} + \nu \frac{\partial^2 u'}{\partial y'^2} \quad 4.1.2$$

## ENERGY:

$$u' \frac{\partial T'}{\partial x'} + v' \frac{\partial T'}{\partial y'} = \alpha \frac{\partial^2 T'}{\partial y'^2} \quad 4.1.3$$

The boundary conditions are

at  $y' = 0$  flow conditions  $u' = 0; v' = v_0'$

thermal conditions  $T = T_0$  4.1.4

at  $y' = \delta_u'$  flow conditions  $\frac{\partial u'}{\partial y'} = 0; \frac{\partial^2 u'}{\partial y'^2} = 0; u' = U(x')$

at  $y' = \delta_t'$  thermal conditions  $\frac{\partial T'}{\partial y'} = 0; \frac{\partial^2 T'}{\partial y'^2} = 0; T = T_\infty$

Another boundary condition is realized at the melting surface. Assuming that the ice is at a constant temperature, the melting temperature  $0^\circ\text{C}$ , an energy balance at the melting interface results in

$$\rho L v_0' = k \left. \frac{\partial T'}{\partial y'} \right|_{y'=0} \quad 4.1.5$$

where  $v_0'$  is the injection velocity due to the melting ice.

The following non-dimensional variables are introduced:

$$\begin{aligned}
 u &= \frac{u'}{V}; & v &= \frac{v'}{V}; & U &= \frac{U'}{V}; & v_0 &= \frac{v_0'}{V} \sqrt{Re_D} \\
 x &= \frac{x'}{D}; & r &= \frac{r'}{D}; & y &= \frac{y'}{D} \sqrt{Re_D}; & \delta_u &= \frac{\delta_u'}{D} \sqrt{Re_D}; \\
 \delta_t &= \frac{\delta_t'}{D} \sqrt{Re_D}; & \theta &= \frac{T - T_0}{T_\infty - T_0}; & Re_D &= \frac{VD}{\nu}
 \end{aligned} \tag{4.1.6}$$

where  $V$  is the velocity of the impinging jet and  $D$  is either the jet diameter or slot width depending if the flow is axisymmetrical or two-dimensional. With these substitutions the boundary layer equations become

#### CONTINUITY

$$\frac{\partial(r^n u)}{\partial x} + \frac{\partial(r^n v)}{\partial y} = 0 \tag{4.1.7}$$

#### MOMENTUM

$$u \frac{\partial u}{\partial x} + v \frac{\partial u}{\partial y} = U \frac{dU}{dx} + \frac{\partial^2 u}{\partial y^2} \tag{4.1.8}$$

#### ENERGY

$$u \frac{\partial \theta}{\partial x} + v \frac{\partial \theta}{\partial y} = \frac{1}{Pr} \frac{\partial^2 \theta}{\partial y^2} \tag{4.1.9}$$

and the boundary conditions become

$$\text{at } y = 0; \quad u = 0; \quad v = v_0$$

$$\theta = 0$$

$$\text{at } y = \delta_u; \quad \frac{\partial u}{\partial y} = 0; \quad \frac{\partial^2 u}{\partial y^2} = 0 \quad u = U(x) \quad 4.1.10$$

$$\text{at } y = \delta_t; \quad \frac{\partial \theta}{\partial y} = 0; \quad \frac{\partial^2 \theta}{\partial y^2} = 0 \quad \theta = 1$$

The energy balance at the interface, 4.1.5, becomes

$$v_0 = \frac{\text{Ste}}{\text{Pr}} \left. \frac{\partial \theta}{\partial y} \right|_{y=0} \quad 4.1.11$$

where Ste is the Stefan number defined by

$$\text{Ste} = c_p \left( \frac{T_\infty - T_0}{L} \right) \quad 4.1.12$$

The Stefan number gives the ratio of specific heat of the water to the latent heat for the melting phenomena. It is always positive ( $T_\infty > T_0$ ) for melting. As the temperature range for the water jet is  $0^\circ\text{C}$  to  $100^\circ\text{C}$  the Stefan number is limited to the range  $0 \leq \text{Ste} \leq 1.25$ .

The method of solution of equations 4.1.7, 4.1.8 and

4.1.9 with boundary conditions 4.1.10 and 4.1.11 is the Karman-Pohlhausen integral method [17,18]. A fourth order polynomial is assumed for both the velocity and temperature profiles in the boundary layer.

#### 4.2 Integration of the Boundary Layer Equations

The boundary layer equations are going to be integrated with respect to  $y$  from  $y = 0$  to  $y = \delta$ .

##### CONTINUITY

$$\int_0^{\delta} \frac{\partial}{\partial x} (r^n u) dy + \int_0^{\delta} \frac{\partial}{\partial y} (r^n v) dy = 0$$

Performing the integration and applying the limits

$$\frac{1}{r^n} \int_0^{\delta} \frac{\partial}{\partial x} (r^n u) dy \quad 4.2.1$$

Both  $\delta = \delta_u$  and  $\delta = \delta_t$  will be considered when using the integrated form of the continuity equation 4.2.1.

##### MOMENTUM

Here, integrate equation 4.1.8 from  $y = 0$  to  $y = \delta_u$ .

$$\int_0^{\delta_u} u \left( u \frac{\partial u}{\partial x} + v \frac{\partial u}{\partial y} \right) dy = \int_0^{\delta_u} u U \frac{dU}{dx} dy + \int_0^{\delta_u} u \frac{\partial^2 u}{\partial y^2} dy \quad 4.2.2$$

First integral. Note that

$$u \frac{\partial u}{\partial x} + v \frac{\partial u}{\partial y} = \frac{\partial(u^2)}{\partial x} + \frac{\partial(uv)}{\partial y} + \frac{u^2}{r^n} \frac{dr^n}{dx} = \frac{1}{r^n} \frac{\partial}{\partial x} (r^n u^2) + \frac{\partial(uv)}{\partial y}$$

using the continuity equation 4.1.7. The term  $\frac{u^2}{r^n} \frac{dr^n}{dx}$  vanishes for the two-dimensional case ( $n = 0$ ). The first integral then becomes

$$\int_0^{\delta} u \frac{1}{r^n} \frac{\partial}{\partial x} (r^n u^2) dy + \int_0^{\delta} u \frac{\partial(uv)}{\partial y} dy = - \frac{U^2}{r^n} \frac{d}{dx} (r^n \delta_2) + U \frac{dU}{dx} \int_0^{\delta} u \left( 2 \frac{u^2}{U^2} - \frac{u}{U} \right) dy + Uv_0$$

where boundary conditions 4.1.10 were used and  $\delta_2$  is the momentum thickness defined by

$$\delta_2 = \int_0^{\delta} u \frac{u}{U} \left( 1 - \frac{u}{U} \right) dy \quad 4.2.3$$

The third integral of equation 4.2.2 evaluates to

$$\int_0^{\delta} u \frac{\partial^2 u}{\partial y^2} dy = - \left. \frac{\partial u}{\partial y} \right|_{y=0}$$

using boundary conditions 4.1.10. Combine the second integral of 4.2.2 with the left hand side and multiply by -1 and the momentum equation becomes

$$\frac{U^2}{r^n} \frac{d}{dx} \left( r^n \delta_2 \right) + U \frac{dU}{dx} \int_0^{\delta_2} \left( 1 + \frac{u}{U} - 2 \frac{u^2}{U^2} \right) dy = \frac{\partial u}{\partial y} \Big|_{y=0} + Uv_0$$

note that

$$1 + \frac{u}{U} - 2 \frac{u^2}{U^2} = 1 - \frac{u}{U} + 2 \frac{u}{U} \left( 1 - \frac{u}{U} \right)$$

so

$$\begin{aligned} \int_0^{\delta_2} \left( 1 + \frac{u}{U} - 2 \frac{u^2}{U^2} \right) dy &= \int_0^{\delta_2} \left( 1 - \frac{u}{U} \right) dy + 2 \int_0^{\delta_2} \frac{u}{U} \left( 1 - \frac{u}{U} \right) dy \\ &= \delta_1 + 2\delta_2 \end{aligned}$$

where  $\delta_1$  is the displacement thickness defined by

$$\delta_1 = \int_0^{\delta_2} \left( 1 - \frac{u}{U} \right) dy \quad 4.2.4$$

The final form of the integrated momentum equation is arrived at by dividing by  $U$  and using equation 4.1.11 for  $v_0$  to obtain



$$\frac{U}{r^n} \frac{d}{dx} (r^n \delta_2) + \delta_2 \frac{dU}{dx} \left(2 + \frac{\delta_1}{\delta_2}\right) = \frac{1}{U} \frac{\partial u}{\partial y} \Big|_{y=0} + \frac{Ste}{Pr} \frac{\partial \theta}{\partial y} \Big|_{y=0} \quad 4.2.5$$

## ENERGY

The energy equation is integrated from  $y = 0$  to  $y = \delta_t$ .

$$\int_0^{\delta_t} \left( u \frac{\partial \theta}{\partial x} + v \frac{\partial \theta}{\partial y} \right) dy = \frac{1}{Pr} \int_0^{\delta_t} u \frac{\partial^2 \theta}{\partial y^2} dy$$

Using the continuity equation 4.1.7 and boundary conditions 4.1.10 the left hand side integrates to

$$-\frac{U}{r^n} \frac{d}{dx} (r^n \delta_3) - \delta_3 \frac{dU}{dx} + v_0$$

where  $\delta_3$  is an energy thickness defined by

$$\delta_3 = \int_0^{\delta_t} \frac{u}{U} (1 - \theta) dy \quad 4.2.6$$

The right hand side becomes

$$\frac{1}{Pr} \int_0^{\delta_t} \frac{\partial^2 \theta}{\partial y^2} dy = - \frac{1}{Pr} \frac{\partial \theta}{\partial y} \Big|_{y=0}$$

Multiplying by -1 and substituting for  $v_0$  from equation 4.1.11, the integrated energy equation is

$$\frac{U}{r^n} \frac{d}{dx} (r^n \delta_3) + \delta_3 \frac{dU}{dx} = \left( \frac{1 + Ste}{Pr} \right) \frac{\partial \theta}{\partial y} \Big|_{y=0} \quad 4.2.7$$

The effect of melting is seen to appear in both equations 4.2.5 and 4.2.7 with the presence of the Stefan number. If the Stefan number is zero these equations reduce to those given in [17,18] as the integrated boundary layer equations of an incompressible fluid in the presence of a pressure gradient for either axisymmetric or two-dimensional flow.

#### 4.3 Velocity and Temperature Distributions

A fourth order polynomial is chosen to represent the velocity and temperature distributions in the boundary layer.

##### (a) Velocity Profile

Assume the form of the velocity profile as

$$u = U(a_0 + a_1 \eta_1 + a_2 \eta_1^2 + a_3 \eta_1^3 + a_4 \eta_1^4) \quad 4.3.1$$

where

$$\eta_1 = \frac{y}{\delta_u} \quad 4.3.2$$

The constants  $a_0$  to  $a_4$  are evaluated using boundary conditions 4.1.10 and evaluating the momentum equation 4.1.8 at  $y = 0$ .

$$\text{at } y = 0; \quad \eta_1 = 0 \quad u = 0$$

$$\text{so } a_0 = 0$$

4.3.3(a)

$$\text{at } y = \delta_u; \quad \eta_1 = 1; \quad \frac{\partial u}{\partial y} = 0$$

$$\text{so } a_1 + 2a_2 + 3a_3 + 4a_4 = 0$$

4.3.3(b)

$$\text{at } y = \delta_u; \quad \eta_1 = 1; \quad \frac{\partial^2 u}{\partial y^2} = 0$$

$$\text{so } a_2 + 3a_3 + 6a_4 = 0$$

4.3.3(c)

$$\text{at } y = \delta_u; \quad \eta_1 = 1; \quad u = U$$

$$\text{so } a_1 + a_2 + a_3 + a_4 = 1$$

4.3.3(d)

$$\text{at } y = 0; \quad \eta_1 = 0; \quad v_0 \frac{\partial u}{\partial y} \Big|_{y=0} = U \frac{dU}{dx} + \frac{\partial^2 u}{\partial y^2} \Big|_{y=0}$$

$$\text{so } 6\lambda_0' a_1 - 2a_2 = \Lambda$$

4.3.3(e)

where

$$\lambda_0' = \frac{v_0 \delta_u}{6}$$

4.3.4

and

$$\Lambda = \delta \frac{2}{u} \frac{dU}{dx} \quad 4.3.5$$

The five conditions 4.3.3(a) to (e) are sufficient to evaluate the five unknown constants  $a_0$  to  $a_4$ . The system of equations may be represented in matrix form as

$$\begin{bmatrix} 1 & 0 & 0 & 0 & 0 \\ 0 & 1 & 2 & 3 & 4 \\ 0 & 0 & 1 & 3 & 6 \\ 0 & 1 & 1 & 1 & 1 \\ 0 & 6\lambda'_0 & -2 & 0 & 0 \end{bmatrix} \begin{bmatrix} a_0 \\ a_1 \\ a_2 \\ a_3 \\ a_4 \end{bmatrix} = \begin{bmatrix} 0 \\ 0 \\ 0 \\ 1 \\ \Lambda \end{bmatrix} \quad 4.3.6$$

The solution of 4.3.6 results in

$$a_0 = 0; \quad a_1 = \frac{2 + \frac{\Lambda}{6}}{1 + \lambda'_0}; \quad a_2 = \frac{6\lambda'_0 - \frac{\Lambda}{2}}{1 + \lambda'_0}$$

$$a_3 = -\frac{2 + 8\lambda'_0 - \frac{\Lambda}{2}}{1 + \lambda'_0}; \quad a_4 = \frac{1 + 3\lambda'_0 - \frac{\Lambda}{6}}{1 + \lambda'_0}$$

and the velocity profile is given by

$$\frac{u}{U} = \frac{1}{1 + \lambda'_0} \{ F(\eta_1) + \frac{\Lambda}{6} G(\eta_1) + \lambda'_0 H(\eta_1) \} \quad 4.3.7$$

where

$$F(\eta_1) = 2\eta_1 - 2\eta_1^3 + \eta_1^4$$

$$G(\eta_1) = \eta_1 - 3\eta_1^2 + 3\eta_1^3 - \eta_1^4 \quad 4.3.8$$

$$H(\eta_1) = 6\eta_1^2 - 8\eta_1^3 + 3\eta_1^4$$

The functions  $F$ ,  $G$ , and  $H$  are shown in Figure 4.2. Velocity profiles for a range of  $\Lambda$ , the pressure gradient parameter, with  $\lambda'_0 = 0$  are shown in Figure 4.3 and the profiles for a range of  $\lambda'_0$  when  $\Lambda = 6$  are shown in Figure 4.4. The effect of melting on the velocity profile is very small as indicated by Figure 4.4. The parameter  $\lambda'_0$  is a melting parameter and is related to the Stefan number.

For the case of no melting,  $\lambda'_0 = 0$  these profiles are only valid in the range,  $-12 \leq \Lambda \leq +12$  [17,18]. The lower limit is the point of separation in this theory and the upper limit corresponds to the case when the velocity profiles pop [18], that is  $\frac{u}{U} > 1$  for a value of  $\eta_1$  between 0 and 1. The condition,  $\frac{u}{U} > 1$  is physically unrealistic for steady isothermal flow. When melting is present this condition is modified slightly to  $-12 \leq \Lambda \leq 12(1 + 2\lambda'_0)$ . Also, for the case of no melting the velocity profile reduces to the one presented in [17] in his discussion of the Karman-Pohlhausen integral method. The case of melting on a flat

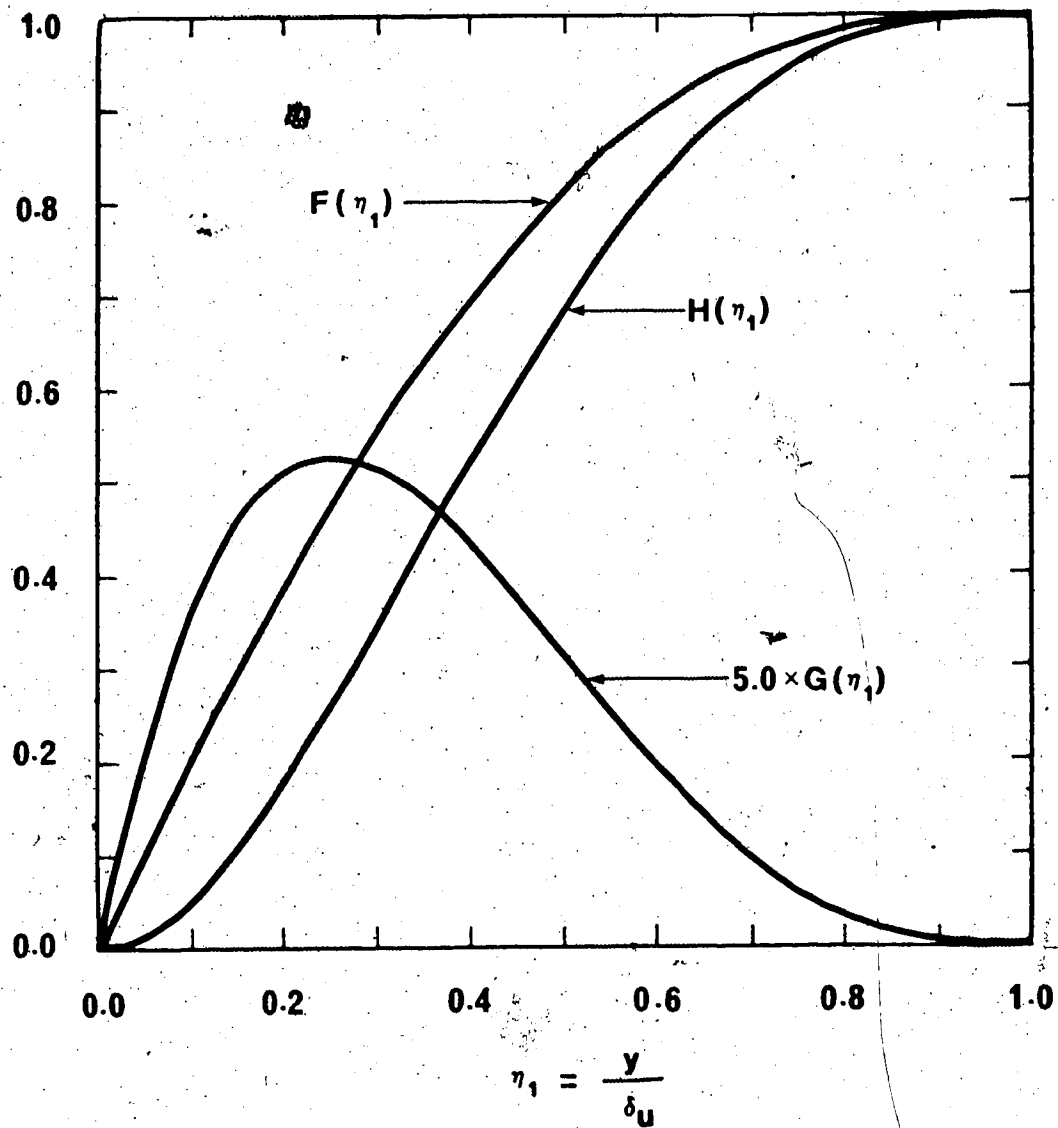


Figure 4.2 Velocity and temperature profile functions

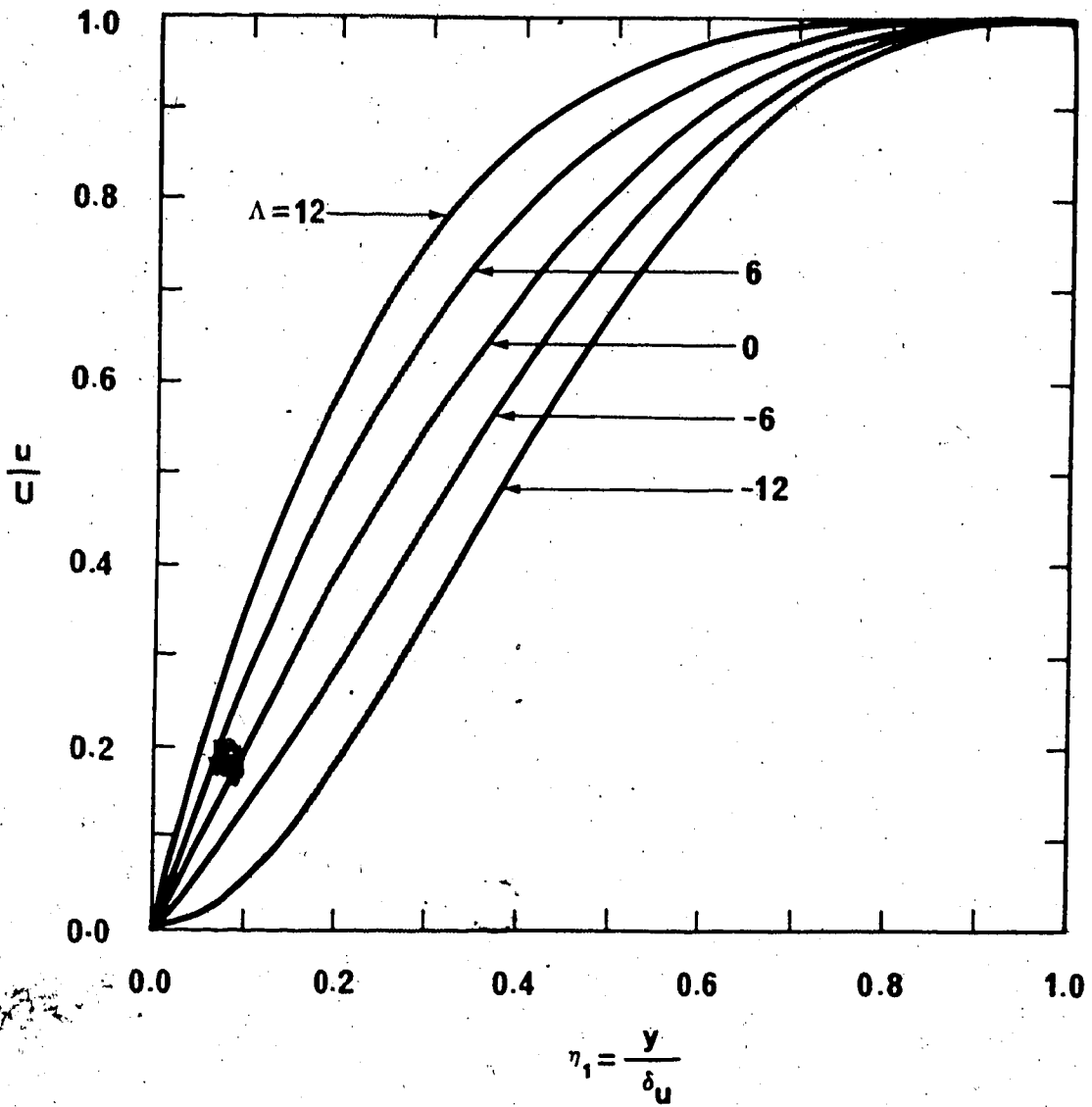


Figure 4.3 Velocity profiles , Ste. = 0 , effect of pressure gradient

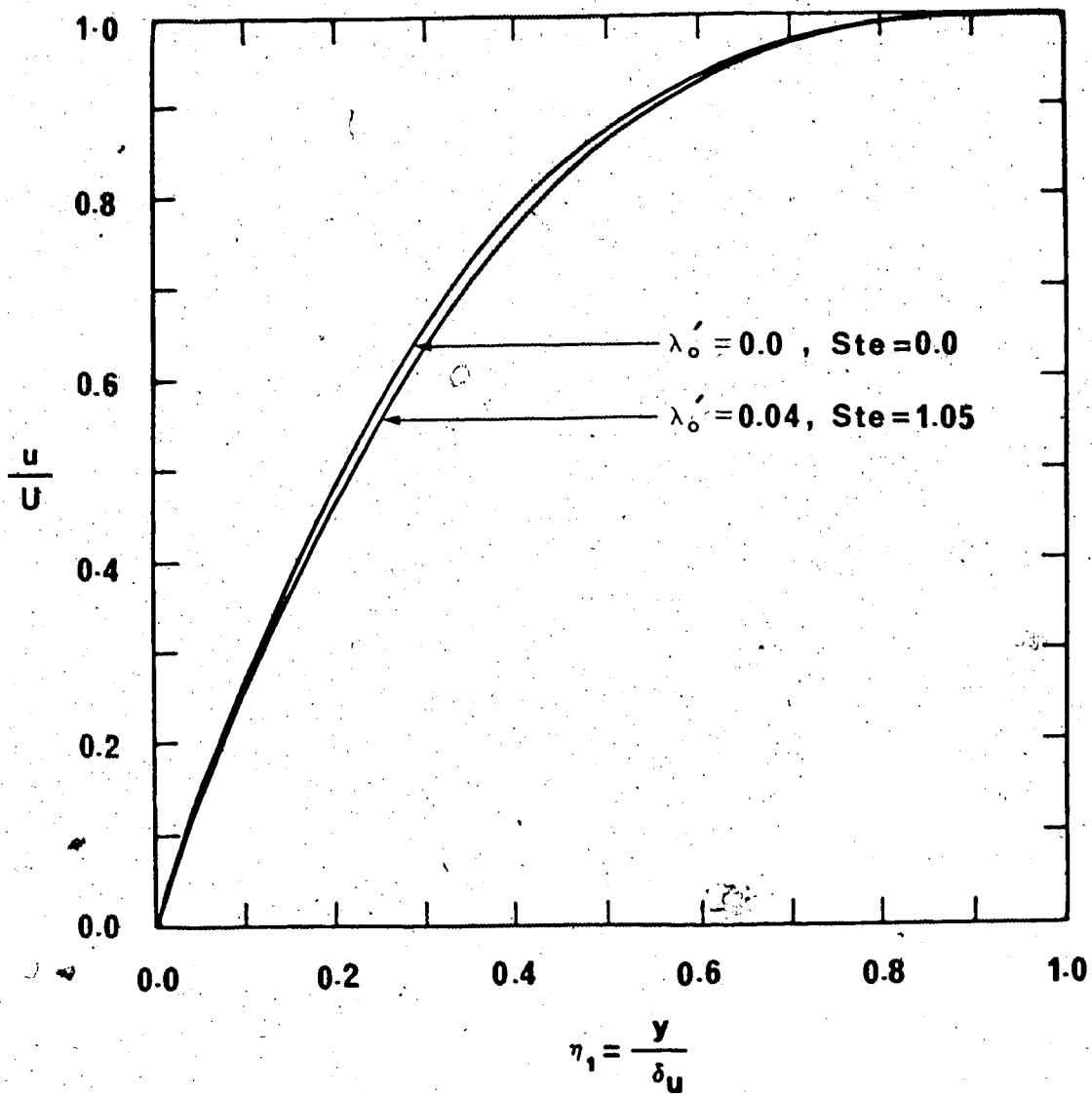


Figure 4.4 Velocity profiles ,  $\Lambda = 6$  , effect of melting .



plate was studied by Pozvonkov, Shurgalskii and Akselrod [19]. The above profile reduces to their profile when  $\Lambda = 0$ , that is for the case of zero pressure gradient.

(b). Temperature Profile

A fourth order polynomial is also chosen to represent the temperature profile. Assume

$$\theta = b_0 + b_1\eta + b_2\eta^2 + b_3\eta^3 + b_4\eta^4 \quad 4.3.9$$

where

$$\eta = \frac{y}{\delta_t} \quad 4.3.10$$

To evaluate the constants, boundary conditions 4.1.10 and the energy equation 4.1.9 evaluated at  $y = 0$  are used

$$\text{at } y = 0; \quad \eta = 0; \quad \theta = 0$$

$$\text{so } b_0 = 0 \quad 4.3.11(a)$$

$$\text{at } y = \delta_t; \quad \eta = 1; \quad \frac{\partial \theta}{\partial y} = 0$$

$$\text{so } b_1 + 2b_2 + 3b_3 + 4b_4 = 0 \quad 4.3.11(b)$$

$$\text{at } y = \delta_t; \quad \eta = 1; \quad \frac{\partial^2 \theta}{\partial y^2} = 0$$

$$\text{so } b_2 + 3b_3 + 6b_4 = 0 \quad 4.3.11(c)$$

$$\text{at } y = \delta_t; \quad \eta = 1; \quad \theta = 1$$

$$\text{so } b_1 + b_2 + b_3 + b_4 = 1 \quad 4.3.11(d)$$

$$\text{at } y = 0; \quad \eta = 0; \quad v_0 \frac{\partial \theta}{\partial y} \Big|_{y=0} = \frac{1}{Pr} \frac{\partial^2 \theta}{\partial y^2} \Big|_{y=0}$$

$$\text{so } 6\lambda_0 Pr b_1 - 2b_2 = 0 \quad 4.3.11(e)$$

where

$$\lambda_0 = \frac{v_0 \delta_t}{6} \quad 4.3.12$$

This system of equations may be represented in matrix form as

$$\begin{bmatrix} 1 & 0 & 0 & 0 & 0 \\ 0 & 1 & 2 & 3 & 4 \\ 0 & 0 & 1 & 3 & 6 \\ 0 & 1 & 1 & 1 & 1 \\ 0 & 6\lambda_0 Pr & -2 & 0 & 0 \end{bmatrix} \begin{bmatrix} b_0 \\ b_1 \\ b_2 \\ b_3 \\ b_4 \end{bmatrix} = \begin{bmatrix} 0 \\ 0 \\ 0 \\ 1 \\ 0 \end{bmatrix} \quad 4.3.13$$

Comparison of the system 4.3.13 with the system 4.3.6 reveals that replacing  $\eta_1$  by  $\eta$ ,  $\lambda_0'$  by  $\lambda_0 \text{Pr}$  and setting  $\Lambda = 0$  makes the two systems identical. Therefore the temperature profile is given by

$$\theta = \frac{1}{1 + \lambda_0 \text{Pr}} \{F(\eta) + \lambda_0 \text{Pr} H(\eta)\} \quad 4.3.14$$

where the functions  $F$  and  $H$  are those given by equation 4.3.8. Figure 4.5 shows the temperature profiles for various Stefan numbers. The parameters  $\lambda_0$  and  $\lambda_0'$  are melting parameters related to the Stefan number. From equation 4.1.11 for the melting velocity, evaluating the derivative from equation 4.3.14 and using equation 4.3.12 one obtains

$$\frac{6\lambda_0}{\delta_t} = \frac{\text{Ste}}{\text{Pr}} \frac{2}{\delta_t (1 + \text{Pr}\lambda_0)}$$

or

$$\text{Ste} = 3\lambda_0 \text{Pr} (1 + \lambda_0 \text{Pr}) \quad 4.3.15$$

and solving for  $\lambda_0 \text{Pr}$

$$\lambda_0 \text{Pr} = \left(0.25 + \frac{\text{Ste}}{3.0}\right)^{1/2} - 0.5 \quad 4.3.16$$

The relationship between  $\lambda_0$  and  $\lambda_0'$  is found from equations

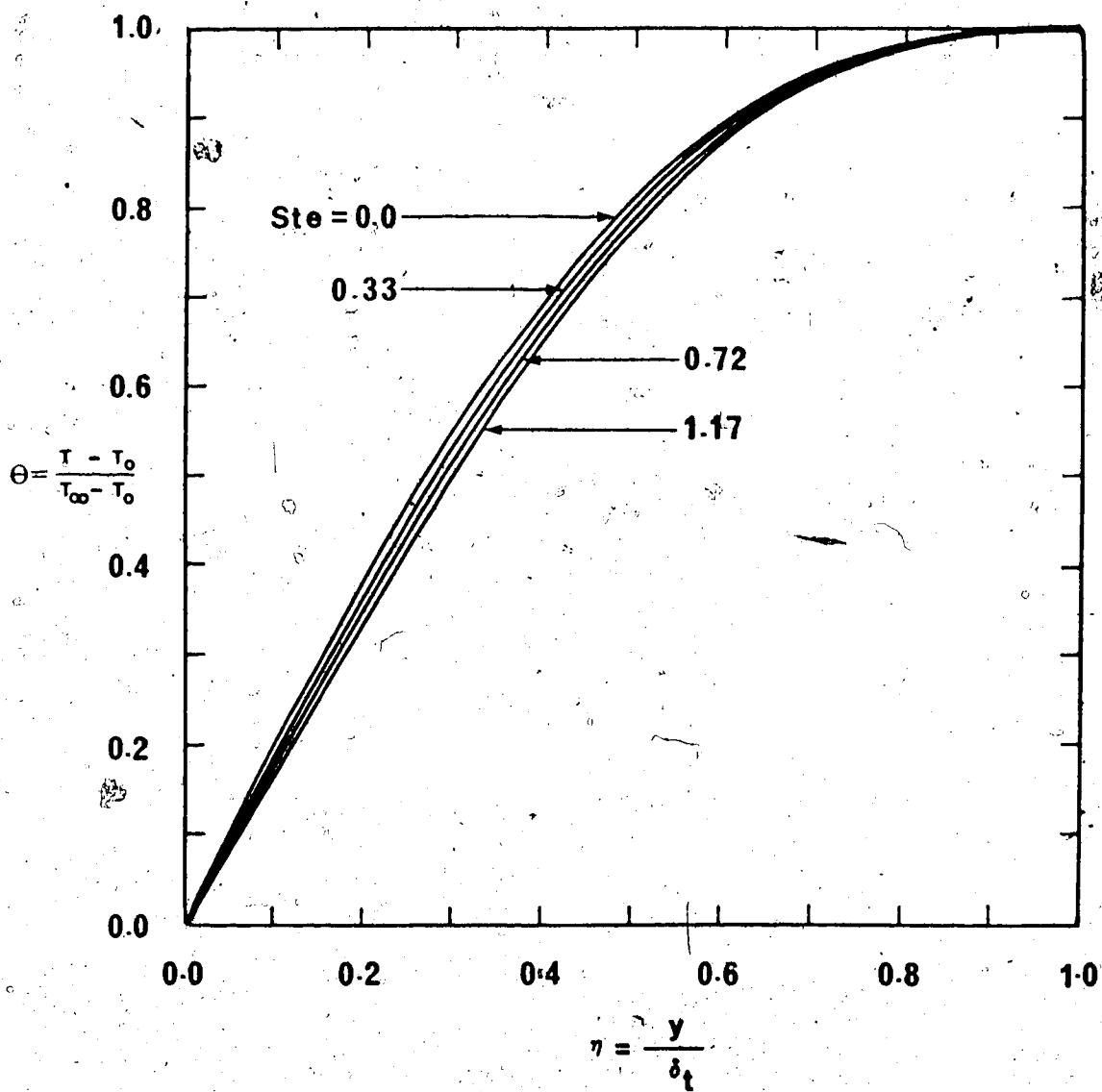


Figure 4.5 Temperature profiles, effect of melting.

4.3.4 and 4.3.10

$$\lambda_0 = \frac{\delta_t}{\delta_u} \lambda_0' = m \lambda_0' \quad 4.3.17$$

where

$$m = \frac{\delta_t}{\delta_u} \quad 4.3.18$$

is the ratio of boundary layer thicknesses.

With the velocity and temperature profiles 4.3.7 and 4.3.14 the thickness parameters defined by equations 4.2.4, 4.2.3 and 4.2.6 may be evaluated. As  $\delta_u$  and  $\delta_t$  are not known only the ratio's  $\frac{\delta_1}{\delta_u}$ ,  $\frac{\delta_2}{\delta_u}$ , and  $\frac{\delta_3}{\delta_t}$  may be found. Define

$$\Delta_1 = \frac{\delta_1}{\delta_u} = \int_0^1 (1 - \frac{u}{U}) d\eta_1$$

$$\Delta_2 = \frac{\delta_2}{\delta_u} = \int_0^1 (1 - \frac{u}{U}) \frac{u}{U} d\eta_1 \quad 4.3.19$$

$$\Delta_3 = \frac{\delta_3}{\delta_t} = \int_0^1 \frac{u}{U} (1 - \theta) d\eta$$

Using the velocity and temperature profiles these integrals result in

$$\Delta_1 = \frac{1}{1 + \lambda'_0} \left\{ \frac{3}{10} - \frac{\Lambda}{120} + \frac{2\lambda'_0}{5} \right\} \quad 4.3.20$$

$$\Delta_2 = \frac{1}{63(1 + \lambda'_0)^2} \left\{ \frac{3}{15} - \frac{\Lambda^2}{144} + \frac{\Lambda\lambda'_0}{10} + \frac{156}{10} \lambda'_0 + \frac{3}{5} \right\} \quad 4.3.21$$

For the case of no melting,  $\lambda'_0 = 0$ , these expressions reduce to those reported in Schlichting [17]. To evaluate  $\Delta_3$  a relationship between  $\eta$  and  $\eta_1$  must be established. The relationship is

$$\eta_1 = m\eta \quad 4.3.22$$

from equations 4.3.2 and 4.3.10 where  $m$  is the boundary layer thickness ratio in equation 4.3.18. The integral  $\Delta_3$  can now be evaluated as

$$\Delta_3 = \frac{1}{(1 + \lambda'_0)(1 + \lambda_0 \text{Pr})} \{ C_1(m) + \Lambda C_2(m) + \lambda'_0 C_3(m) + \lambda_0 \text{Pr} C_4(m) + \lambda_0 \text{Pr} \Lambda C_5(m) + \lambda_0 \text{Pr} \lambda'_0 C_6(m) \} \quad 4.3.23$$

where

$$C_1(m) = \frac{2m}{15} - \frac{3m^3}{140} + \frac{m^4}{180}$$

$$C_2(m) = \frac{m}{90} - \frac{m^2}{84} + \frac{9}{1680} m^3 - \frac{65}{216} m^4$$

$$C_3(m) = \frac{m^2}{14} - \frac{3m^3}{35} + \frac{m^4}{60}$$

4.3.24

$$C_4(m) = \frac{m}{5} - \frac{m^3}{14} + \frac{m^4}{105}$$

$$C_5(m) = \frac{m}{60} - \frac{2}{105} m^2 + \frac{m^3}{112} - \frac{m^4}{630}$$

$$C_6(m) = \frac{8}{35} m^2 - \frac{m^3}{7} + \frac{m^4}{35}$$

This value of  $\Delta_3$  reduces to the one reported by Schlichting [17] for a case of no melting,  $\lambda_0 = \lambda'_0 = 0$ , on a flat plate,  $\Lambda = 0$ , for a Prandtl number greater than one. When the Prandtl number is greater than one the ratio of the boundary layer thicknesses is less than one.

#### 4.4 Solution of the Integral Equations

The solution procedure described below is that outlined in Schlichting [17] extended to solve both the momentum and energy equations. First, the solution procedure for the momentum equation will be described.

From the velocity profile 4.3.7 and the temperature profile 4.3.14, the velocity gradient and temperature gradient at the wall can be evaluated

$$\left. \frac{\partial u}{\partial y} \right|_{y=0} = \frac{U}{\delta_u} \left( \frac{2 + \frac{\Lambda}{6}}{1 + \lambda'_0} \right) \quad 4.4.1$$

$$\left. \frac{\partial \theta}{\partial y} \right|_{y=0} = \frac{2}{\delta_t (1 + \text{Pr} \lambda'_0)} \quad 4.4.2$$

Substituting those expressions into the momentum integral equation 4.2.5 and noting that  $\frac{\delta_1}{\delta_2} = \frac{\Delta_1}{\Delta_2}$  results in

$$\frac{U}{r^n} \frac{d(r^n \delta_2)}{dx} + \delta_2 \frac{dU}{dx} \left( 2 + \frac{\Delta_1}{\Delta_2} \right) = \frac{U}{\delta_u} \frac{(2 + \frac{\Lambda}{6})}{(1 + \lambda'_0)} + \frac{\text{Ste}}{\text{Pr} \delta_t} \frac{2}{(1 + \text{Pr} \lambda'_0)}$$

Multiplying by  $\delta_u$  and noting  $\Delta_2 = \frac{\delta_2}{\delta_u}$

$$\frac{U}{2\Delta_2 r^n} \frac{d}{dx} (r^n \delta_2^2) + \frac{\delta_2^2}{\Delta_2} \frac{dU}{dx} \left( 2 + \frac{\Delta_1}{\Delta_2} \right) = \frac{2 + \frac{\Lambda}{6}}{1 + \lambda'_0} + \frac{\text{Ste}}{\text{Pr} \delta_t} \frac{2}{(1 + \text{Pr} \lambda'_0)}$$

Introduce the substitutions

$$z = \delta_2^2 \quad 4.4.3$$



$$k = \delta_2^2 \frac{dU}{dx} = z \frac{dU}{dx} \quad 4.4.4$$

The function  $k$  is a known function as

$$k = \frac{\delta_2^2}{\delta_u^2} \delta_u^2 \frac{dU}{dx} = \Delta_2^2 \Lambda \quad 4.4.5$$

from equations 4.2.3 and 4.3.5. Multiply the momentum equation by  $\Delta_2$  and expand the derivative to get

$$\frac{dz}{dx} = \frac{z}{U} \left\{ \Delta_2 \left( \frac{2 + \frac{\Lambda}{6}}{1 + \lambda_0} + \frac{2St\epsilon}{Prm(1 + Pr\lambda_0)} \right) - k \left( 2 + \frac{\Delta_1}{\Delta_2} \right) - \frac{U}{\frac{dU}{dx}} \frac{dr^n}{r^n} k \right\} \quad 4.4.6$$

The last term in ( ) disappears for the two-dimensional case. An alternative form for this last term is

$$\frac{U}{\frac{dU}{dx}} \frac{dr^n}{r^n} k = \frac{Uz}{r^n} \frac{dr^n}{dx} \quad 4.4.7$$

by equation 4.4.4. To eliminate the derivative,  $\frac{dr^n}{dx}$ , a simple transformation is used. Let

$$z^* = z(r^n)^2 \quad 4.4.8$$

and the momentum equation 4.4.6 becomes

$$\frac{dz^*}{dx} = \frac{2(r^n)^2}{U} \left\{ \Delta_2 \left( \frac{2 + \frac{\lambda}{\delta}}{1 + \lambda_0'} + 6\lambda_0' \right) - k \left( 2 + \frac{\Delta_1}{\Delta_2} \right) \right\} \quad 4.4.9$$

using equation 4.3.15 for the Stefan number and equation 4.3.17. Note that for the two-dimensional case  $n = 0$ ,  $z = z^*$  and equations 4.4.6 and 4.4.9 are identical.

As the integral energy equation 4.2.7 is very similar in form to the integral momentum equation 4.2.5 the same procedure is used to obtain an equation similar to equation 4.4.6. The transformed energy equation is

$$\frac{dW}{dx} = \frac{2}{U} \left\{ \Delta_3 \left( \frac{(1 + Ste)}{Pr} \cdot \frac{2}{(1 + Pr\lambda_0')} \right) - \tilde{L} - \frac{U}{dx} \frac{dr^n}{dx} \frac{\tilde{L}}{r^n} \right\} \quad 4.4.10$$

where

$$W = \delta_3^2 \quad 4.4.11$$

$$\tilde{L} = \delta_3^2 \frac{du}{dx} = W \frac{dU}{dx} \quad 4.4.12$$

Again to remove the derivative of  $(r^n)$ , the transformation

similar to the one used for the momentum equation is introduced. Let

$$W^* = W(r^n)^2 \quad 4.4.13$$

and using equation 4.3.15 for the Stefan number the integral energy equation becomes

$$\frac{dW^*}{dx} = \frac{2(r^n)^2}{\Delta_3} \left\{ \frac{2}{Pr(1 + \lambda_0 Pr)} + 6\lambda_0 \right\} - \tilde{L} \quad 4.4.14$$

A Runge-Kutta technique [20] is used to solve equations 4.4.9 and 4.4.14. The right hand side of both equations are functions of the pressure gradient parameter  $\Delta$ , and the boundary layer thickness ratio  $m$  for a given Stefan number, velocity distribution and surface shape. In order to start the integration procedure the initial values of  $\Delta$  and  $m$  must be known at the stagnation point. Equations 4.4.6 and 4.4.10 exhibit a singular behavior at the stagnation point where the velocity  $U$  is zero. As the derivatives,  $\frac{dz}{dx}$  and  $\frac{dW}{dx}$  are finite at the stagnation point, the terms in the brackets  $\{ \}$  on the right hand side of each equation must be zero at the stagnation point. Therefore two stagnation conditions exist and are given by

$$\Delta_2 \left\{ \frac{2 + \frac{\Delta_1}{6}}{1 + \lambda_0} + 6\lambda_0 \right\} - k \left( 2 + \frac{\Delta_1}{\Delta_2} \right) - k \frac{U}{dx} \frac{dr^n}{r^n} = 0 \quad 4.4.15$$

and

$$\Delta_3 \left\{ \frac{2}{Pr(1 + \lambda_0 Pr)} + 6\lambda_0 \right\} - \tilde{L} - \tilde{L} \frac{U}{\frac{dU}{dx}} \frac{\frac{dr^n}{dx}}{r^n} = 0 \quad 4.4.16$$

For the two-dimensional case,  $n = 0$ , the terms involving  $r^n$  and  $\frac{dr^n}{dx}$  vanish. For the axisymmetric case,  $n = 1$ , and this term must be evaluated at the stagnation point,  $x = 0$ .

Assume that

$$\lim_{x \rightarrow 0} \frac{U}{\frac{dU}{dx}} \frac{\frac{dr^n}{dx}}{r^n} = 1 \quad 4.4.17$$

In the region of the stagnation point the velocity may be represented by  $U = \beta x$  where  $\beta$  is a constant. Also  $r \approx x$  near the stagnation point. With these approximations the assumption of equation 4.4.17 is true. The stagnation conditions now become

$$\Delta_2 \left\{ \frac{2 + \frac{\Lambda}{6}}{1 + \lambda_0} + 6\lambda_0 \right\} - k \left( 2 + \frac{\Delta_1}{\Delta_2} \right) - nk = 0$$

and

4.4.18

$$\Delta_3 \left\{ \frac{2}{Pr(1 + \lambda_0 Pr)} + 6\lambda_0 \right\} - \tilde{L} - n\tilde{L} = 0.$$

These two equations are solved simultaneously to find the starting values of the parameters  $\Lambda$  and  $m$ . The values determined depend on the Stefan number and whether the flow is axisymmetrical or two-dimensional. Figure 4.6 shows the variation of  $\Lambda$  and  $m$  with Stefan number for two-dimensional flow. Figure 4.7 shows the same variation for the axisymmetrical case. Schlichting [17] reports the values of  $\Lambda$  at the stagnation point for the case of no melting and they coincide with the values found from the solution of equation 4.4.18.

Once the values of  $\Lambda$  and  $m$  are known at the stagnation point, call them  $\Lambda_0$  and  $m_0$ , a Runge-Kutta integration technique may be used as follows. The first assumption is that the boundary layer thickness ratio  $m_0$  is constant [19]. This assumption was found to be acceptable as the functions involved in the boundary layer equations are only weak functions of  $m$ . The integration of the momentum equation 4.4.9 is carried out step by step in the form

$$z_{p+1}^* = z_p^* + \left( \frac{dz^*}{dx} \Big|_p + \frac{dz^*}{dx} \Big|_{p+1} \right) \frac{(x_{p+1} - x_p)}{2} \quad 4.4.19$$

This is a Runge-Kutta method of order two [20]. To start the iteration values of  $z_0^*$ ,  $\frac{dz^*}{dx} \Big|_0$  and  $\frac{dz^*}{dx} \Big|_1$  must be known. As  $\Lambda_0$  and  $m_0$  are known the value of  $k$  at the stagnation point,  $k_0$ , may be found from equation 4.4.5. Then  $z_0$  is

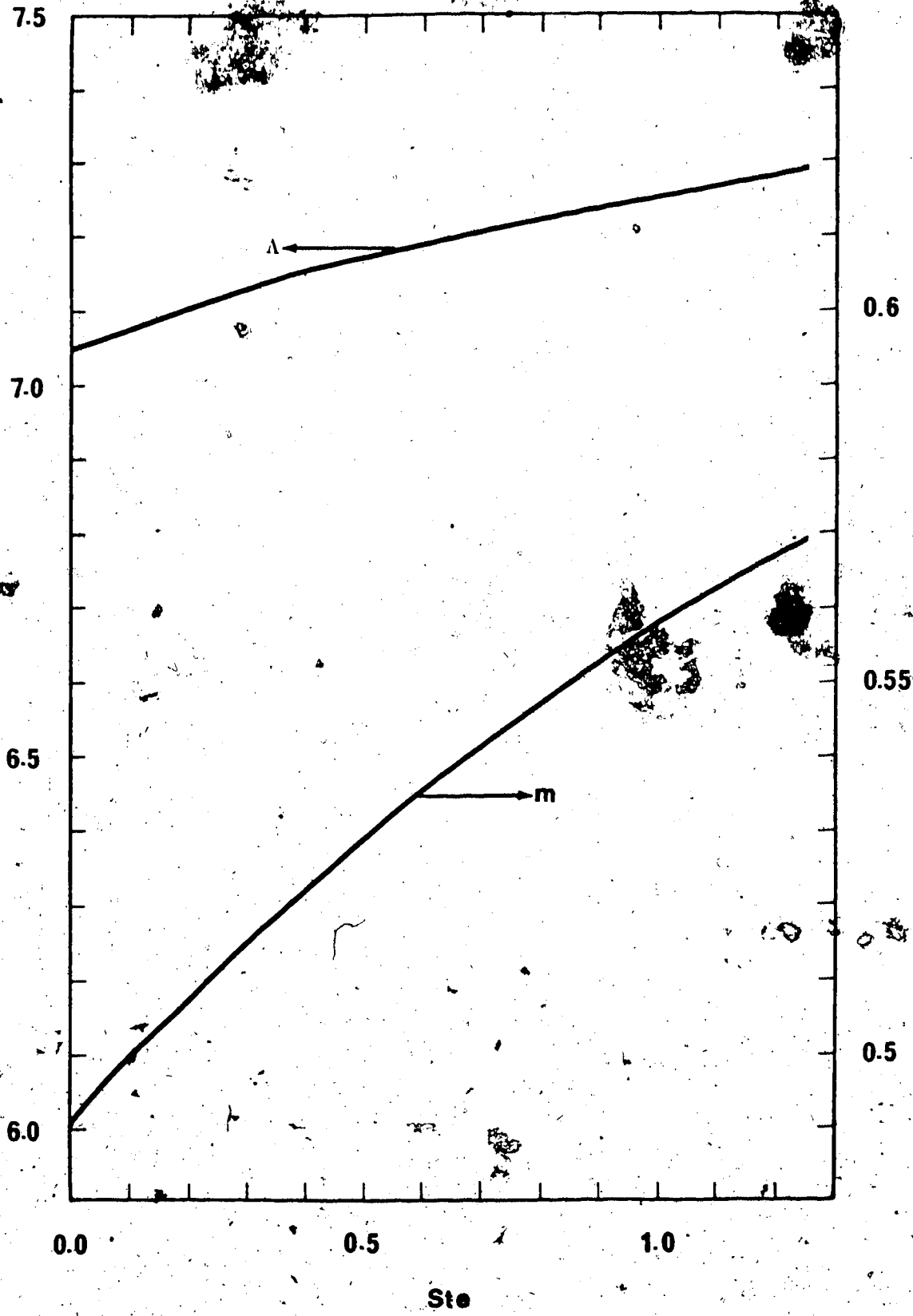


Figure 4.6 Two-dimensional starting values

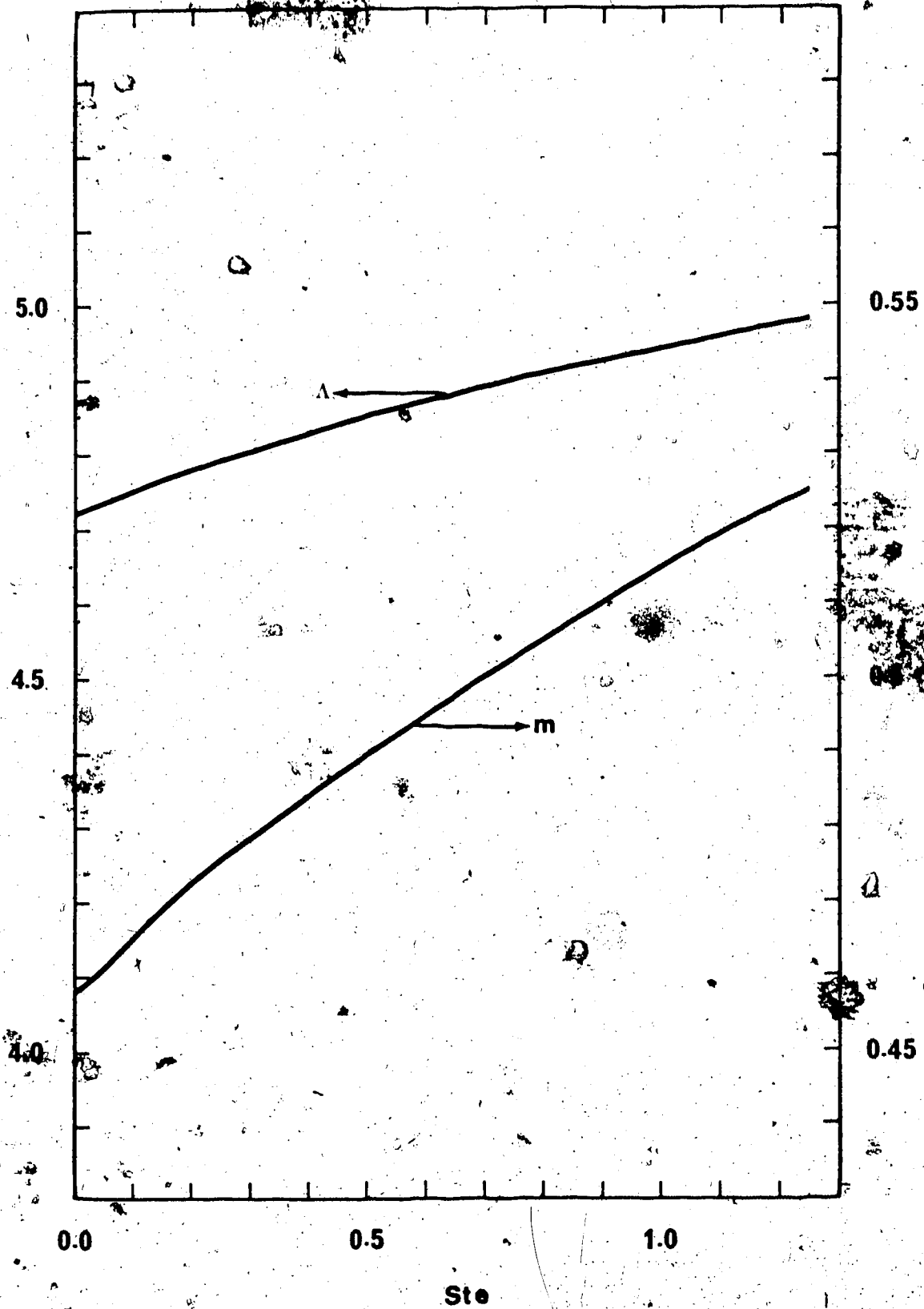


Figure 4.7 Axisymmetric starting values

given by equation 4.4.4 and  $z_0^*$  by 4.4.8. For the axisymmetrical case  $z_0^*$  is zero as  $r^n$  is zero at the stagnation point. In the two-dimensional case  $z_0^* = z_0$ . To evaluate  $\left. \frac{dz^*}{dx} \right|_0$  equation 4.4.8 is differentiated and evaluated at the stagnation point

$$\left. \frac{dz^*}{dx} \right|_0 = \left[ (r^n)^2 \frac{dz}{dx} + 2(r^n) \frac{dr^n}{dx} z \right] \Big|_0$$

For the axisymmetrical case,  $n = 1$ , and value of  $r^n$  at the stagnation point is zero so

$$\left. \frac{dz^*}{dx} \right|_0 = 0 \quad \text{axisymmetric case} \quad 4.4.20$$

For the two-dimensional case  $n = 0$  and

$$\left. \frac{dz^*}{dx} \right|_0 = \left. \frac{dz}{dx} \right|_0$$

The general form of the differential equation for the two-dimensional case is

$$\frac{dz}{dx} = \frac{F(k)}{U} \quad 4.4.21$$

in accordance with equation 4.4.9. The function  $F(k)$  is



not known explicitly but is known implicitly through the pressure gradient parameter  $\Lambda$ . To find  $\frac{dz}{dx}|_0$ , L'Hopital's rule is used because of the singularity at the stagnation point. So

$$\frac{dz}{dx}|_0 = \frac{\frac{dF}{dk} \frac{dk}{dx}|_0}{\frac{dU}{dx}|_0}$$

Using equation 4.4.4 to evaluate  $\frac{dk}{dx}$

$$\frac{dz}{dx}|_0 = \frac{\frac{dF}{dk} \left( \frac{dz}{dx} \frac{dU}{dx} + \frac{k}{\frac{dU}{dx}} \frac{d^2U}{dx^2} \right)|_0}{\frac{dU}{dx}|_0}$$

Solving for  $\frac{dz}{dx}|_0$

$$\frac{dz}{dx}|_0 = \frac{\frac{dF}{dk} k \frac{d^2U}{dx^2}}{\left(1 - \frac{dF}{dk}\right) \left(\frac{dU}{dx}\right)^2}|_0$$

For the stagnation points considered in this study the velocity distributions in the vicinity of the stagnation point are represented by  $U = \beta x$ . Therefore  $\frac{d^2U}{dx^2} = 0$  and

$$\frac{dz}{dx}|_0 = 0 \quad \text{for two-dimensional flows}$$

The linear velocity distribution near the stagnation point is valid for blunt bodies only.

Using  $\Lambda_0$  and  $m_0 \left. \frac{dz^*}{dx} \right|_1$  is calculated with  $r^n|_1$  and  $U|_1$  by equation 4.4.9. Now  $z_1^*$  can be calculated from equation 4.4.19. Using equation 4.4.8,  $z_1$  can be found and from equation 4.4.4  $k_1$  is found. As  $k$  is a universal function of  $\Lambda$  by equation 4.4.5 the equation

$$k(\Lambda) - k_1 = 0 \quad 4.4.23$$

can be solved to give the pressure gradient parameter at the new position 1. Once  $z_1$  has been found all of the relevant parameters, the boundary layer thicknesses can be found using equations 4.4.3 and 4.3.19. With a new value for the pressure gradient parameter the procedure is repeated until the whole boundary layer has been calculated.

A similar technique is used to solve the energy equation and the result is the thermal boundary thickness  $\delta_t$ . The assumption of constant boundary layer thickness ratio is checked as follows. In the Runge-Kutta solutions the primary output variables are  $z$  and  $W$ . These were determined independently of each other. They are related as follows.

$$z = \delta_2^2 = \frac{\delta_2^2}{\delta_u^2} \frac{\delta_u^2}{\delta_t^2} \frac{\delta_t^2}{\delta_3^2} \delta_3^2 = \frac{\Delta_2^2}{m^2 \Delta_3^2} W$$

and solving for m

$$m = \left( \frac{\Delta_2^2}{\Delta_3} \frac{W}{z} \right)^{1/2}$$

4.4.24

This value is then compared with the value found at the stagnation point to check whether the boundary thickness ratio was constant.

Appendix 2 gives a description of a complete solution procedure, potential flow plus boundary layer calculation, and also the computer program used for the calculation.

## CHAPTER V

### TWO-DIMENSIONAL JET IMPINGEMENT ON A FLAT SURFACE

For the case of two-dimensional flow when a free surface forms, an exact solution for the inviscid incompressible jet impinging on a flat surface is available by using the complex variable and conformal mapping techniques given by Michell [21] and Ehrich [22]. Miyazaki and Silberman [23] used the results of [22] for the potential flow field analysis of the impinging two-dimensional jet and then used a finite difference technique to solve for the skin friction and heat transfer in the laminar boundary layer region near the stagnation point. The results of [23] will be used to verify the validity of the finite element potential flow solution of Chapter III and the integral boundary layer solution of Chapter IV. A discussion of the methods of solution of [23] and comparison with the finite element method and integral boundary layer solution follows.

#### 5.1 Exact Solution of the Potential Flow Field

The methods of complex variables and conformal mappings may be used to determine the exact flow field solution of an incompressible, inviscid two-dimensional jet impinging on a flat surface [21,22]. A schematic of the flow

field using the non-dimensionalization of equations 2.1.12 is shown in Figure 5.1. The relevant results for use in a boundary layer analysis are reported in [23] and are repeated here for future reference. They are

$$H = \frac{1}{2} \left\{ 1 - \frac{\sqrt{\gamma}}{\pi} \ln \left( \frac{\sqrt{\gamma} - 1}{\sqrt{\gamma} + 1} \right) \right\} / \left\{ \sqrt{\gamma - 1} + \sqrt{\gamma} \right\} \quad 5.1.1$$

$$U_f = \sqrt{\gamma - 1} + \sqrt{\gamma} \quad 5.1.2$$

$$X = \frac{1}{\pi U_f} \left\{ \sqrt{\gamma - 1} \tan^{-1} \left( \frac{2\sqrt{\gamma - 1} \frac{U_s}{U_f}}{1 + \left(\frac{U_s}{U_f}\right)^2} \right) + \ln \left( \frac{1 + \frac{U_s}{U_f}}{1 - \frac{U_s}{U_f}} \right) \right. \\ \left. + \sqrt{\gamma} \tan^{-1} \left( \frac{2\sqrt{\gamma} \frac{U_s}{U_f}}{1 - \left(\frac{U_s}{U_f}\right)^2} \right) \right\} \quad 5.1.3$$

where  $H$  is the dimensionless nozzle-plate spacing,  $U_s$  is the velocity on the impingement surface or mainstream velocity for the boundary layer,  $U_f$  is the velocity on the free surface and  $\gamma$  is a parameter defined by equation 5.1.2.

For a given nozzle-plate spacing equation 5.1.1 is solved for  $\gamma$  and the velocity on the free streamline evaluated by equation 5.1.2. Equation 5.1.3 then yields the distribution of velocity on the impingement surface. The distributions of the mainstream velocity for  $H = \infty, 3.0, 1.0, 0.5$

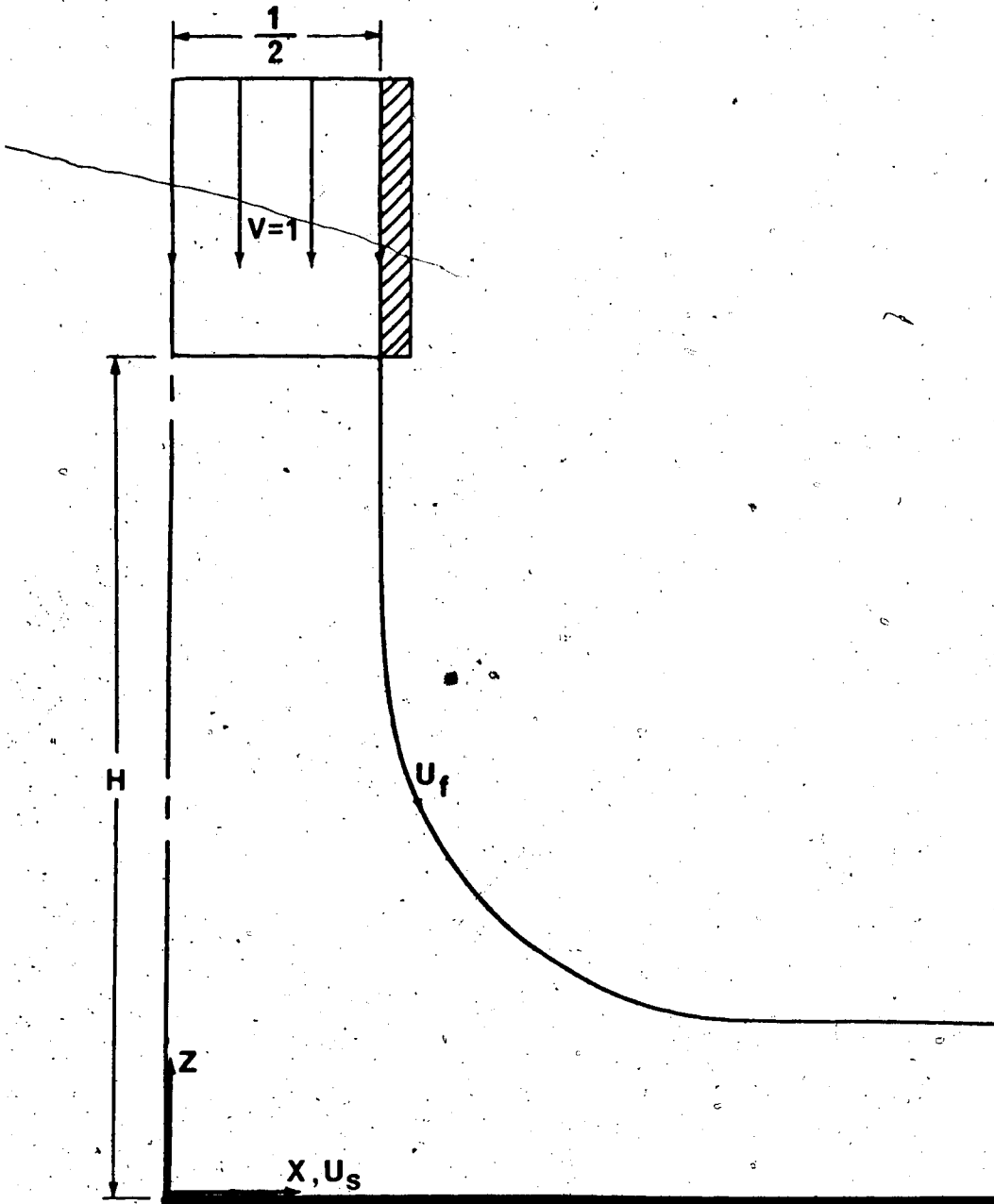


Figure 5.1 Two-dimensional jet impinging on a flat surface

and 0.25 are shown in Figure 5.2. The curves for  $H = \infty$  and  $H = 3.0$  are essentially the same.

The solution for  $H = \infty$  can also be found by considering the normal impact of two equal uniform jets, one originating at  $+\infty$  and the other at  $-\infty$ . The analysis is described in [1] in some detail. When  $H = \infty$  the solution of equation 5.1.1 yields  $\gamma = 1$  and the velocity on the free surface is  $U_f = 1$  by equation 5.1.2. When  $\gamma = 1$ , equation 5.1.3 reduces to the velocity distribution described in [1]. Also given in [1] is an equation specifying the position of the free streamline for  $H = \infty$ . The free surface is described by the equation

$$z = \frac{1}{2} + \frac{1}{\pi} \ln \left\{ \coth \left\{ \frac{\pi}{4} (2x - 1) \right\} \right\} \quad 5.1.4$$

and is shown in Figure 5.3.

As shown in Figure 5.2 the rate of change of mainstream velocity decreases continually with increasing distance from the stagnation point for an infinite nozzle-plate spacing. However, as the nozzle-plate spacing is reduced the velocity rises more rapidly than linear at a point near the lip of the nozzle. This effect may be better seen by differentiating the velocity distribution to obtain the velocity gradient. Explicit differentiation of equation 5.1.3 yields

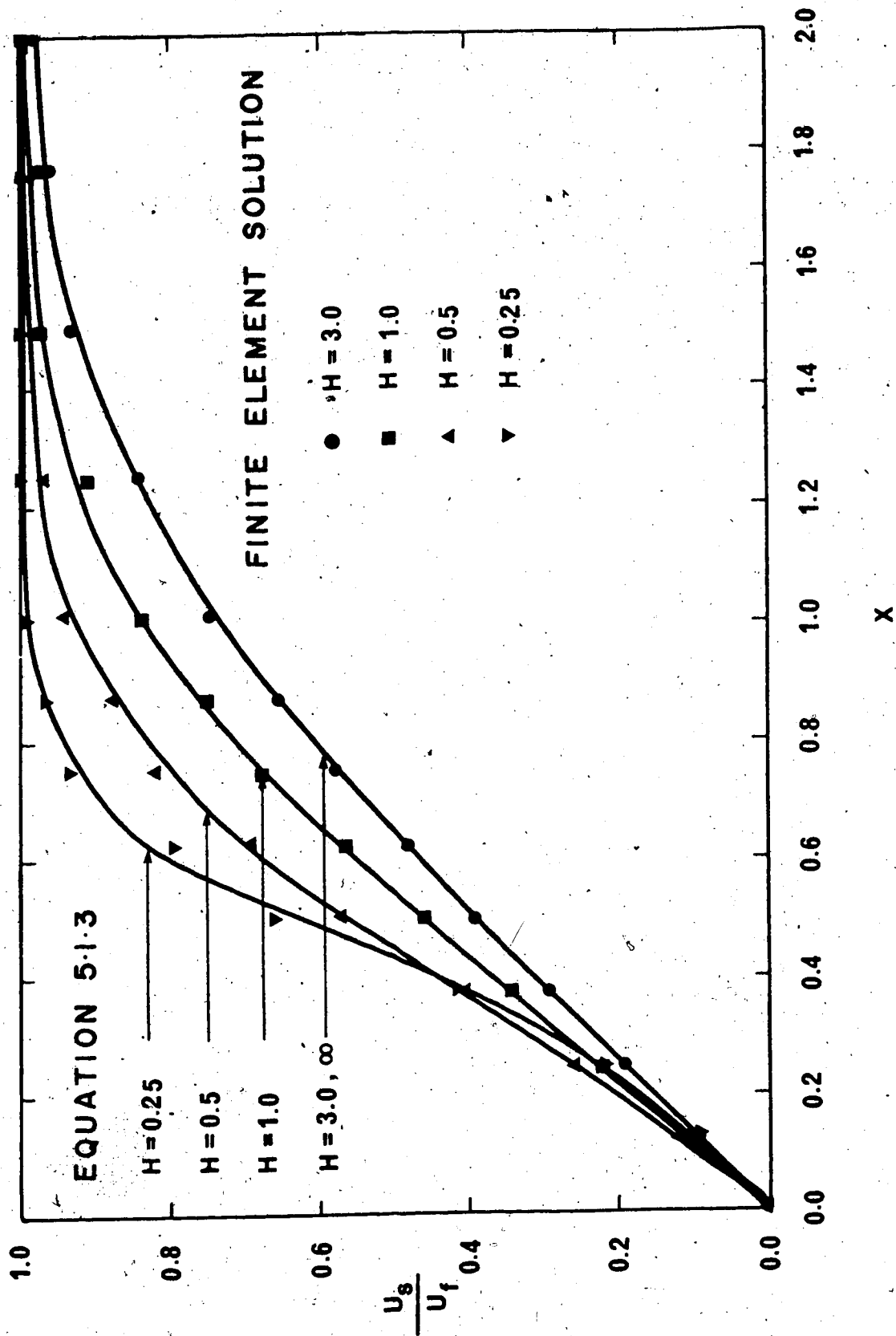


Figure 5.2 Velocity distributions, two-dimensional jet impinging on a flat surface



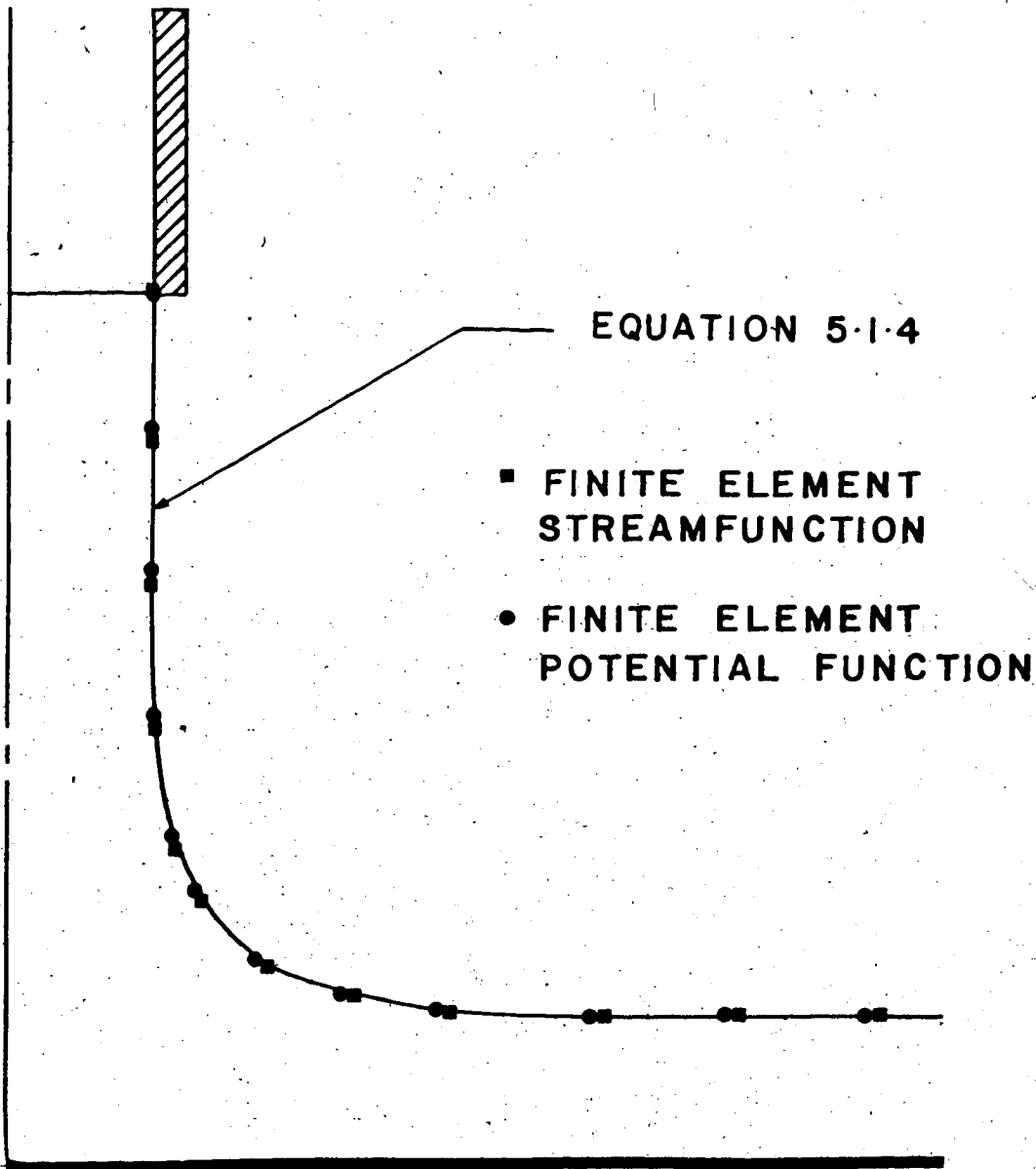


Figure 5.3 Position of the free surface , two-dimensional jet impinging on a flat surface ,  $H \rightarrow \infty$

$$\frac{d\left(\frac{U_s}{U_f}\right)}{dx} = \left[ \frac{1}{\pi U_f} \left\{ \frac{2(\gamma-1)\left(1 - \left(\frac{U_s}{U_f}\right)^2\right)}{\left(1 + \left(\frac{U_s}{U_f}\right)^2\right)^2 + 4(\gamma-1)\left(\frac{U_s}{U_f}\right)^2} + \frac{2}{1 - \left(\frac{U_s}{U_f}\right)^2} + \frac{2\gamma\left(1 + \left(\frac{U_s}{U_f}\right)^2\right)}{\left(1 - \left(\frac{U_s}{U_f}\right)^2\right)^2 + 4\gamma\left(\frac{U_s}{U_f}\right)^2} \right\} \right]^{-1} \quad 5.1.5$$

Figure 5.4 shows the mainstream velocity gradient distribution for nozzle-plate spacings of  $H = \infty, 3.0, 1.0, 0.5$  and  $0.25$ . As  $H$  decreases from infinity a peak in the velocity gradient distribution curve occurs at a distance from the stagnation point equal to the slot half width or at a point near the lip of the nozzle.

The explanation of this phenomena follows the discussion in [23]. When the nozzle is placed far away from the impingement surface the jet is deflected gradually far in advance of the impingement surface. As the nozzle-plate spacing is reduced the velocity at the lip of the nozzle increases, that is  $U_f > 1$ , and by continuity the velocity closer to the stagnation streamline must decrease. Also, the flow must turn more sharply in a region which is continually decreasing in area, as the nozzle-plate spacing is reduced. With decreasing nozzle-plate spacing the streamlines are packed closer together. Because the velocity is defined as the derivative of the stream function, the velo-

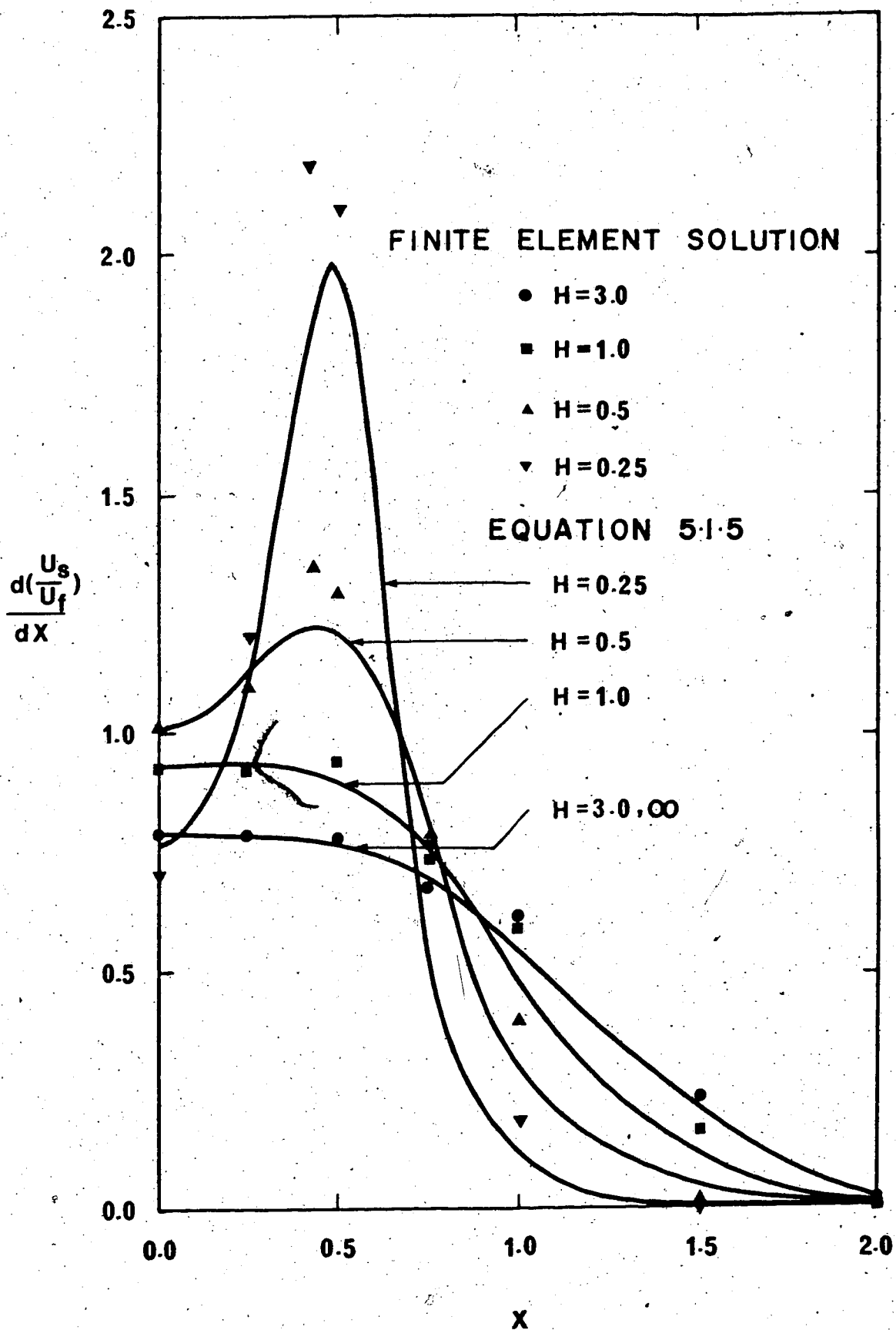


Figure 5.4 Velocity gradient distributions, two-dimensional jet impinging on a flat surface

city will be greater if the streamlines are closer together. Consequently, the mainstream velocity rises faster than the case when  $H = \infty$ .

The finite element program was run for the nozzle-plate spacing of  $H = 3.0, 1.0, 0.5$  and  $0.25$ . The case,  $H = 3.0$  was run with both the potential function formulation and the stream function formulation. All the other cases were run with the potential function formulation only. As shown in Figure 5.2 the finite element program approximates the distribution of mainstream velocity correctly for the various nozzle-plate spacings. The position of the free surface, which is part of the solution, is also found accurately by the finite element method as shown in Figure 5.3. Limits of accuracy depend on the number of nodes chosen for the approximation and the spacings of these nodes. In general, more nodes are required when the velocity is changing rapidly or when the shapes of the boundaries are changing rapidly. For the gradient of velocity, a cubic spline interpolation as described in Appendix 2 is used to numerically differentiate the computed velocity distribution. As with any numerical differentiation, errors become magnified. For the case  $H = 3.0$  the finite element method accurately approximates the gradient of mainstream velocity as shown in Figure 5.4. The velocity varies smoothly and numerical differentiation introduces very little error. But for the case of  $H = 0.25$  the velocity gradient has a sharp peak and to be able to predict accurately the exact

shape of this curve many more nodes than were used for the case of  $H = 3.0$  would be required.

## 5.2 Heat Transfer

Miyazaki and Silberman computed the heat transfer near the stagnation point by a finite difference technique. The resulting heat transfer curves showing the parameter  $Nu_D/\sqrt{Re_D}$  versus distance from the stagnation point for a Prandtl number of ten and nozzle-plate spacings of  $H = \infty$ , 1.5, 1.0 and 0.5 are shown in Figure 5.5. The parameter  $Nu_D/\sqrt{Re_D}$  is related to the temperature gradient at the wall. Forming an energy balance at the interface

$$h(T_\infty - T_0) = k \left. \frac{\partial T}{\partial y'} \right|_{y'=0} \quad 5.2.1$$

and introducing the non-dimensional variables of equation 4.1.6 one obtains

$$\frac{h}{k} = \frac{\sqrt{Re_D}}{D} \left. \frac{\partial \theta}{\partial y} \right|_{y=0}$$

Rearranging and forming a Nusselt number

$$\frac{Nu_D}{\sqrt{Re_D}} = \left. \frac{\partial \theta}{\partial y} \right|_{y=0} \quad 5.2.2$$

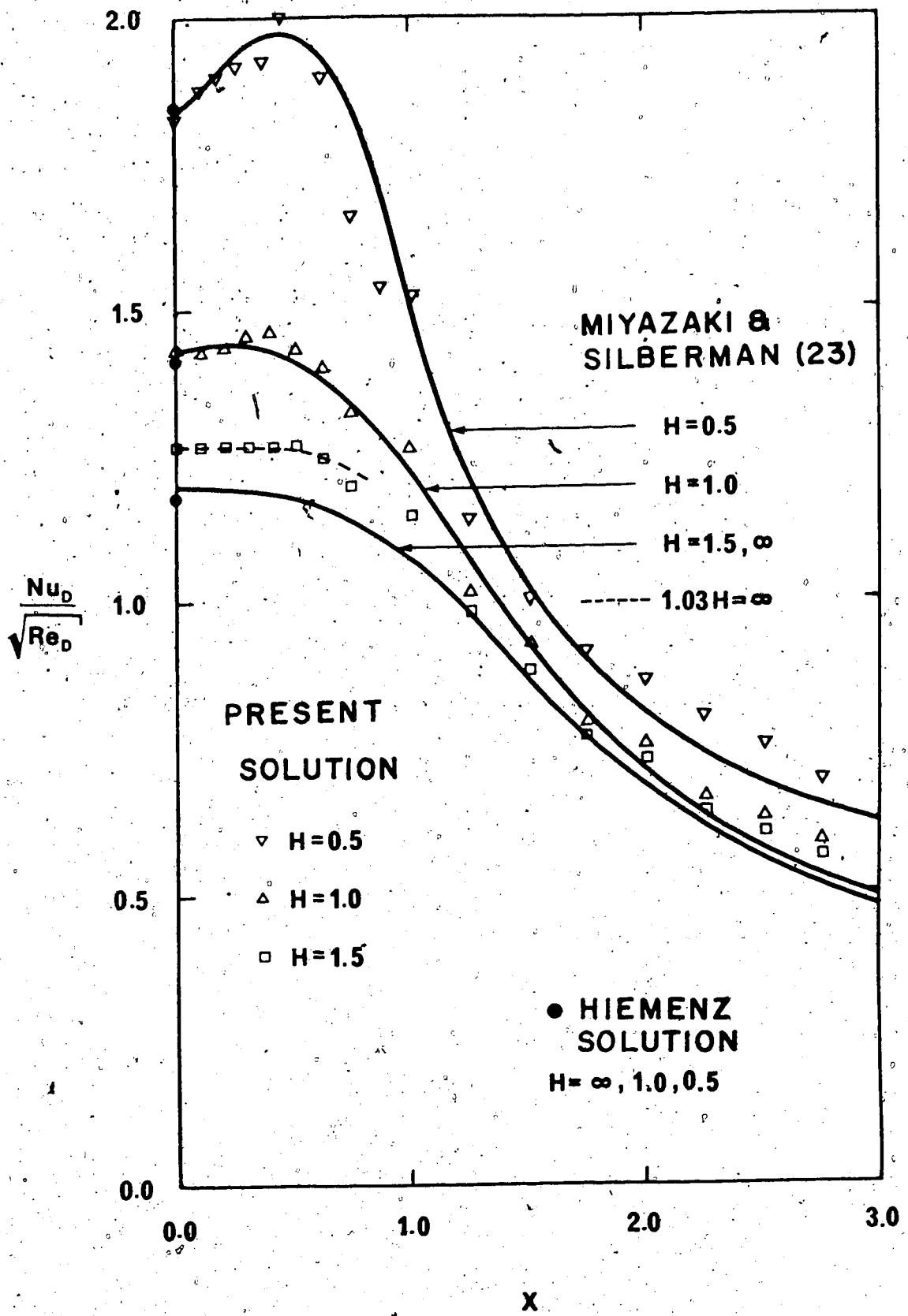


Figure 5.5 Heat transfer near the stagnation point of a two-dimensional jet impinging on a flat surface

As the nozzle-plate spacing is reduced a peak in the heat transfer curve appears near the lip of the nozzle. From the discussion of the gradient of velocity in the last section it would seem that the heat transfer near the stagnation point is directly related to the gradient of the mainstream velocity. To show this relationship the simple case of Hiemenz stagnation point flow discussed in White [18] will be used.

The stagnation point flow of an infinite fluid or Hiemenz flow is one of the few flows having an exact solution of the complete Navier-Stokes equations. The solution is described in [18] and involves a similarity parameter  $\eta$ , defined as

$$\eta = y' \sqrt{\frac{\left(\frac{dU_s'}{dx'}\right)_0}{\nu}} \quad 5.2.3$$

and a non-dimensional form of the stream function  $F(\eta)$  defined by

$$\psi' = \left\{ \left(\frac{dU_s'}{dx'}\right)_0 \nu \right\}^{1/2} x' F(\eta) \quad 5.2.4$$

where  $\left(\frac{dU_s'}{dx'}\right)_0$  is the mainstream velocity gradient at the stagnation point and  $\nu$  is the kinematic viscosity. The mainstream velocity for this stagnation point flow rises

linearly with the distance from the stagnation point or

$$U'_s = \beta x' \quad 5.2.5$$

where the parameter  $\beta$  may be thought of as the velocity gradient at the stagnation point.

$$\left(\frac{dU'_s}{dx'}\right)_0 = \beta \quad 5.2.6$$

Substitution of equations 5.2.3 and 5.2.4 into the Navier-Stokes momentum equation yields an ordinary differential equation for  $F$ .

$$\frac{d^3 F}{d\eta^3} + F \frac{d^2 F}{d\eta^2} - \left(\frac{dF}{d\eta}\right)^2 + 1 = 0 \quad 5.2.7$$

with boundary conditions

$$F(0) = F'(0) = 0; \quad F'(\infty) = 1 \quad 5.2.8$$

The solution of 5.2.7 with boundary conditions 5.2.8 is available in either [17] or [18] in tabular or graphical form.

Now consider the energy equation and a dimensionless temperature defined by



$$\theta(\eta) = \frac{T - T_0}{T_\infty - T_0} \quad 5.2.9$$

where  $T_\infty$  is the ambient fluid temperature and  $T_0$  the surface temperature. The energy equation, neglecting viscous dissipation becomes

$$\frac{d^2\theta}{d\eta^2} + \text{PrF} \frac{d\theta}{d\eta} = 0 \quad 5.2.10$$

using equations 5.2.3, 5.2.4 and 5.2.9. The boundary conditions are

$$\theta(0) = 0; \quad \theta(\infty) = 1 \quad 5.2.11$$

Equation 5.2.10 with boundary conditions 5.2.11 can be directly integrated to give

$$\theta(\eta) = \frac{\int_0^\eta \exp \left\{ - \text{Pr} \int_0^\eta F ds \right\} d\eta}{\int_0^\infty \exp \left\{ - \text{Pr} \int_0^\eta F ds \right\} d\eta} \quad 5.2.12$$

The heat transferred at the wall is then given by

$$\begin{aligned} q_w &= h(T_0 - T_\infty) = -k \left. \frac{\partial T}{\partial y'} \right|_{y'=0} \\ &= -k(T_\infty - T_0) \left\{ \int_0^\infty \exp(-\text{Pr} \int_0^\eta F ds) d\eta \right\}^{-1} \sqrt{\frac{dU'_s}{(dx')_0}} \quad 5.2.13 \end{aligned}$$

Forming a Nusselt number results in

$$\text{Nu}_D = \frac{hD}{k} = D \sqrt{\frac{\left(\frac{dU'_s}{dx'}\right)_0}{\nu}} G(\text{Pr}) \quad 5.2.14$$

where  $G(\text{Pr})$  is given by

$$G(\text{Pr}) = \left\{ \int_0^\infty \exp(-\text{Pr} \int_0^n F ds) dn \right\}^{-1} \quad 5.2.15$$

For Prandtl number equal to ten  $G(\text{Pr})$  is 1.3388 from [18].

Using the non-dimensionalizations of equation 2.1.12, equation 5.2.6 becomes

$$\beta = \left(\frac{dU'_s}{dx'}\right)_0 = \frac{V}{D} \left(\frac{dU'_s}{dx}\right)_0 \quad 5.2.16$$

and evaluating equation 5.1.5 at the stagnation point,

$U_s = 0$ , gives

$$\left(\frac{dU'_s}{dx'}\right)_0 = \frac{\pi U_f^2}{4\gamma} \quad 5.2.17$$

Substituting equations 5.2.16 and 5.2.17 into equation 5.2.14 and using the value of  $G(\text{Pr})$  for a Prandtl number of ten yields

$$Nu_D = \frac{hD}{k} = 1.3388 D \sqrt{\frac{V\pi U_f^2}{4D\gamma v}}$$

and rearranging gives

$$\frac{Nu_D}{\sqrt{Re_D}} = 1.3388 U_f \sqrt{\frac{\pi}{4\gamma}} \quad 5.2.18$$

The solutions of equations 5.1.1, 5.1.2 and 5.2.18 for various nozzle-plate spacings and a Prandtl number of ten are given in Table 1.

Table 1. Exact solutions of a two-dimensional jet impinging on a flat surface.

H	$\gamma$	$U_f$	$Nu_D/\sqrt{Re_D}$
$\infty$	1	1	1.186
3.0	1.00000594	1.000771	1.187
2.0	1.000263	1.016355	1.206
1.5	1.004080	1.065911	1.262
1.0	1.044880	1.234042	1.432
0.5	1.474190	1.902776	1.859
0.25	3.451139	3.423336	2.186

The values of  $Nu_D/\sqrt{Re_D}$  for  $H = \infty, 1.0$  and  $0.5$  given in Table 1 are shown at the stagnation point on Figure 5.5. They correspond to the heat transfer calculated

by the finite difference and integral boundary layer methods at the stagnation point. Therefore, Heimenz flow is valid at the stagnation point for a finite jet. Because the velocity in Heimenz flow is linear by equation 5.2.5, the gradient of velocity will be constant. By equation 5.2.14 this implies a constant Nusselt number and constant heat transfer in the region of the stagnation point. As the Nusselt number varies as the square root of the velocity gradient, by equation 5.2.14, the Nusselt number and heat transfer are not constant for the case of the finite jet. As seen by this analysis the peaks in the gradient of velocity distribution are directly related to the peaks observed in the heat transfer curves.

To compare the integral boundary layer technique of Chapter IV with the finite difference method of [23], the integral boundary layer solution was computed for nozzle-plate spacings of  $H = 1.5, 1.0, 0.5$  and  $0.25$  for the case of no melting and a Prandtl number of ten. The non-dimensional heat transfer  $Nu_D/\sqrt{Re_D}$  is modeled correctly by the integral boundary layer solution for nozzle-plate spacings of  $1.0$  and  $0.5$  as shown in Figure 5.5. The seemingly oscillatory nature of the integral boundary layer solution is due to the inaccuracies in calculating the velocity gradient by cubic spline interpolation.

The discrepancy for the case of  $H = 1.5$  is explained as follows. Miyazaki and Silberman [23] concluded that the velocity distribution curves for  $H = \infty$  and  $H = 1.5$  were

identical. As shown by equation 5.2.14 the Nusselt number varies as the square root of the streamwise velocity gradient at the stagnation point. Evaluating equation 5.2.17 for  $H = \infty$  and  $H = 1.5$  result in

$$\left(\frac{dU_s}{dx}\right)_0^{1/2} = 0.886 \quad \text{for } H = \infty$$

5.2.19

$$\left(\frac{dU_s}{dx}\right)_0^{1/2} = 0.914 \quad \text{for } H = 1.5$$

The curve presented by Miyazaki and Silberman [23] for  $H = \infty, 1.5$  probably used the velocity distribution of equation 5.1.3 for  $H = \infty$ . The finite element solution used a nozzle-plate spacing of  $H = 1.5$ . Therefore the finite element solution should be  $0.914/0.886$  times greater than the solution presented in [23]. This is actually the case as shown in Figure 5.5.

The solution for a nozzle-plate spacing of  $H = 0.25$  was attempted but because of the large velocity gradients present, as shown in Figure 5.4, the boundary layer solution failed. As was pointed out in Chapter IV the range of pressure gradient parameter for which the solution is valid is  $-12 \leq \Lambda \leq 12 (1 + 2\lambda_0')$ . The lower limit corresponds to separation and the upper limit to the case where the velocity profiles pop [18]. When the nozzle-plates spacing is 0.25 the large velocity gradients imply that a large pressure gradient is present.

In both cases, for too small a pressure gradient  $\Lambda < -12$ , and for too large a pressure gradient  $\Lambda > +12$  ( $1 + 2\lambda_0'$ ) the integral boundary layer solution is not valid. The boundary layer equations 4.1.2 and 4.1.3 no longer apply and to solve the problem in the regions  $\Lambda < -12$  or  $\Lambda > 12$  ( $1 + 2\lambda_0'$ ) another method of solution must be considered.

The errors introduced by the finite element method and integral boundary layer solution are caused by many factors. The number of nodes chosen affects the accuracy of the calculated velocities. In general, the more nodes used to approximate the flow field, the greater the accuracy will be but more computer time is required. Therefore there is a trade off between accuracy and computer time used. From comparison of the finite element generated velocity distribution and the exact solution equation 5.1.3 the approximate accuracy for all cases of nozzle-plate spacings is less than  $\pm 5$  percent. The same number of nodes were used in each case. The greatest errors occur when the velocity is changing very rapidly, that is when  $H = 0.25$ . The accuracy of the velocity gradient calculation depends primarily on the accuracy of the cubic spline numerical differentiation procedure. Again comparing the finite element solution to the exact solution of equation 5.1.5 in Figure 5.4 the approximate accuracy is  $\pm 20$  percent. Again, greater accuracy is achieved when the velocity gradient does not change very rapidly, that is for  $H = 3.0$ .

In the calculation of the heat transfer there are

two main sources of error. One is the error introduced by the approximation of integrating the boundary layer equations and using a fourth order polynomial for the velocity and temperature profiles. The other error is introduced by the approximation of the velocity gradient in the cubic spline approximation. With the Nusselt number being proportional to the square root of the velocity gradient and an error in the velocity gradient of  $\pm 20$  percent the maximum error in the Nusselt number is approximately  $\pm 10.6$  percent. Because of the averaging quality of the integral solution an approximate guess to the error in the calculation of the Nusselt number is between 10 and 15 percent.

## CHAPTER VI

### AXISYMMETRIC JET IMPINGEMENT

As mentioned previously there are two distinct cases of jet flows. Both cases apply to axisymmetric and two-dimensional jets. The first occurs when a gaseous jet issues into a gaseous medium or a liquid jet issues into a liquid medium. Here, entrainment of the ambient fluid by the jet greatly affects the velocity profile of the jet. The second case occurs when a liquid jet issues into a gaseous medium. This jet is virtually unaffected by the ambient fluid and a free surface forms between the liquid jet and the surroundings.

The impingement characteristics of these two jet flows are slightly different. The flow regions for the case of the entrained jet are well known. Near the nozzle exit a potential core region exists, surrounded by a mixing region between the jet and the ambient fluid. A few jet widths or diameters downstream the mixing region has spread inwards to engulf the potential core. Beyond this point the mixing continues and the velocity distribution adjusts itself so as to conserve linear momentum. In this region the velocity profiles are self-similar. When the jet impinges on a surface, in the stagnation region, a strong essentially inviscid jet-surface interaction produces a change in flow



direction [24]. Far from the stagnation point a wall jet forms and the velocity profiles are again self-similar. A transition zone exists between each of the above regions.

The flow regions for the case of the free surface jet are slightly different. The velocity profile present at the exit of the nozzle persists until the stagnation region begins to change the kinetic energy of the jet into pressure energy. In the impingement region and resulting flow over the surface Watson [25] recognizes four distinct flow regions. These are shown in Figure 6.1 and are described below.

1. A stagnation region, where the velocity on the surface rises rapidly from zero at the stagnation point to the free streamline velocity at a distance from the stagnation point equal to approximately the nozzle diameter. When  $x' \ll D$  the flow can be described by the stagnation flow of an infinite fluid where the mainstream velocity rises linearly with  $x'$ . This is the Hiemenz stagnation point flow described in [17] or [18].
2. A flat plate region at a greater distance  $x'$  where there is no pressure gradient and the flow is similar to Blasius flow over a flat plate.
3. A transition region where the boundary layer includes the whole flow field and the velocity profile changes from the flat plate profile to the fully-developed similarity profile.

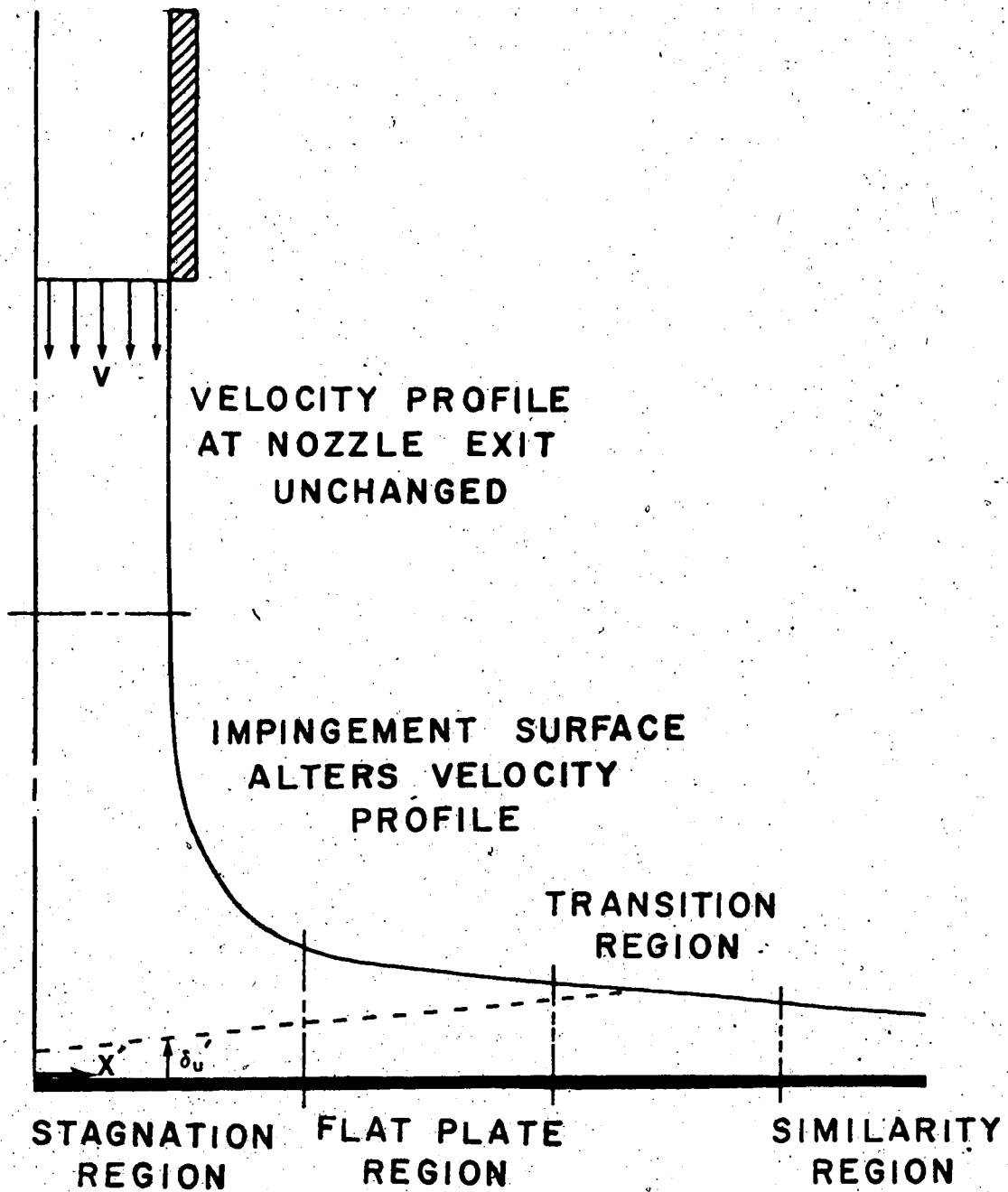


Figure 6.1 Flow regions of an impinging jet

4. A similarity region where the fully developed similar profile persists. A hydraulic jump will eventually occur and the thickness of the liquid on the plate suddenly increases.

The above regions apply only to laminar flow. As region 1 has a strong favorable pressure gradient, transition to turbulence is not likely to occur there. A more likely place for transition is in region 2 where the pressure gradient is essentially zero. Of course transition to turbulence will depend on a number of factors, jet Reynolds number, free stream turbulence, and length scales and surface roughness. Only laminar boundary layers are considered in this study.

#### 6.1 Previous Work

The main problem in determining the flow field characteristics of axisymmetric jets is that the stream function and the potential function both do not satisfy Laplace's equation and thus the methods of complex variables are not useful. Therefore, numerical and experimental methods must be attempted. Leclerc [26] used an electrical analogy to solve for the potential flow of an axisymmetric jet impinging on a flat plate. Brady and Ludwig [27] computed the velocity on a flat plate due to an axisymmetric jet by experimentally measuring the pressure distribution on the surface. Their interest was in the ground flow characteristics of VTOL and STOL aircraft jets. Scholtz and Trass

[28] used a separation of variables technique and a truncated series solution to solve for the flow field in a non-uniform impinging jet. Sarpkaya and Hiriart [16] used the finite element method of [11] and also Belotserkovsky's integral method to solve for the potential flow associated with aerodynamic jet thrust reversers.

Other investigators [29]-[39] have made experimental and theoretical investigations into the flow field and heat transfer of impinging axisymmetric jets. The effects of entrainment are important and some of the parameters and effects dealt with are nozzle-plate spacing, turbulence levels and length scales, size of jet and size of target surface, jet Reynolds number and Prandtl number. The pressure distribution measured on the surface is important for determining the velocity on the impingement surface.

In this chapter the flow and heat transfer characteristics of an axisymmetric laminar jet impinging on a surface will be investigated. Two effects were modelled by the finite element method and integral boundary layer analysis. These are the effect of nozzle-plate spacing and the effect of surface curvature. Also the shear stress on the impingement surface is determined. The effects of melting on the heat transfer will be considered in the next chapter.

## 6.2 Flow Field of Axisymmetric Jet Impingement

The finite element program was run for an axisymmetric jet impinging on a flat surface for nozzle-plate spacings

of  $H = 0.25, 0.5, 1.0$  and  $3.0$ . The radial surface velocity distributions are shown in Figure 6.2. The velocity distributions for the cases of  $1.0$  and  $3.0$  are essentially the same and therefore the case of  $H = 1.0$  corresponds to the case of infinite nozzle-plate spacing. This is contrasted with the two-dimensional case where the infinite nozzle-plate spacing is modelled by  $H = 3.0$ . In the region  $x \leq 0.25$  the velocities for all three nozzle plate spacings are approximately equal, although the velocity gradients are very different. This is shown in Figure 6.3 where the velocity gradients for  $H = 3.0, 1.0, 0.5$  and  $0.25$  were calculated by the finite element method and cubic spline interpolation technique. As was present in the two-dimensional case errors occur due to numerical differentiation of the computed velocities. Peaks occur in the gradient of velocity curves at a radial distance near the lip of the nozzle. Similar to the two-dimensional case, these peaks are related to peaks which occur in the heat transfer curves. A difference from the two-dimensional case is that a peak occurs in the case  $H = 1.0, \infty$  for the axisymmetric jet. There is no peak in the gradient of velocity curve for  $H = 3.0, \infty$  in the two-dimensional case. The peak in the axisymmetric case is due to the rapidly decreasing flow area near the lip of the nozzle so that by continuity requirements, the velocity must increase more rapidly than in the two-dimensional case.

The velocity distribution predicted by Leclerc's

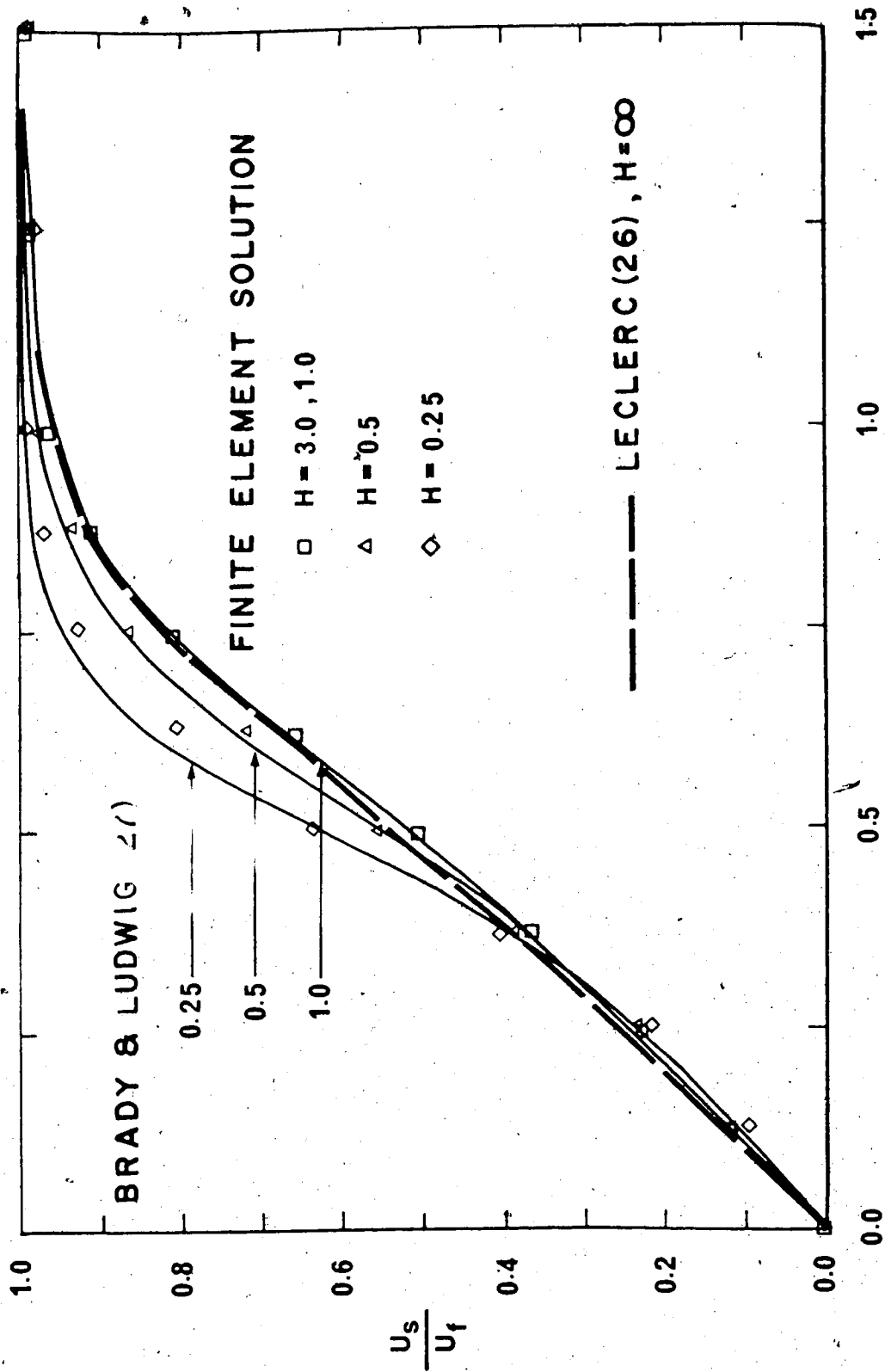


Figure 6.2 Velocity distributions, axisymmetric jet impinging on a flat surface

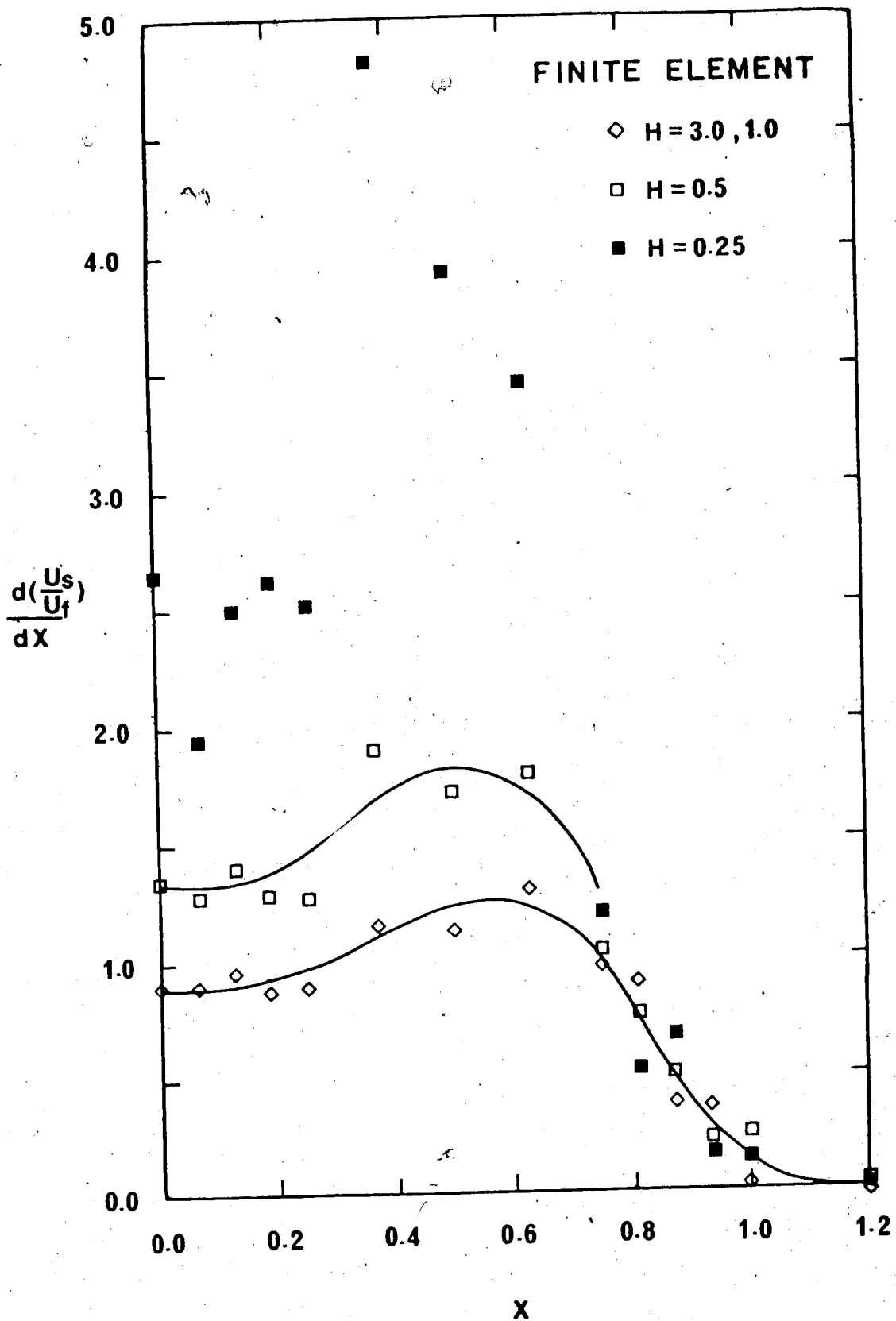


Figure 6.3 Velocity gradient distributions , axisymmetric jet impinging on a flat surface

electrical analogy [26] for  $H = \infty$  and by the experimental method of Brady and Ludwig [27] for  $H = \infty, 0.5$  and  $0.25$  are also shown in Figure 6.2. Agreement between the finite element method and the experimental methods is quite good for the case of  $H = 1.0$  and  $H = 0.5$ , but the accuracy suffers when  $H = 0.25$ . All three cases had the same number of nodes in the finite element mesh and the decrease in accuracy is due to the increase in velocity gradient. A large change in velocity requires more nodes for accurate representation.

The same argument for the increase in velocity gradient with a decrease in nozzle-plate spacing as given for the two-dimensional case also applies for axisymmetric jet impingement.

To consider the effect of a curved impingement surface the finite element program was run with a nozzle-plate spacing of  $H = 3.0$  for an axisymmetric jet impinging on curved paraboloid surfaces. The paraboloid cross-sections were of the form

$$w = ar^2 \qquad 6.2.1$$

for various values of the parameter  $a$ , ( $a = 0, 0.05, 0.1, 0.2, 0.5$  and  $1.0$ ). The coordinate directions  $w$  and  $r$  along with the resulting velocity profiles are shown in Figure 6.4. The radius of curvature  $R$  and curvature  $K$  are found by the formula



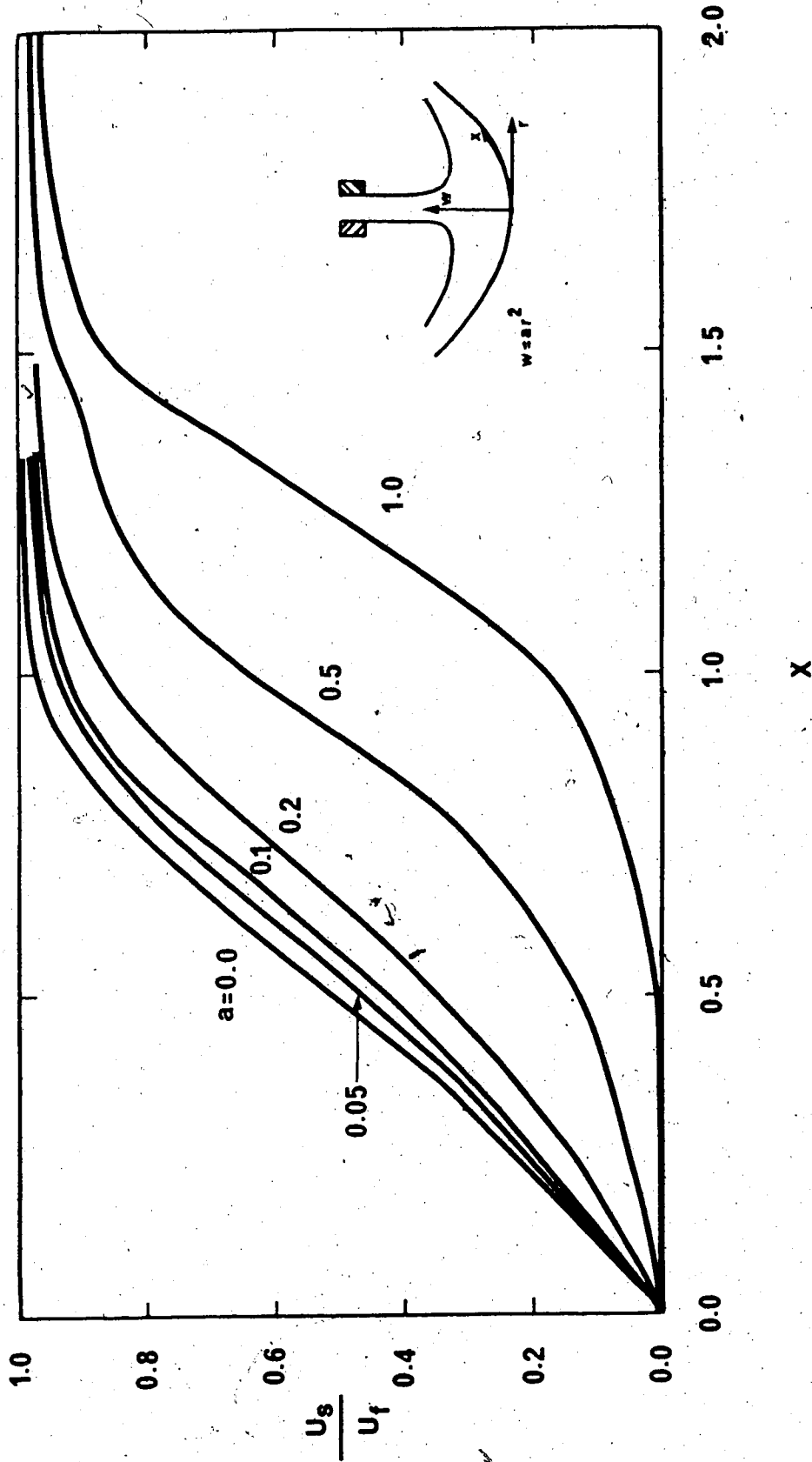


Figure 6.4 Velocity distributions, axisymmetric jet impinging on curved surfaces

$$R = \frac{1}{K} = \frac{[1 + (\frac{dw}{dr})^2]^{3/2}}{\frac{d^2w}{dr^2}} \quad 6.2.2$$

and for the family given by equation 6.2.1, one obtains

$$R = \frac{1}{K} = \frac{(1 + 4a^2r^2)^{3/2}}{2a} \quad 6.2.3$$

The smallest radius of curvature and largest curvature occur at  $r = 0$ , the stagnation point. Table 2 shows the radii of curvature and curvature for the family of paraboloids considered.

Table 2. Radii of curvature and curvature for a family of paraboloids given by  $w = ar^2$  at  $r = 0$ .

a	K	R
0	0	$\infty$
0.05	0.1	10
0.1	0.2	5
0.2	0.4	2.5
0.5	1.0	1.0
1.0	2.0	0.5

For the boundary layer equations to be valid the relationship  $\frac{\delta u}{R} \ll 1$  must hold [18]. Using the non-dimensional variables of equation 4.1.6 and the relationship  $R = \frac{R'}{D}$  the curvature criteria becomes  $\frac{\delta u}{R} (Re_D)^{-1/2} \ll 1$ . If this criteria is not fulfilled then the complete Navier-Stokes equations including curvature effects must be considered [45]. If  $\frac{\delta u}{R} (Re_D)^{-1/2} \ll 1$  is valid, then the effects of a change in surface shape are felt through the external pressure gradient the surface imposes on the flow. For flow on the concave side of the paraboloid the pressure gradient is favourable and tends to delay separation. For flow on the convex side, the pressure gradient is unfavorable and tends to increase the chances of separation occurring. Only the flow on the concave side of the paraboloid was considered assuming that the curvature criteria,  $\frac{\delta u}{R} (Re_D)^{-1/2} \ll 1$ , was satisfied.

### 6.3 Heat Transfer of Axisymmetric Jet Impingement

With the velocity distributions of the previous section the boundary layer solution described in Chapter IV may be used to find the heat transfer characteristics of the impinging axisymmetric jet. As outlined in the previous chapter concerning the two-dimensional jet the Nusselt number was found to be proportional to the square root of the velocity gradient at the wall. The analysis for the axisymmetric jet is the same as both the two-dimensional and

axisymmetric stagnation point flows are of the same type. If boundary layer equations are considered, they both belong to the class of Falkner-Skan wedge flows [18]. The difficulty for axisymmetric jet impingement lies in finding the parameter  $\beta$  in the expression

$$U'_s = \frac{\beta}{2} x' \quad 6.3.1$$

As the exact solution is available for the two-dimensional jet, the parameter  $\beta$  was found as shown by equations 5.2.16 and 5.2.17.

The governing equation for axisymmetric Heimenz stagnation point flow is [18]

$$\frac{d^3 F}{d\eta^3} + F \frac{d^2 F}{d\eta^2} + \frac{1}{2} \left( 1 - \left( \frac{dF}{d\eta} \right)^2 \right) = 0 \quad 6.3.2$$

with

$$u' = \frac{\beta x'}{2} \frac{dF}{d\eta} \quad 6.3.3$$

$$\psi' = \frac{x'^2}{2} \sqrt{\beta \nu} F(\eta) \quad 6.3.4$$

and

$$\eta = y' \sqrt{\frac{\beta}{\nu}}$$

similar to that for the two-dimensional case. The only difference is the presence of the factor 1/2 in the above equations. The boundary conditions are the same as for the two-dimensional case, that is  $F(0) = F'(0) = 0$  and  $F'(\infty) = 1$ . The energy equation and thermal boundary conditions are identical with those of the two-dimensional case, that is equations 5.2.10 and 5.2.11. The solution is again equation 5.2.12 but the non-dimensional stream function  $F$  is obtained from the solution of equation 6.3.2. The expression for the Nusselt number is given by equation 5.2.14 and is repeated here for reference.

$$Nu_D = D \sqrt{\frac{\beta}{\nu}} G(\text{Pr}) \quad 6.3.5$$

The value of  $G(\text{Pr})$  for axisymmetric stagnation point flow and a Prandtl number of 13.7 is 1.3296 as given by White [18]. This compares with the two-dimensional value of 1.4557 for a Prandtl number of 13.7. The physical properties, assumed constant for this problem, must be calculated at some reference temperature. Three possible choices are the wall temperature, the film temperature and the jet bulk temperature. The wall temperature, 0°C, was chosen as the reference temperature for calculating the physical properties. A discussion on the applicability of this assumption is given in the next chapter. Using the non-dimensionalization of equation 2.1.12, equation 6.3.1 becomes

$$\beta = 2 \left( \frac{dU_s'}{dx} \right)_0 = \frac{2V}{D} \left( \frac{dU_s}{dx} \right)_0 \quad 6.3.6$$

similar to equation 5.2.16. Substituting equation 6.3.6 into equation 6.3.5 and rearranging results in

$$\frac{Nu_D}{\sqrt{Re_D}} = \sqrt{2 \left( \frac{dU_s}{dx} \right)_0} G(Pr) \quad 6.3.7$$

As no exact solution for axisymmetric jet impingement exists the values of  $\beta$ , the velocity gradient at the wall, may be obtained from the finite element and cubic spline interpolation. The values of the velocity gradient at the stagnation point from Figure 6.3 and the heat transfer parameter from equation 6.3.7 are shown in Table 3 for various nozzle-plate spacings.

Table 3. Axisymmetric jet impingement heat transfer on a flat surface.

H	$\left( \frac{dU_s}{dx} \right)_0$	$\frac{Nu_D}{\sqrt{Re_D}}$
1.0, $\infty$	0.91	1.8
0.5	1.28	2.13
0.25	2.52	3.57

The values of  $Nu_D/\sqrt{Re_D}$  from Table 3 at the stagnation point for  $H = \infty, 1.0,$  and  $0.5$  are shown in Figure 6.5. Also shown are the heat transfer curves generated by the boundary layer analysis. The case of  $H = 0.25$  was attempted but the velocity gradients were too large. Large velocity gradients imply a large pressure gradient parameter  $\Lambda$ , and the solution is not valid for large  $\Lambda$  as previously described. The scatter in the data is due to the numerical differentiation procedure of the cubic spline interpolation approximation coupled with the integration procedure. Peaks in these heat transfer curves correspond to the peaks in the velocity gradient distribution curves of Figure 6.3.

The trends in heat transfer on curved surfaces can be inferred from the velocity distribution curves in Figure 6.4. The heat transfer for the curve  $w = 0$  is same as shown in Figure 6.5 for  $H = 3.0, 1.0$ . As the parameter  $a$  increases, the velocity gradient at the stagnation point decreases as shown in Figure 6.4. Therefore, the stagnation point heat transfer will also decrease with increasing curvature. This trend is the same as concluded by Cheng and Williams [54]. For the cases  $a = 0.05, 0.1$  and  $0.2$  the heat transfer curves will only slightly differ from the flat surface case  $a = 0$ . This is evident because the velocity distributions for these four cases are similar. For the cases  $a = 0.5, 1.0$  the velocity gradient in the region near the stagnation point is very small. Heat transfer by conduction will predominate over convective heat transfer

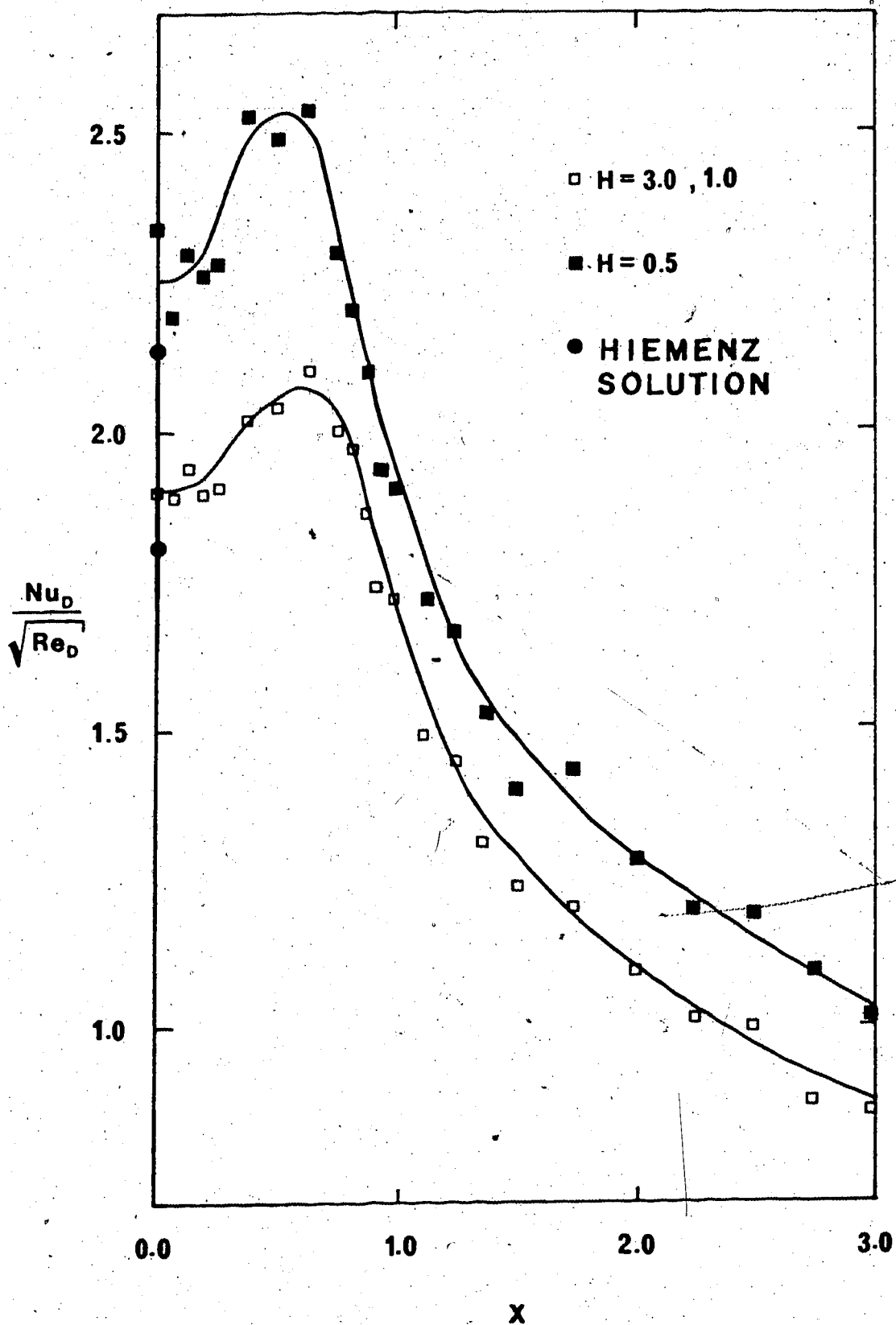


Figure 6.5 Heat transfer near the stagnation point of an axisymmetric jet impinging on a flat surface



in the region of the stagnation point for these two cases.

Also of interest is the shear stress generated on the surface due to the impinging jet. The shear stress will be important if erosion effects are present in the transfer mechanisms. A possible situation where this would happen is the impingement cutting of a frozen sand or gravel. Define a shear stress coefficient as

$$C_{\tau} = \frac{\mu \left. \frac{\partial u'}{\partial y'} \right|_{y'=0}}{\frac{1}{2} \rho V^2} \quad 6.3.8$$

Introducing the non-dimensional variables of equation 4.1.6 results in

$$\frac{1}{2} C_{\tau} \sqrt{Re_D} = \left. \frac{\partial u}{\partial y} \right|_{y=0} \quad 6.3.9$$

Equation 4.4.1 is used to evaluate the velocity gradient in the direction normal to the wall. Figure 6.6 shows the shear stress distribution on the impingement surface as calculated by the integral boundary layer analysis. From equation 4.4.1 and equation 6.3.9 the shear stress parameter is proportion to the ratio  $U/\delta_u$ . The shear stress parameter is zero at the stagnation point as the free stream velocity is zero there also. For the region near the stagnation point,  $\delta_u$ , the boundary layer thickness, is con-

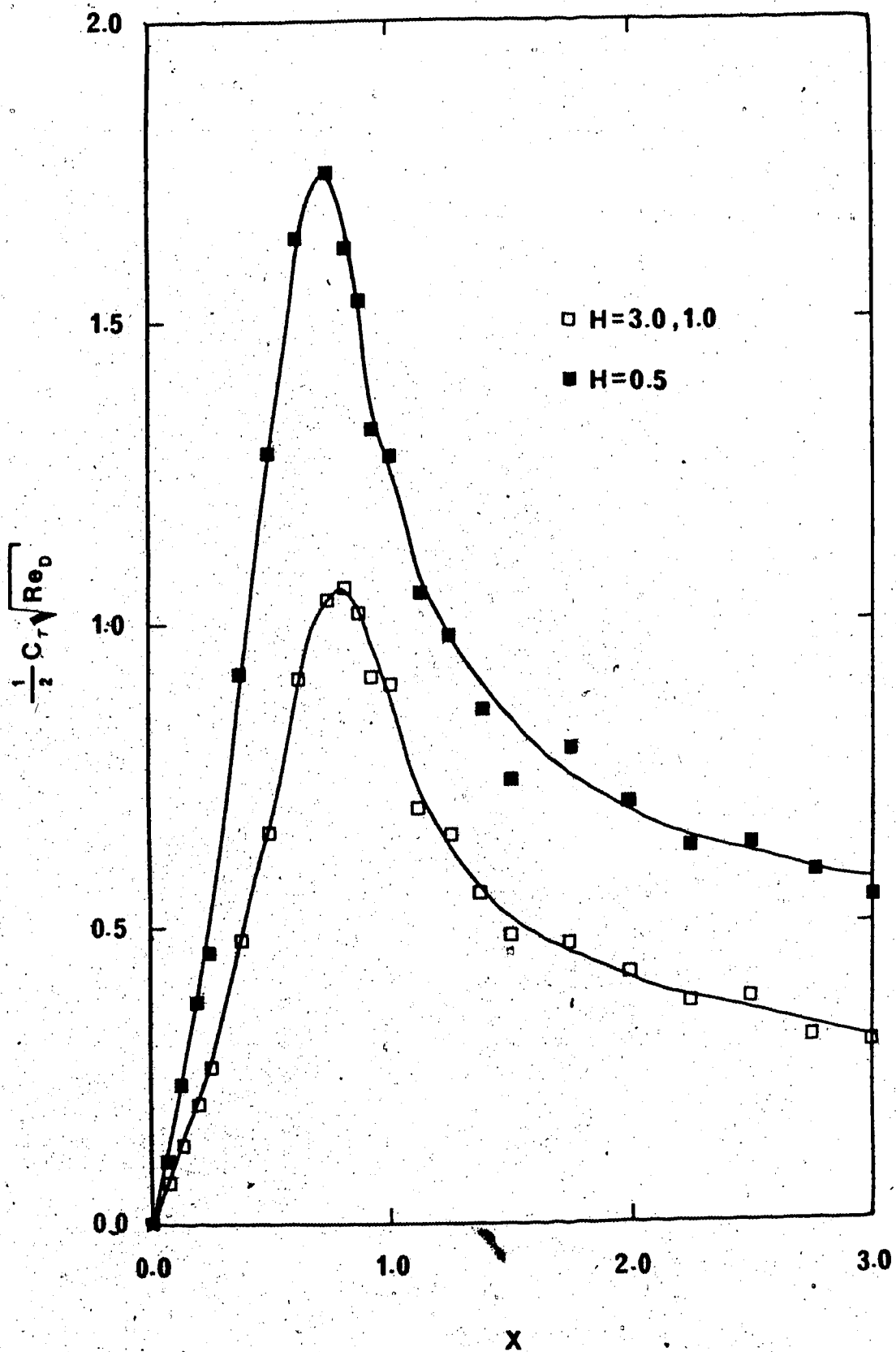


Figure 6.6 Shear stress on a flat surface due to axisymmetric jet impingement

stant and  $U$  rises from zero as shown in figure 6.2. Therefore, the shear stress parameter rises from zero in a manner similar to the rise in the velocity. The smaller nozzle-plate spacing produces a larger shear stress parameter because a greater rise in free stream velocity is experienced for smaller nozzle-plate spacings as shown in Figure 6.2. As the radial distance increases the mainstream velocity becomes constant and the boundary layer thickness increases. These two effects combine together to produce the peaks in the shear stress parameter curves near the lip of the nozzle. The subsequent decrease in shear stress is due to the continual increase in boundary layer thickness while the mainstream velocity remains constant.

The combined effect of shear stress and melting will be discussed in the next chapter.

## CHAPTER VII

### MELTING AND EROSION CAUSED BY AXISYMMETRIC JET IMPINGEMENT

The melting and erosion of a frozen material by the action of a water jet presents a very complex problem. Because of this complexity, investigations on melting by impinging jets have been experimental in nature. In this chapter the melting and erosion of frozen material is analyzed by the methods of the previous chapters. The effect of melting on the heat transfer of an axisymmetric jet impinging on an ice surface is shown. An attempt to model the melting of a block of ice results in the steady state heat transfer rate as a function of Stefan number. To obtain a physical perspective of the melting process, photographs were taken at various time intervals during the melting of a block of ice. Finally the effect of shear stress and erosion on the cutting action of the jet is discussed.

#### 7.1 Previous Work

Recently experimental investigations on the melting of ice with a water jet have been made. Savino, Zumdieck and Siegal [40] have studied the effect of freezing and melting on the heat transfer coefficient at a stagnation

point and found that the phase change had little effect on the heat transfer coefficient. However, they only considered small temperature differences between the jet and the ice and the Stefan number was small in their study,  $Ste \leq 0.14$ . Yen [41] experimentally studied the heat transfer characteristics of a bubble-induced water jet impinging on an ice surface. In this case the water jet is submerged and entrainment is an important factor. As previously mentioned Mellor [42] has presented a number of potential applications for the cutting of ice with continuous high pressure jets. Two recent experimental studies by Yen and Zehnder [43] and Gilpin [44] have shown the effects of melting a block of ice with a water jet. In [43] the mass of ice removed by the ablation process was the primary measured quantity. They found that the weight-loss versus time curves were essentially linear implying a constant melting rate. Gilpin [44] recognized two distinct regimes of melting heat transfer, characterized by the shape of the cavity in the ice produced by the impinging water jet. The first was a smooth cavity shape occurring at Reynolds numbers in the range,  $2 \times 10^3 \leq Re_D \leq 4 \times 10^4$ . Heat transferred during steady state cutting of the ice was found to be correlated by

$$Nu_D = 0.4 Re_D^{0.65}$$

7.1.1

The exponent 0.65 indicates a heat transfer rate slightly greater than that for purely laminar flow. Smoothness in cavity shape implies that a laminar boundary layer is present and the increased rate of heat transfer is due to the turbulent free stream of the jet. The second case was a rough cavity shape indicating highly turbulent flow. The Reynolds number range for this case was  $5 \times 10^3 \leq Re_D \leq 7 \times 10^4$ . Obviously either mode of heat transfer can exist for a range of Reynolds numbers and the mode which does exist depends on the experimental conditions at the time the experiment takes place. For the rough case the heat transfer was correlated by

$$Nu_D = 0.17 Re_D^{0.8} \quad 7.1.2$$

The exponent 0.8 is characteristic of turbulent forced convection heat transfer.

## 7.2 Melting Ice with a Water Jet

The boundary layer solution was run for an axisymmetric jet impinging on a flat ice surface. The heat transfer distribution near the stagnation point for a range of Stefan numbers is shown in Figure 7.1. Since the water temperature is limited to the range 0°C to 100°C the Stefan number,  $\frac{C_p(T_\infty - T_0)}{L}$ , is limited to the range 0 to 1.25. The nozzle-

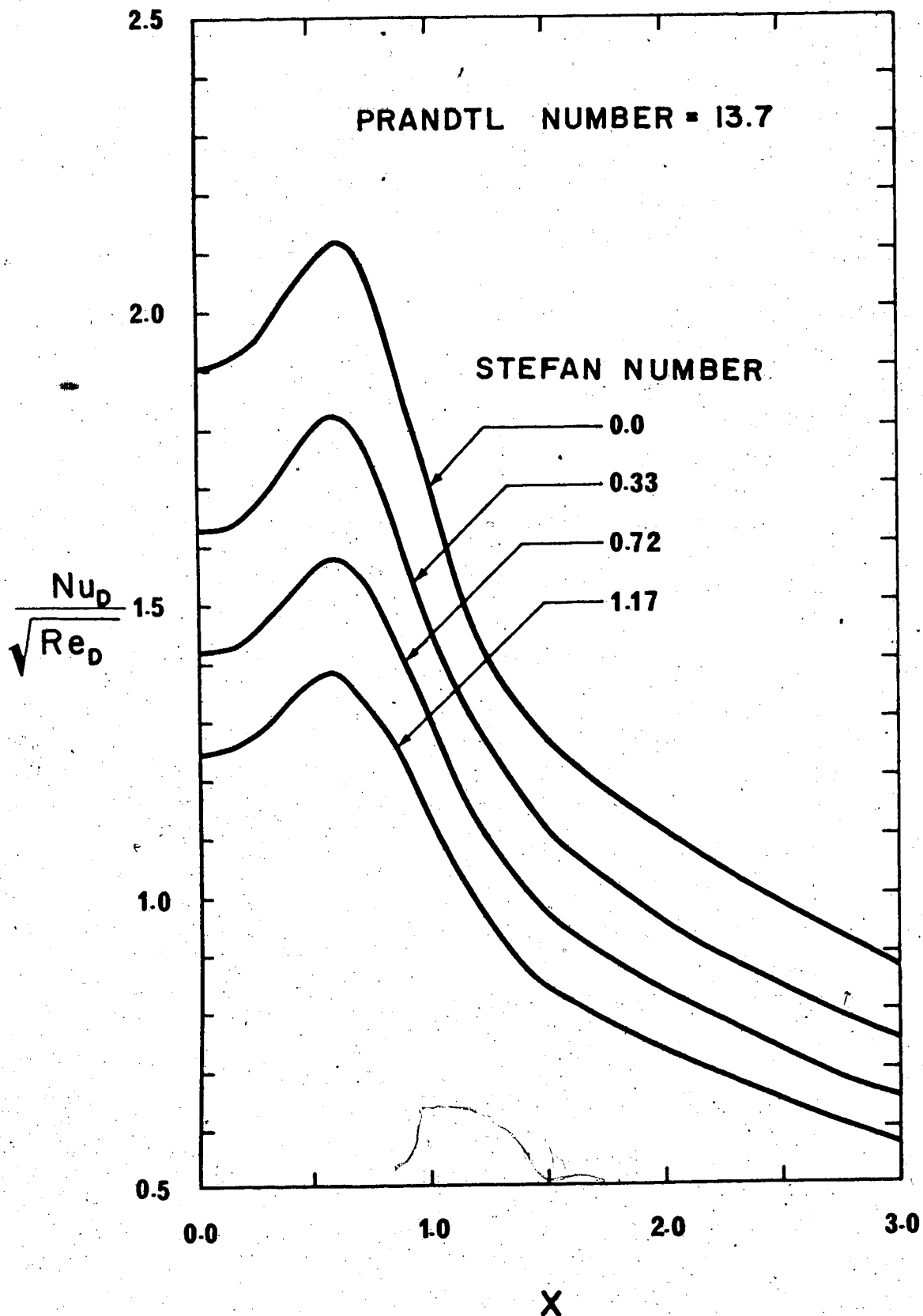


Figure 7.1 Heat transfer from an axisymmetric jet to a flat surface, effect of melting

plate spacing used was  $H = 3.0$ . For increasing Stefan number the heat transfer parameter  $Nu_D/\sqrt{Re_D}$ , decreases. The shape of the heat transfer curve is independent of the Stefan number but shifts downwards with increasing Stefan number. The decrease in heat transfer with increasing Stefan number may be explained as follows. From equation 5.2.2, the heat transfer parameter is equal to the non-dimensional temperature gradient at the wall. Obviously, as the bulk temperature of the jet is increased more ice will be melted and a thicker layer of near freezing water will be formed. With the thicker layer of colder water, the temperature gradient at the wall decreases. A shielding of the ice surface by the newly melted water layer takes place.

The finite element method and integral boundary layer solution were used to model the continuous melting of a block of ice by a water jet. The solution procedure proceeded as follows. First, the axisymmetric jet flow field on a flat surface was solved by the finite element method. The integral boundary layer solution was then solved to obtain the distribution of melting velocity,  $v_0$ , along the ice surface. If the position of the ice surface before the melting started was  $z_t$  then the new position of the ice surface after a non-dimensional time  $\Delta t$  is

$$z_{t+\Delta t} = z_t - |v_0| \Delta t \quad 7.2.1$$



using the coordinate system described in Figure 7.2. An adjustment of the new ice surface position now takes place to ensure that the finite element mesh does not become too distorted from its original shape. If  $z_{t0}$  is the original position of the stagnation point and  $z_{(t+\Delta t)0}$  the new position of the stagnation point after melting has taken place, then the melted ice surface is adjusted according to the transformation

$$z_A = z_{t+\Delta t} - (z_{(t+\Delta t)0} - z_{t0}) \quad 7.2.2$$

where  $z_A$  gives the adjusted ice surface shape. This transformation ensures that the stagnation point remains at the same vertical distance from the Tip of the nozzle. The transformation for the first time step is shown schematically in Figure 7.2. With this transformation the origin of the coordinate system remains at the stagnation point.

Physically the adjustment of the ice surface may correspond to two entirely different situations. As the distance between the nozzle and the stagnation point remains constant the first situation occurs when the nozzle moves with the same velocity as the melting surface. The relative velocity between the water jet and the ice surface is  $V$ , the dimensional water jet velocity. The second case occurs if the nozzle remains stationary and the ice surface melts away from the nozzle. Although the distance between the

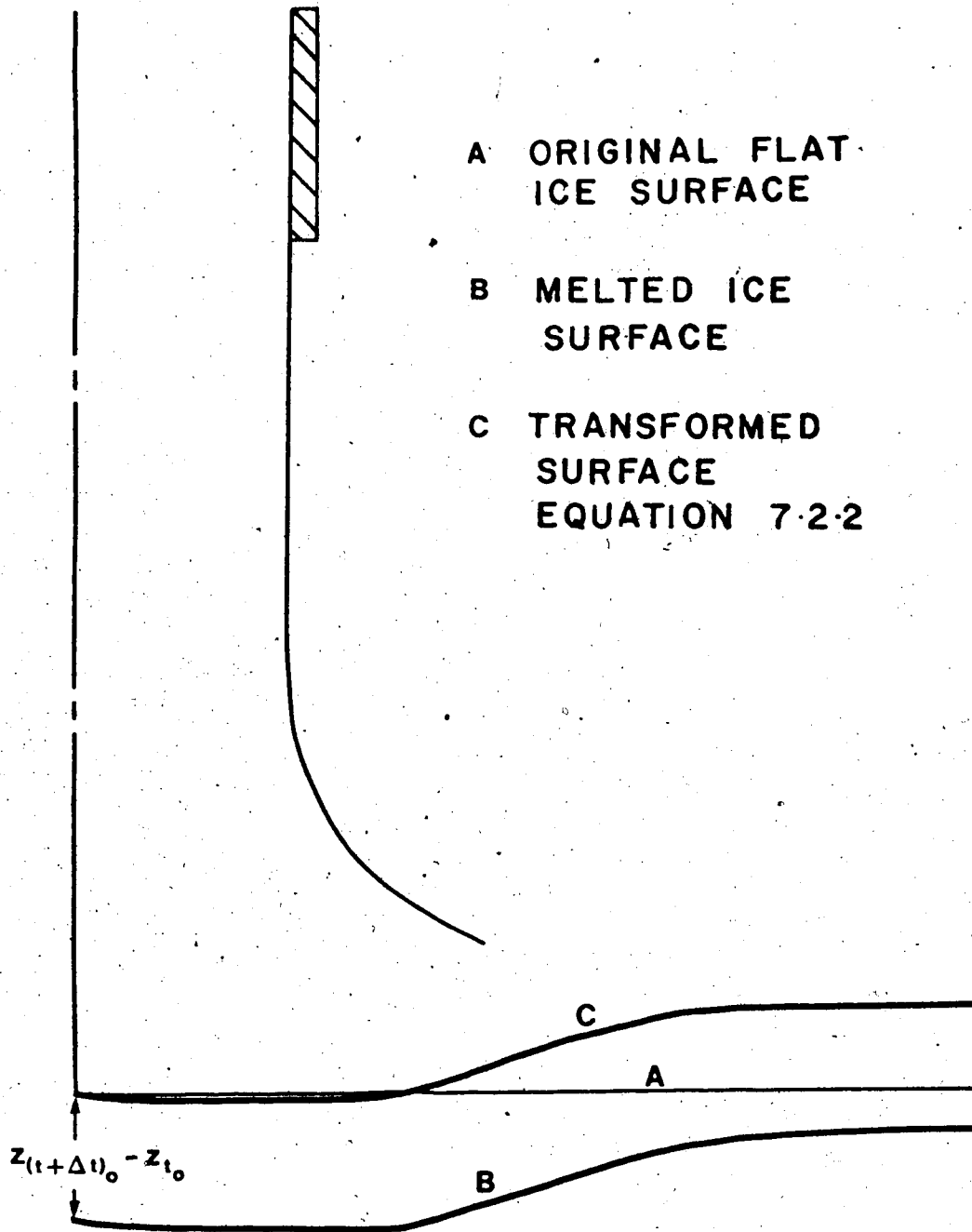


Figure 7.2 Adjustment of the melted surface

nozzle and the stagnation point is physically increasing, a nozzle-plate spacing of  $H = 1.0$  models all cases in the range  $1.0 \leq H \leq \infty$  as previously discussed. The initial nozzle-plate spacing for this case was  $H_0 = 3.0$  and the adjustment of the ice surface does not alter the potential flow analysis. However, the relative velocity between the water jet and the ice surface is now  $V - v_0'$ . The program was run assuming the relative velocity was  $V$ , that is, the first case was considered. As will be shown later the magnitude of the melting velocity is so small that the distinction between these two cases is negligible.

The complete computer program was run for Stefan numbers of  $Ste = 0.2, 0.33, 0.72, \text{ and } 1.17$ . A typical time history profile of the ice interface is shown in Figure 7.3 for a Stefan number of 0.33. A time step of  $\Delta t = 1$  was used for this run. The non-dimensional times for the ice interface profiles shown are  $t = 0, 5, 10, 20 \text{ and } 30$ . The ice profile is almost flat for the region  $0 \leq X \leq 0.75$ . As time increases the ice profile becomes steeper in the region  $1.0 \leq X \leq 1.75$ . The program was stopped after 30 iterations because separation was predicted. Separation occurs when the pressure gradient parameter  $\Lambda$  becomes less than  $-12$  as previously discussed.

The assumption of quasi-steady state flow made in Chapter IV may now be verified. Consider a typical flow

$$V = 3 \text{ m/sec} \quad D = 0.5 \text{ cm} \quad \nu = 1.74 \times 10^{-6} \frac{\text{m}^2}{\text{sec}} \quad \text{at } 0^\circ\text{C}$$

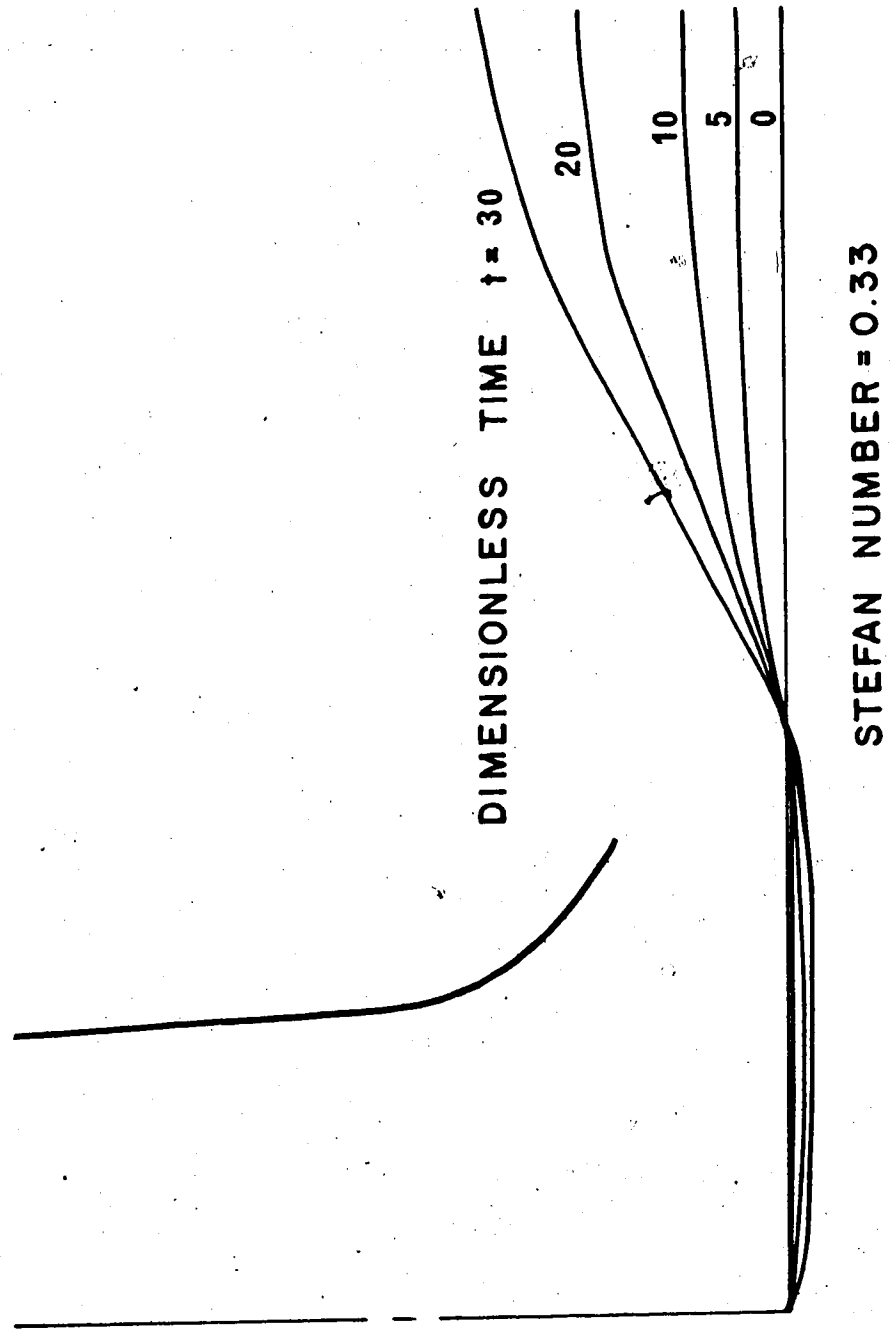


Figure 7.3 Typical profiles of the ice interface

The Reynolds number for this flow is approximately  $8.6 \times 10^3$ . For a Stefan number of 0.33, the non-dimensional melting velocity is approximately  $v_0 = 0.04$ . Therefore the actual melting velocity for this problem is

$$v_0' = \frac{v_0 V}{\sqrt{Re_D}} = \frac{0.04 \times 3 \text{ m/sec}}{\sqrt{8.6 \times 10^3}} \approx 1.3 \times 10^{-3} \frac{\text{m}}{\text{sec}}$$

or only about 0.04 percent of the incoming jet velocity. Because the melting velocity is such a small percentage of the incoming jet velocity the flow may be assumed to be at steady-state.

Also because of this small percentage the difference between the two cases of relative velocity will be very small. Therefore, the jet impingement problem may be modelled by the case where the nozzle moves with the same velocity as the melting ice surface.

As shown in Figure 7.3 the shape of the ice profile in the flat region is constant for the last ten iterations. The constant shape implies a constant melting velocity along the whole flat region of the ice profile. Steady state melting was assumed when the ice profile in the flat region had reached a constant shape. The melting velocity  $v_0$  is then used to calculate the steady state heat transfer rate.

From equations 4.1.11 and 5.2.2 the heat transfer parameter is given by

$$\frac{Nu_D}{\sqrt{Re_D}} = \frac{v_0 P_r}{Ste} \quad 7.2.2$$

For the case of no melting both the melting velocity and the Stefan number are zero and equation 7.2.2 is indeterminate. Figure 7.4 shows the steady state heat transfer parameter versus Stefan number. The region near Stefan number equal to zero is shown by a dotted line to indicate that the steady state results for this region are not known because of the indeterminateness of equation 7.2.2. Also shown are the stagnation point values from Figure 7.1. As the Stefan number increases, the difference between the initial stagnation point melting velocity and the steady state melting velocity increases. This trend leads to the assumption that the steady state heat transfer rate is the stagnation point heat transfer rate for a Stefan number equal to zero. Therefore, for small Stefan numbers the initial stagnation point melting velocity may be used to calculate steady state heat transfer rates but at larger Stefan numbers differences of up to about ten percent would result if stagnation point values were used instead of the steady state value.

The next problem was that of deciding on a reference temperature. As pointed out in the derivation of the boundary layer equation, the physical properties were assumed to be constant. The water temperature varies from the melting temperature at the wall to the bulk temperature

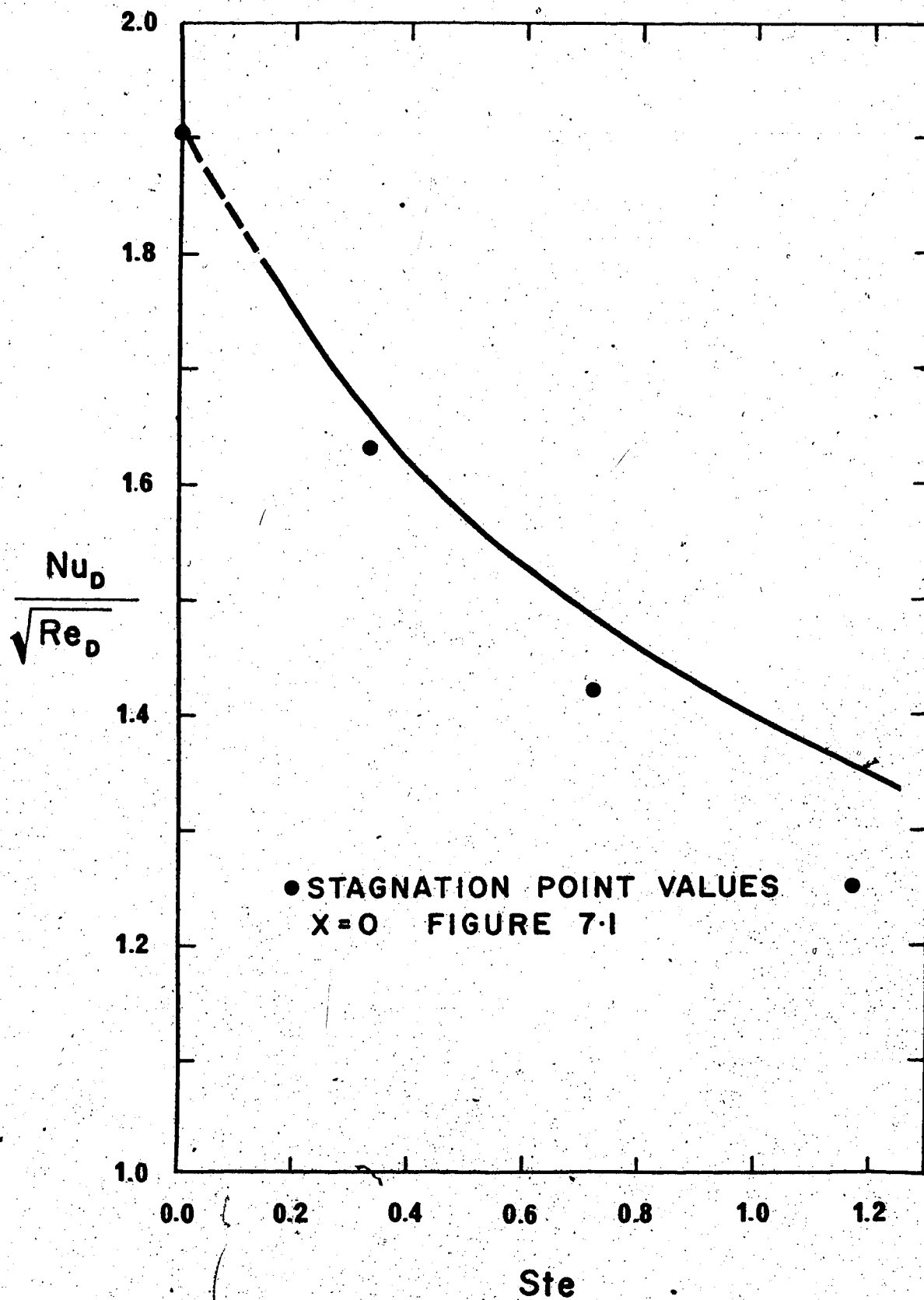


Figure 7.4 Steady-state heat transfer due to axisymmetric jet impingement

of the jet in the free stream across a thin boundary layer and the problem of which temperature in this range is to be used for calculating the physical properties arises. This is a problem as the viscosity of water varies greatly over the range of Stefan numbers considered [46]. The heat transfer curves for reference temperatures based on the wall temperature, the film temperature and the bulk temperature are shown in Figure 7.5. A significant variation in the heat transfer parameter is noticed depending on which reference temperature is used. To determine which reference temperature is best suited to describe this heat transfer process some experiments should be made and the heat transfer calculated based on each of the three reference temperatures. A comparison could then be made with Figure 7.5. Another possible solution would be to attempt a variable property numerical solution for this jet impingement heat transfer problem.

To gain some physical insight into this forced convection melting heat transfer problem a series of simple experiments were conducted. The experimental apparatus is shown schematically in Figure 7.6. A jet of water was vertically directed at a block of ice for varying amounts of time.

The water was pumped from a constant temperature tank and the temperature of water and flow rate were recorded. After completion of run, the block of ice was removed from the apparatus and the block was cut in half to reveal the profile of the hole produced by the impinging water jet. A





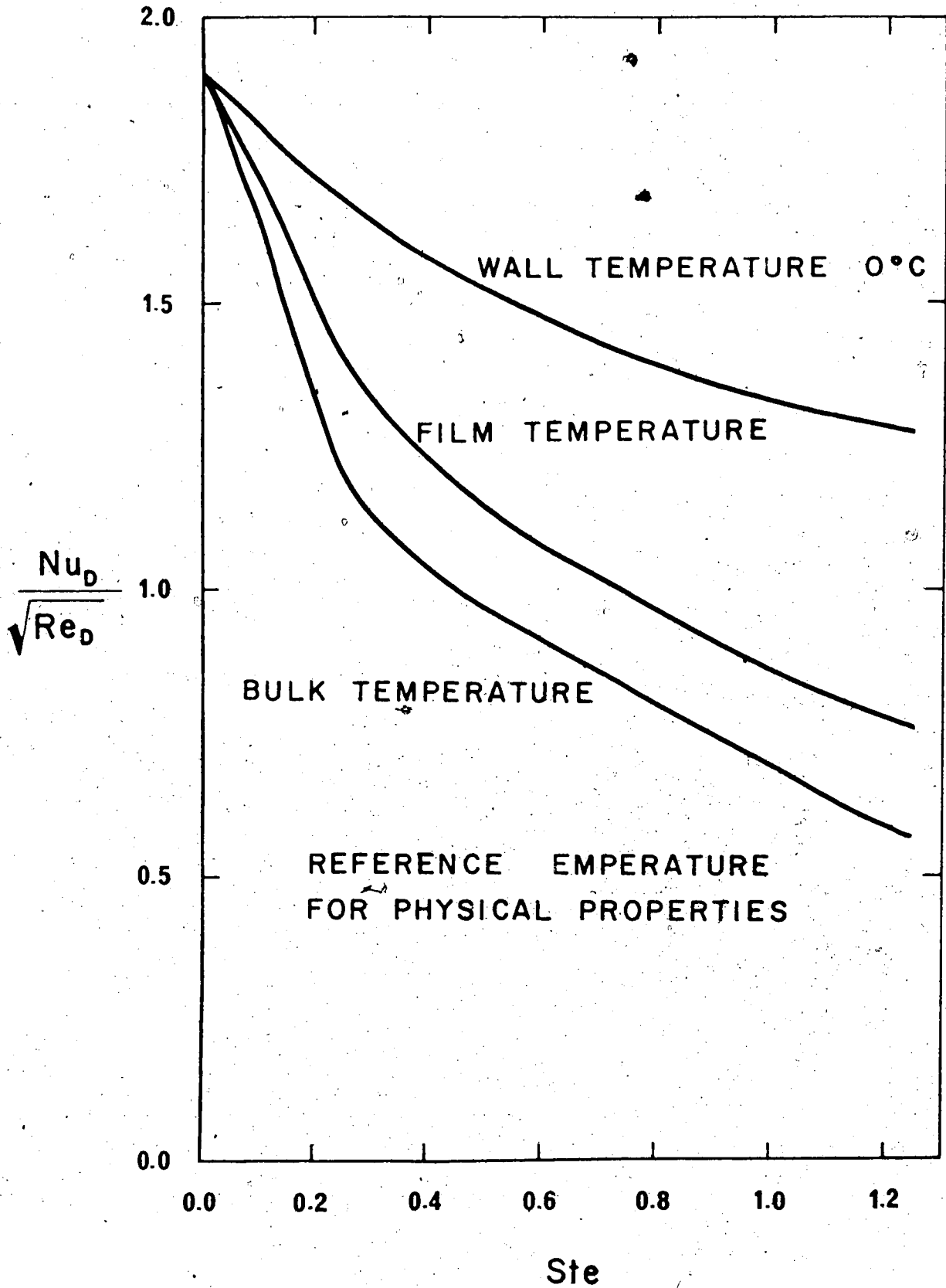


Figure 7.5 Effect of reference temperature for calculating physical properties.

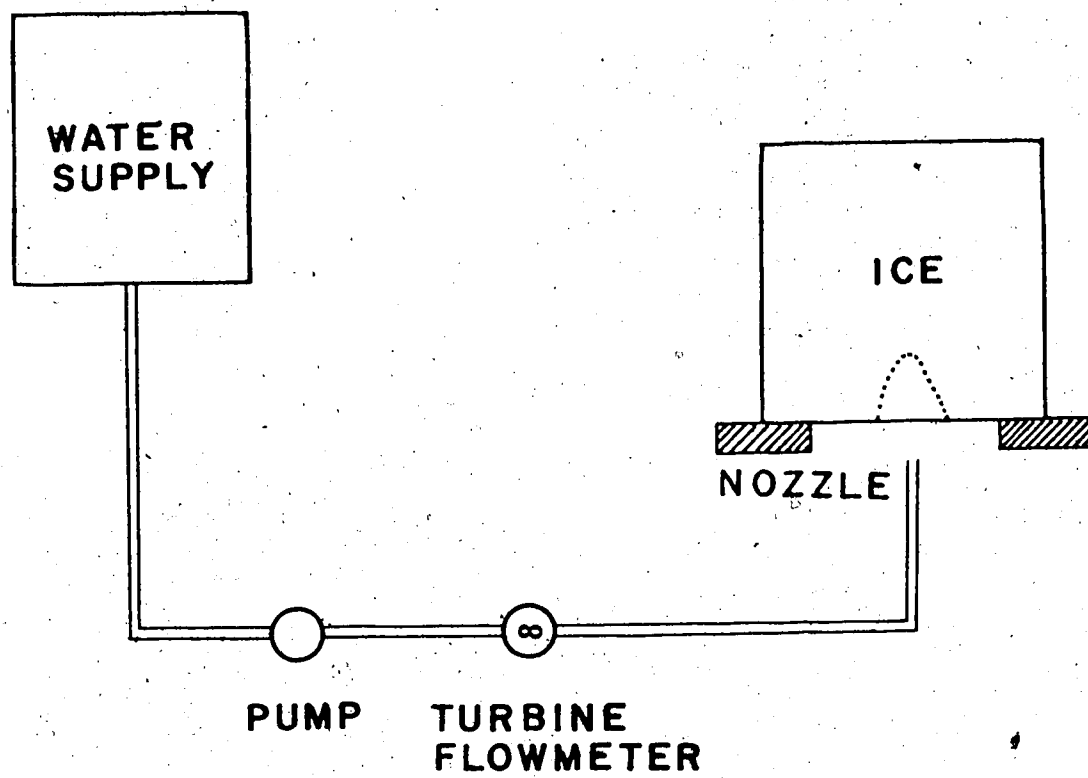


Figure 7.6 Experimental apparatus

photograph of the resulting ice profile was then taken. The time history of the ice interface was obtained by allowing the jet to impinge on the ice surface for various times. A 1.27 cm diameter jet of water at a temperature of 25°C, Stefan number of 0.31, was directed at an initially flat block of ice for times of 6, 10, 20, 40 and 80 seconds. The resulting photographs are shown in Plate 1. The jet velocity was approximately 0.76 meters/second. Using the wall temperature as reference temperature this corresponds to a jet Reynolds number of  $Re_D = 5.4 \times 10^3$ . To compare the photographs with the curves in Figure 7.3 a reference time must be established. Knowing

$$v_0 = \frac{v_0'}{V} \sqrt{Re_D}; \quad t = \frac{t'}{t_R}; \quad z = \frac{z'}{D} \quad \text{and}$$

$$z' = v_0' t'; \quad z = v_0 t$$

where  $t_R$  is a reference time results in

$$t_R = \frac{D}{V} \sqrt{Re_D} \quad 7.2.3$$

For the present case the reference time is 1.22 seconds. The times considered in the experiment then correspond to non-dimensional times of 4.9, 8.2, 16.4, 32.8 and 65.6. A

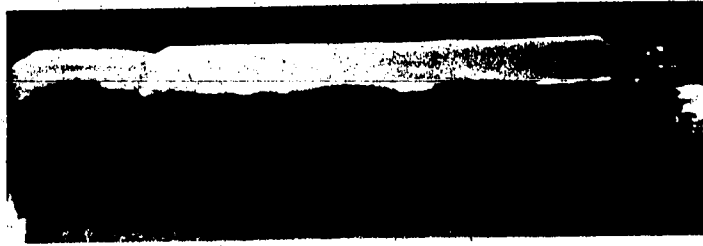
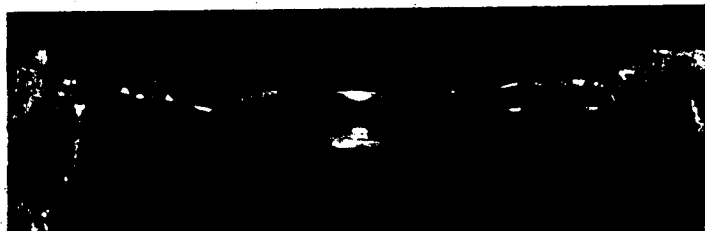
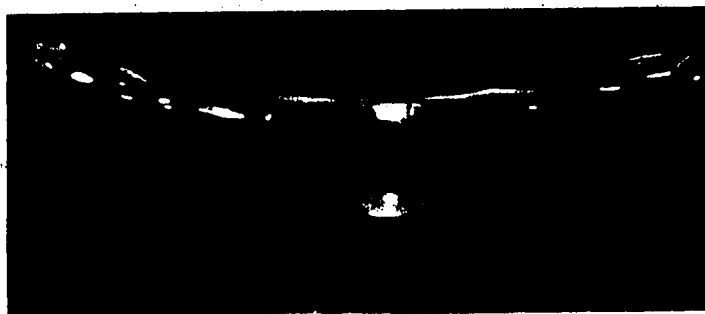
1a)  $t' = 6$  seconds,  $t = 4.9$ 1b)  $t' = 10$  seconds,  $t = 8.2$ 1c)  $t' = 20$  seconds,  $t = 16.4$ 1d)  $t' = 30$  seconds,  $t = 32.8$ 1e)  $t' = 80$  seconds,  $t = 65.6$ 

Plate 1. Time history of a block of ice melted  
by a water jet.  $D = 1.27\text{cm}$ ,  $V = 0.76\text{m/sec}$   
 $Re_D = 5.4 \times 10^3$ ,  $Ste = 0.31$ .

discussion of the photographs follows.

Plate 1a. A very shallow hole is present. The shape of the ice interface looks like that in Figure 7.3 for non-dimensional time of 5 in the region  $X \leq 1.5$ . Beyond this point, transition to turbulent flow is present, increasing the heat transfer and changing the shape of the ice interface.

Plate 1b. A deeper hole is shown. Note the flatness of the region near the stagnation point and the sudden rise in profile shape. The region of turbulent flow can be seen very clearly.

Plate 1c. An even more sharply defined laminar type region. A stagnation region still exists near the stagnation point.

Plate 1d. A very sharp distinction at the end of the laminar flow region. The flow is separated and continual application of the jet just deepens the cavity and increases the steepness of the cavity wall. The stagnation region is still very flat.

Plate 1e. The flow has melted away the sharp lip shown in Plate 1d and has reattached to the block of ice. The formation of another lip, and then separation is predicted to occur. This pattern of separation and reattachment is predicted until the hole has formed nearly vertical walls and the flow is continually separated.

From comparison between the photographs and the predicted results of Figure 7.3 the conclusions are:

1. That a flat region exists near the stagnation point.
2. That the computer program is valid only in the region  $0 \leq X \leq 1.5$  because transition to turbulence is likely to occur beyond this point.
3. That the computer program predicts separation accurately. Also the computer analysis is not valid after separation has been predicted to occur.

The effect of shear stress as well as heat transfer may be important in some applications where a jet is used to cut a frozen medium such as frozen gravel or sand.

Assume now that in addition to the heat transfer the removal rate of the material is directly proportional to the shear stress so

$$v_0' = \frac{k}{\rho L} \left. \frac{\partial T}{\partial y'} \right|_{y'=0} + c \left. \frac{\partial u'}{\partial y'} \right|_{y'=0} \quad 7.2.4$$

where  $c$  is a proportionality factor. Introducing the non-dimensionalizations of equations 4.1.6 and equation 6.3.8 results in

$$v_0 = \frac{Ste}{Pr} \left. \frac{\partial \theta}{\partial y} \right|_{y=0} + \frac{1}{2} \frac{c}{D} c_\tau \sqrt{Re_D} \quad 7.2.5$$

A problem arises because the value of the factor  $c$  is unknown. To determine the effect of shear stress the program was run

for the case  $\frac{c}{D} \sqrt{Re_D} = 1$  and the resulting shape of the interface after one melting time step is shown in Figure 7.7. The contribution of the shape due to melting is shown for comparison. The shape of the interface in Figure 7.7 resembles the inverse of the shear stress coefficient curve of Figure 6.6 which was expected considering the form of equation 7.2.5.

The exact value of the parameter  $c$  is unknown but the effects of varying the parameter  $\frac{c}{D} \sqrt{Re_D}$  are possible to predict with the present program. It is recommended that an experimental program be set up to determine what factors affect the parameter  $c$  and what its value might be for certain materials.



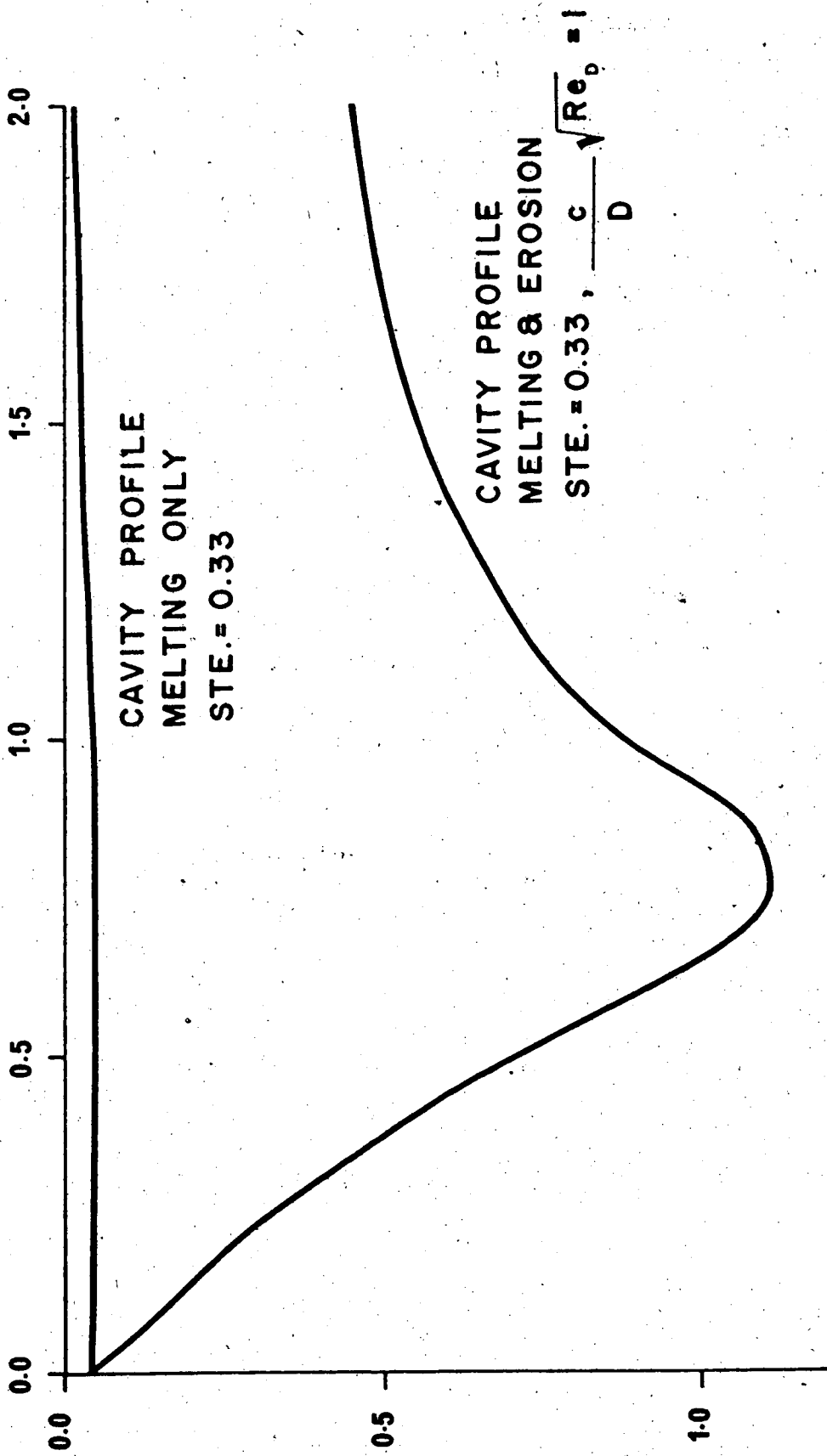


Figure 7.7 Profiles of a melted surface , with and without erosion

## CHAPTER VIII

### CONCLUSIONS AND RECOMMENDATIONS

This thesis was motivated by a desire to be able to predict the melting characteristics of a water jet impinging on an ice surface. With this in mind an analytical solution for laminar jet impingement has been derived. Both two-dimensional and axisymmetric flows are dealt with. The solution is divided into two parts, a potential flow problem which is solved by the finite element method and a boundary layer problem, solved by the Karman-Pohlhausen integral method.

The potential flow solution is valid for all jet impingement free surface type flows where gravity effects can be neglected. The physical effects dealt with are the distance from the nozzle-exit to the impingement surface and the impingement surface shape. From the potential flow solution the position of the free surface and the velocity distribution on the impingement surface used for the boundary layer analysis, are found.

The boundary layer solution is valid for laminar boundary layers on arbitrarily shaped surfaces. However, if the curvature of the surface becomes too large the boundary layer equations are no longer applicable and the complete Navier Stokes equations, including curvature effects,

must be considered. Another restriction on the applicability of the solution is imposed by the integral solution technique. The Karman-Pohlhausen integral technique is limited by extreme values in pressure gradient which may be present in the flow. The lower limit corresponds to the case of separation where the boundary layer equations are no longer valid. For the upper limit, the integral technique predicts velocity profiles which are unreasonable from a physical point of view. Therefore the solution is not valid in regions of highly adverse and highly favorable pressure gradients. The boundary layer solution is valid for laminar boundary layers in the presence of a laminar free stream. Although a laminar boundary layer can arise from the impingement of a turbulent jet, the free stream is turbulent which increases the heat transfer on the impingement surface.

The finite element method proved very versatile in handling all the different types of jet flows considered. Although an iterative procedure was required in locating the free surface, the finite element method was efficient for solving these potential flow problems. Because of the complex nature of the jet impingement melting problem the integral solution provides the easiest method of calculating the boundary layer. Although the accuracy is affected by the approximate nature of the integral technique, the averaging effect of integrating the boundary layer equations produces reasonable results.

The conclusions from this work will be summarized in point form.

1. The finite element method is generally known to be an effective means of solving field problems with complex boundaries. In this thesis, it was shown that the finite element technique is also a convenient method to use when the boundaries are not fixed a priori but are determined by the flow field itself. This was the situation for the free surface and the melting surface. Care must be taken, however, to ensure that there are a sufficient number of nodes to accurately represent the flow field. In general more nodes are required when there are large changes in the velocity or when the shape of the boundary changes rapidly.

2. For a stagnation point flow the heat transfer rate is directly related to the square root of the mainstream velocity gradient along the impingement surface. This correlation provides a means of qualitatively measuring the heat transfer rates on the impingement surface. For example, in the case of a jet impinging into a cavity it was observed that the velocity gradient at the stagnation point was significantly reduced when the radius of curvature of the cavity tip was of the order of the radius of the jet. A corresponding reduction in the rate of heat transfer occurs. Also in the case of a jet impinging on a flat surface for nozzle-plate spacings of one jet diameter or less significant increases in the velocity gradients occurred near the lip of the nozzle. Again a region of high heat

transfer exists near the lip of the nozzle.

3. There are three effects that make the heat transfer rate at the stagnation point of a water jet melting a cavity in ice different from that which would normally be associated with stagnation point flow. First there is the effect of injection of cold water into the boundary layer that is caused by the melting. It is noted that this effect produces a decrease in heat transfer rate of up to sixty percent for very hot water in the jet. The second effect is produced by the highly temperature dependent properties of water near the freezing point. Although this effect was not analysed in detail it appears that the choice of the reference temperature at which fluid properties are calculated will result in a fifty percent uncertainty in the dimensionless heat transfer rates. The final effect is produced by the fact that the shape of the cavity melted in the ice affects the flow field at the stagnation point and thus the heat transfer rate. On the basis of the calculated heat transfer to a parabolic shaped cavity a significant effect of the cavity shape may have been expected. However, the cavity formed by melting was found to have a very flat bottom and the resulting change in heat transfer rate was only about ten percent at most.

4. When cutting frozen sand or gravel the effects of shear stress are probably important. The present work assumed direct proportionality between cutting rate and shear stress, although the constant of proportionality was

unknown.

This work is a start to predicting the melting rates of water jets impinging on ice surfaces. This knowledge could have practical application wherever ice formation was a problem and its removal necessary for the continued operation of an industrial machine or component. Further to this work, the effect of turbulence on the melting process should be investigated. Also experimental work should be carried out to determine:

- a. which reference temperature should be used for calculating the physical properties;
- b. the value of the constant of proportionality  $c$ , when concerned with shear stress as a removal mechanism.

## REFERENCES

1. Milne-Thomson, L.M., Theoretical Hydrodynamics, 5th Ed., Macmillan, 1968.
2. Batchelor, G.K., An Introduction to Fluid Dynamics, Cambridge University Press, 1967.
3. Lamb, H., Hydrodynamics, Dover, 1932.
4. Robertson, J.M., Hydrodynamics in Theory and Application, Prentice-Hall, 1965.
5. Kantorovich, L.V. and Krylov, V.I., Approximate Methods of Higher Analysis, Translated from 3rd Russian Ed., by C.D. Benster, P. Noordhoff, The Netherlands, 1964.
6. Sokolnikoff, I.S., "Variational Methods", Chapter 7, Mathematical Theory of Elasticity, McGraw Hill, 1956.
7. Zienkiewicz, O.C., The Finite Element Method in Engineering Science, 2nd Ed., McGraw Hill, 1971.
8. Huebner, K.H., The Finite Element Method for Engineers, Wiley, 1975.
9. Norrie, D.H. and deVries, G., The Finite Element Method: Fundamentals and Applications, Academic Press, 1973.
10. Zienkiewicz, O.C. and Cheung, Y.K., "Finite Elements in the Solution of Field Problems", The Engineer, Vol. 24, September, 1965, pp. 507-510.
11. Chan, S.T.K., Finite Element Analysis of Irrotational Flows of an Ideal Fluid, Ph.D. Thesis, U. of C. Davis, University Microfilms, 1971.
12. deVries, G. and Norrie, D.H., "The Application of the Finite Element Technique to Potential Flow Problems", Trans. A.S.M.E., Journal of Applied Mechanics, Ser. E, Vol. 38, December, 1971, pp. 798-802.

13. Martin, H.C., "Finite Element Analysis of Fluid Flows", Proc. of 2nd Conf. on Matrix Methods in Structural Mechanics, (AFFDL-TR-68-150), Wright Patterson Air Force Base, Dayton, Ohio, October, 1968.
14. Argyris, J.H. and Mareczek, G., "Potential Flow Analysis by Finite Elements", Ing-Arch., Vol. 42, No. 1, December, 1972, pp. 1-25.
15. Chan, S.T.K. and Larock, B.E., "Fluid Flows from Axisymmetric Orifices and Values", A.S.C.E., Vol. 99, No. HY1, Proc. Paper 9465, January, 1973, pp. 81-97.
16. Sarpkaya, T. and Hiriart, G., "Analysis of Curved Target Type Thrust Reversers", A.I.A.A. J., Vol. 13, No. 2, February, 1975, pp. 185-192.
17. Schlichting, H., Boundary Layer Theory, 6th Ed., Translated by J. Kestin, McGraw-Hill, 1968.
18. White, F.M., Viscous Fluid Flows, McGraw-Hill, 1974.
19. Pozvonkov, F.M., Shurgalskii, E.F. and Akselrod, L.S., "Heat Transfer at a Melting Flat Plate Under Conditions of Forced Convection and Laminar Boundary Layer", International Journal of Heat and Mass Transfer, Vol. 13, 1970, pp. 957-962.
20. Conte, S.D., and deBoor, C., Elementary Numerical Methods, An Algorithmic Approach, 2nd Ed., McGraw Hill, 1972.
21. Mitchell, J.H., "On the Theory of Free Streamline", Philosophical Transactions of the Royal Society, Vol. 181A, 1890, pp. 389-431.
22. Ehrlich, F.F., "Some Hydrodynamic Aspects of Values", A.S.M.E. Paper 55-A-114, 1955.
23. Miyazaki, H. and Silberman, E., "Flow and Heat Transfer on a Flat Plate Normal to a Two-Dimensional Laminar Jet Issuing from a Nozzle of Finite Height", International Journal of Heat and Mass Transfer, Vol. 15, 1972, pp. 2097-2107.
24. Donaldson, C. duP. and Snedeker, R.S., "A Study of Free Jet Impingement. Part I. Mean Properties of Free and Impinging Jets", Journal of Fluid Mechanics, Vol. 45, Part 2, 1971, pp. 281-319.



25. Watson, E.J., "The Radial Spread of a Liquid Jet over a Horizontal Plane", Journal of Fluid Mechanics, Vol. 20, Part 3, 1964, pp. 481-499.
26. Leclerc, A., "Deviation d'un Jet Liquide Par Une Plaque Normal à Son Axe. Determination de la Surface Libre Par Analogie Electrique", (Deviation of a Liquid Jet by Means of a Plate Normal to the Axis of the Former. Determination of the Free Surface by Electrical Analogy), La Houille Blanche, November/ December, 1950, p. 816.
27. Brady, W.G. and Ludwig, G., "Theoretical and Experimental Studies of Uniform Impinging Jets", American Helicopter Society Journal, Vol. 8, No. 2, April, 1963, pp. 1-13.
28. Scholtz, M.T. and Trass, O., "Mass Transfer in a Non-Uniform Impinging Jet", AIChE Journal, January, 1970, pp. 82-96.
29. Brdlik, P.M. and Savin, V.K., "Heat Transfer Between an Axisymmetric Jet and a Plate Held Normal to the Flow", Journal of Engineering Physics, Vol. 8, No. 2, 1965, pp. 146-155.
30. Brdlik, P.M. and Savin, V.K., "Heat Transfer in the Vicinity of the Stagnation Point in an Axisymmetric Jet Flowing over Surfaces Normal to the Flow", Journal of Engineering Physics, Vol. 10, No. 4, 1966, pp. 423-428.
31. Donaldson, C. duP., Snedeker, R.S. and Margolis, D.P., "A Study of Free Jet Impingement. Part 2. Free Jet Turbulence Structure and Impingement Heat Transfer", Journal of Fluid Mechanics, Vol. 45, Part 3, 1971, pp. 477-512.
32. Sitharamayya, S. and Raju, K.S., "Heat Transfer Between an Axisymmetric Jet and a Plate Held Normal to the Flow", Canadian Journal of Chemical Engineering, Vol. 47, 1969, pp. 365-368.
33. Ravuri, R. and Tabakoff, W., "A Numerical Solution for the Heat Transfer Between an Axisymmetric Air Jet and a Heated Plate", A.S.M.E. Paper 75-WM-HT-106, 1975.
34. Tani, I. and Komatsu, Y., "Impingement of a Round Jet on a Flat Surface", 11th International Conference on Applied Mechanics, 1966, pp. 672-676.

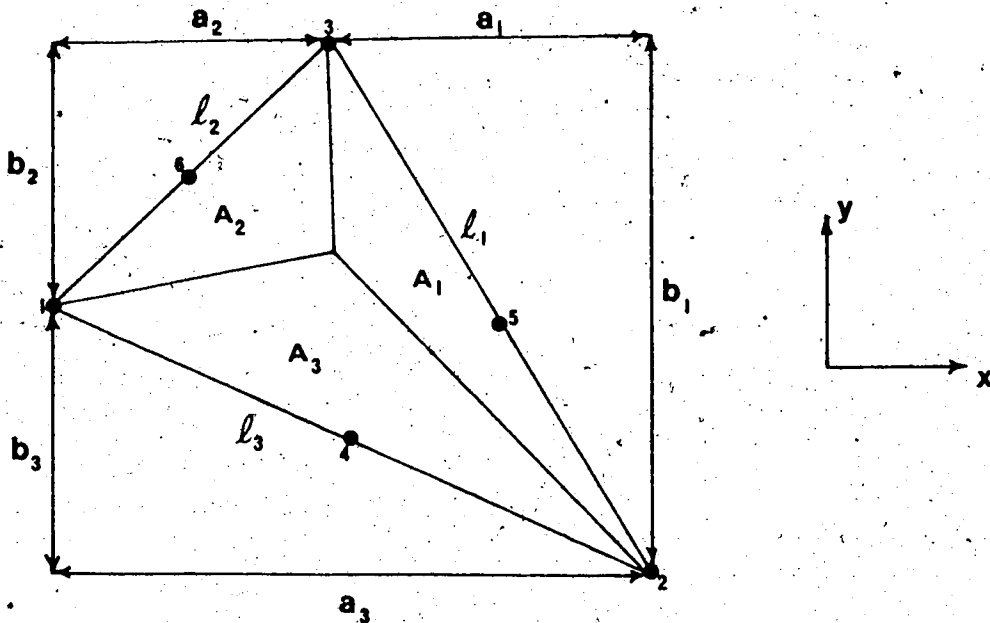
35. Chaudhury, Z.H., "Heat Transfer in a Radial Liquid Jet", Journal of Fluid Mechanics, Vol. 20, Part 3, 1964, pp. 501-511.
36. Beltaos, S. and Rajarathnam, N., "Impinging Circular Turbulent Jets", Journal of the Hydraulics Division, A.S.C.E., Vol. 100, 1974, pp. 1313-1328.
37. Glauser, M.B., "The Wall Jet", Journal of Fluid Mechanics, Vol. 1, 1956, pp. 625-643.
38. Gordon, R. and Akfirat, J.C., "The Role of Turbulence in Determining Heat Transfer Characteristics of Impinging Jets", International Journal of Heat and Mass Transfer, Vol. 8, 1965, pp. 1261-1272.
39. Traci, R.M. and Wilcox, D.C., "Free Stream Turbulence Effects on Stagnation Point Heat Transfer", A.I.A.A. Journal, Vol. 13, No. 7, 1975, pp. 890-896.
40. Savino, J.M., Zumdick, J.F. and Siegal, R., "Experimental Study of Freezing and Melting of Flowing Warm Water at a Stagnation Point on a Cold Plate", Fourth International Heat Transfer Conference, Cu 2.10, 1970, Paris.
41. Yen, Y.C., "Heat Transfer Characteristics of a Bubble Induced Water Jet Impinging on an Ice Surface", International Journal of Heat and Mass Transfer, Vol. 18, 1975, pp. 917-926.
42. Mellor, M., "Cutting Ice with Continuous Jets", Second International Symposium on Jet Cutting Technology, Paper G5, April, 1974, Cambridge, pp. G5-65-G5-76.
43. Yen, Y.C. and Zehnder, A., "Melting Heat Transfer with Water Jet", International Journal of Heat and Mass Transfer, Vol. 16, 1973, pp. 219-223.
44. Gilpin, R.R., "The Ablation of Ice by a Water Jet", Transactions of the C.S.M.E., Vol. 2, No. 2, 1973-1974, pp. 91-96.
45. Plotkin, A., "The Flow of a Laminar Incompressible Jet Along a Parabola", Transactions of the A.S.M.E., Ser. E, Journal of Applied Mechanics, March, 1972, pp. 13-17.
46. Krieth, F., Principles of Heat Transfer, 3rd Ed., Intext Educational Publishers, New York, 1973.

47. Sparrow, E.M. and Lee, L., "Analysis of the Flow Field and Impingement Heat/Mass Transfer Due to a Non-Uniform Slot Jet", Transactions of the A.S.M.E., Ser. C, Journal of Heat Transfer, May, 1975, pp. 191-197.
48. Baines, W.D. and Keffer, J.F., "Shear Stress and Heat Transfer at a Stagnation Point", International Journal of Heat and Mass Transfer, Vol. 19, pp. 21-26, 1976.
49. Schnurr, N.M., Williamson, J.W. and Tatom, J.W., "An Analytical Investigation of the Impingement of Jets on Curved Deflectors", A.S.M.E. Journal, Vol. 10, No. 11, 1972, pp. 1430-1435.
50. Yen, Y.C. and Tien, C., "Laminar Heat Transfer over a Melting Plate, the Modified Leveque Problem", Journal of Geophysical Research, Vol. 68, Part 3, 1963, pp. 3673-3678.
51. Merk, H.J., "The Influence of Melting and Anomalous Expansion on the Thermal Convection in Laminar Boundary Layers", Applied Scientific Research, Sec. A, Vol. 4, 1954, pp. 435-452.
52. Tien, C. and Yen, Y.C., "The Effect of Melting on Forced Convection Heat Transfer", Journal of Applied Meteorology, Vol. 4, August, 1965, pp. 523-527.
53. Griffin, O.M., "Heat, Mass, and Momentum Transfer During the Melting of Glacial Ice in Sea Water", Transactions of the A.S.M.E., Ser. C, Journal of Heat Transfer, August, 1973, pp. 317-323.
54. Cheng, E.H. and Williams, J.C., "Curvature Effects on Heat Transfer Near a Forward Stagnation Point", 5th International Heat Transfer Conference, 1974.
55. Ahlberg, J.H., Nielson, E.N. and Walsh, J.L., The Theory of Splines and Their Application, "The Cubic Spline", Chapter 2, Academic Press, 1967.

## APPENDIX 1

### FINITE ELEMENT MATRIX FORMULATION

In the finite element method described in Chapter III the solution of the potential flow field depended on the formulation of element matrices. By the use of area coordinates, these matrices may be found once and for all. In this appendix the element matrices for a general triangle as shown below for both two-dimensional and axisymmetric flows is briefly discussed. The notation of Chapter III is used. This discussion follows that of Chan [11].



### A.1 Matrices for Two-Dimensional Flow

From Chapter III the element matrices are

$$S_{ij}^m = \iint_{A^m} (T_i T_j + \hat{T}_i \hat{T}_j) dA \quad (i, j=1-6) \quad A.1$$

$$SL_i^m = \oint_{C^m} x_i \left( \frac{\partial \phi}{\partial n} \right)^a ds \quad A.2$$

with

$$\begin{aligned} \langle T_1, \dots, T_6 \rangle = & \langle (4\varepsilon_1 - 1) \frac{b_1}{2A^m}, (4\varepsilon_2 - 1) \frac{b_2}{2A^m}, \\ & (4\varepsilon_3 - 1) \frac{b_3}{2A^m}, \frac{2(\varepsilon_2 b_1 + \varepsilon_1 b_2)}{A^m}, \\ & \frac{2(\varepsilon_3 b_2 + \varepsilon_2 b_3)}{A^m}, \frac{2(\varepsilon_1 b_3 + \varepsilon_3 b_1)}{A^m} \rangle \quad A.3 \end{aligned}$$

$$\langle X_1, \dots, X_6 \rangle = \langle \varepsilon_1(2\varepsilon_1 - 1), \varepsilon_2(2\varepsilon_2 - 1), \varepsilon_3(2\varepsilon_3 - 1),$$

$$4\varepsilon_1\varepsilon_2, 4\varepsilon_2\varepsilon_3, 4\varepsilon_3\varepsilon_1 \rangle \quad A.4$$

$$\langle a_1, a_2, a_3 \rangle = \langle (x_3 - x_2), (x_1 - x_3), (x_2 - x_1) \rangle \quad A.5$$

$$\langle b_1, b_2, b_3 \rangle = \langle (y_2 - y_3), (y_3 - y_1), (y_1 - y_2) \rangle \quad A.6$$

$$\langle \xi_1, \xi_2, \xi_3 \rangle = \left\langle \frac{A_1}{A^m}, \frac{A_2}{A^m}, \frac{A_3}{A^m} \right\rangle \quad A.7$$

and

$$A^m = (a_1 b_3 - a_3 b_1) / 2 \quad A.8$$

The array  $\hat{T}_i$  is found by replacing the b's with a's in the expression for  $T_i$ .

Now substitution of the appropriate quantities into the matrix equations A.1 and A.2 enables their evaluation. For example to evaluate  $S_{11}$  both  $i$  and  $j$  are set equal to one and

$$\begin{aligned} S_{11}^m &= \iint_{A^m} (T_1 T_1 + \hat{T}_1 \hat{T}_1) dA \\ &= \frac{1}{(2A^m)^2} \iint_{A^m} \left[ (4\xi_1 - 1)^2 b_1^2 + (4\xi_1 - 1)^2 a_1^2 \right] dA \\ &= \frac{a_1^2 + b_1^2}{(2A^m)^2} \iint_{A^m} \left[ 16 \xi_1^2 - 8 \xi_1 + 1 \right] dA \end{aligned}$$

A convenient formula exists for find integrals in area co-

ordinates [8]. For integrating area coordinates over the area of a triangular element

$$\iint_A \xi_1^\alpha \xi_2^\beta \xi_3^\gamma dA = \frac{\alpha! \beta! \gamma!}{(\alpha + \beta + \gamma + 2)!} 2A^m \quad \text{A.9}$$

Using A.9

$$\iint_A 16\xi_1^2 dA = 16 \frac{2! 0! 0!}{(2 + 0 + 0 + 2)!} 2A^m = \frac{8}{3} A^m$$

$$\iint_A 8\xi_1 dA = 8 \frac{1! 0! 0!}{(1 + 0 + 0 + 2)!} 2A^m = \frac{8}{3} A^m$$

$$\iint_A 1 dA = \frac{0! 0! 0!}{(0 + 0 + 0 + 2)!} 2A^m = A^m$$

Combining

$$S_{11}^m = \frac{(a_1^2 + b_1^2)}{4A^m}$$

The remaining components are found in a similar manner. Letting  $P_{ij} = (a_i a_j + b_i b_j) / 12A^m$  the element matrix for the given triangle is given below.

$$S_{11}^m = 3P_{11}$$

$$S_{12}^m = S_{21}^m = -P_{12}$$

$$S_{13}^m = S_{31}^m = -P_{13}$$

$$S_{14}^m = S_{41}^m = 4P_{12}$$

$$S_{15}^m = S_{51}^m = 0$$

$$S_{16}^m = S_{61}^m = 4P_{13}$$

$$S_{22}^m = 3P_{22}$$

$$S_{23}^m = S_{32}^m = -P_{23}$$

$$S_{24}^m = S_{42}^m = 4P_{12}$$

A.10

$$S_{25}^m = S_{52}^m = 4P_{23}$$

$$S_{26}^m = S_{62}^m = 0$$

$$S_{33}^m = 3P_{33}$$

$$S_{34}^m = S_{43}^m = 0$$



$$S_{35}^m = S_{53}^m = 4P_{23}$$

$$S_{36}^m = S_{63}^m = 4P_{13}$$

$$S_{44}^m = 8(P_{33} - P_{12})$$

$$S_{45}^m = S_{54}^m = 8P_{13}$$

$$S_{46}^m = S_{64}^m = 8P_{23}$$

$$S_{55}^m = 8(P_{11} - P_{23})$$

$$S_{56}^m = S_{65}^m = 8P_{12}$$

$$S_{66}^m = 8(P_{22} - P_{13})$$

Now the boundary conditions are considered in order to evaluate the load matrix equation A.2. The symbols  $(\frac{\partial\phi}{\partial n})^1$ ,  $(\frac{\partial\phi}{\partial n})^2$ , and  $(\frac{\partial\phi}{\partial n})^3$  represent the specified normal velocity component on sides  $\ell_1$ ,  $\ell_2$  and  $\ell_3$ . Note that if side  $\ell_i$  is not on the boundary then  $(\frac{\partial\phi}{\partial n})^i$  must be zero. In the problem under consideration these specified normal velocity components are constant over each individual boundary segment.

The integral over the triangular area is given by

$$\oint_{C_m} \phi \left( \frac{\partial \phi}{\partial n} \right)^a ds = \int_{\ell_1} \phi_i \chi_i \left( \frac{\partial \phi}{\partial n} \right)^1 ds + \int_{\ell_2} \phi_i \chi_i \left( \frac{\partial \phi}{\partial n} \right)^2 ds \\ + \int_{\ell_3} \phi_i \chi_i \left( \frac{\partial \phi}{\partial n} \right)^3 ds$$

Consider the first integral

$$\int_{\ell_1} \phi_i \chi_i \left( \frac{\partial \phi}{\partial n} \right)^1 ds = \left( \frac{\partial \phi}{\partial n} \right)^1 \int_{\ell_1} \phi_i \chi_i ds \quad i = 1 \text{ to } 6$$

On side 1  $\xi_1 = 0$  so  $\xi_2 + \xi_3 = 1$  or  $\xi_2 = 1 - \xi_3$  and since the integrations are carried out in a counter clockwise manner  $ds = \ell_1 d\xi_3 = -\ell_1 d\xi_2$  and the integral becomes noting the summation convention.

$$\int_{\ell_1} \phi_i \chi_i \left( \frac{\partial \phi}{\partial n} \right)^1 ds = \left( \frac{\partial \phi}{\partial n} \right)^1 \ell_1 \int_{\ell_1} \left[ \phi_2 \xi_2 (2\xi_2 - 1) \right. \\ \left. + \phi_3 \xi_3 (2\xi_3 - 1) + 4\xi_2 \xi_3 \phi_5 \right] d\xi_3 \\ = \left( \frac{\partial \phi}{\partial n} \right)^1 \ell_1 \int_0^1 \left[ \phi_2 (1 - \xi_3)(1 - 2\xi_3) \right. \\ \left. + \phi_3 \xi_3 (2\xi_3 - 1) + 4(1 - \xi_3)\xi_3 \phi_5 \right] d\xi_3$$

By taking the partial derivatives of the above integral with respect to  $\phi_2$ ,  $\phi_3$  and  $\phi_5$  results in

$$\frac{\partial}{\partial \phi_2} \left[ \int_{\ell_1} \phi \frac{\partial \phi^1}{\partial n} ds \right] = \frac{\frac{\partial \phi^1}{\partial n} \ell_1}{6}$$

$$\frac{\partial}{\partial \phi_3} \left[ \int_{\ell_1} \phi \frac{\partial \phi^1}{\partial n} ds \right] = \frac{\frac{\partial \phi^1}{\partial n} \ell_1}{6}$$

$$\frac{\partial}{\partial \phi_5} \left[ \int_{\ell_1} \phi \left( \frac{\partial \phi}{\partial n} \right)^1 ds \right] = \frac{4 \left( \frac{\partial \phi}{\partial n} \right)^1 \ell_1}{6}$$

Similar results can be obtained by considering the other two integrals. In this way the load matrix is obtained as

$$SL_1 = \left( \left( \frac{\partial \phi}{\partial n} \right)^2 \ell_2 + \left( \frac{\partial \phi}{\partial n} \right)^3 \ell_3 \right) / 6$$

$$SL_2 = \left( \left( \frac{\partial \phi}{\partial n} \right)^3 \ell_3 + \left( \frac{\partial \phi}{\partial n} \right)^1 \ell_1 \right) / 6$$

$$SL_3 = \left( \left( \frac{\partial \phi}{\partial n} \right)^1 \ell_1 + \left( \frac{\partial \phi}{\partial n} \right)^2 \ell_2 \right) / 6$$

A.11

$$SL_4 = 2 \left( \frac{\partial \phi}{\partial n} \right)^3 \ell_3 / 3$$

$$SL_5 = 2\left(\frac{\partial\phi}{\partial n}\right)^1 l_1/3$$

$$SL_6 = 2\left(\frac{\partial\phi}{\partial n}\right)^2 l_2/3$$

A physical interpretation of the load matrix may be obtained by considering the flux of velocity across a boundary surface.

## A.2 Matrices for Axisymmetric Flow

From Chapter III the element matrices are given by

$$SA_{ij}^m = \iint_{A^m} (T_i T_j + \hat{T}_i \hat{T}_j) r dA \quad (i, j = 1 \text{ to } 6) \quad A.12$$

and

$$SLA_i^m = \oint_{C^m} \chi_i \left(\frac{\partial\phi}{\partial n}\right)^a r ds$$

with arrays  $T_i^m$ ,  $\hat{T}_i^m$ ,  $\chi_i$ ,  $a_i$  and  $A^m$  defined as before in two-dimensions. However the array  $b_i$  is defined as

$$\langle b_1, b_2, b_3 \rangle = \langle (r_2 - r_3), (r_3 - r_1), (r_1 - r_2) \rangle \quad A.13$$

Also the variable  $r$  is defined as a radial coordinate as

$$r = r_1 \xi_1 + r_2 \xi_2 + r_3 \xi_3$$

A.14

The procedure is exactly the same as for the two-dimensional case and the element matrix and load matrix for axisymmetric flows are listed below. Here  $P_{ij}$  is used to represent the sum  $(a_i a_j + b_i b_j)/60 A^m$ .

$$SA_{11}^m = 3P_{11}(3r_1 + r_2 + r_3)$$

$$SA_{12}^m = SA_{21}^m = -P_{12}(2r_1 + 2r_2 + r_3)$$

$$SA_{m3}^m = SA_{31}^m = -P_{13}(2r_1 + r_2 + 2r_3)$$

$$SA_{14}^m = SA_{41}^m = P_{11}^o(3r_1 - 2r_2 + r_3) + P_{12}(14r_1 + 3r_2 + 3r_3)$$

$$SA_{15}^m = SA_{51}^m = P_{12}(3r_1 - r_2 - 2r_3) + P_{13}(3r_1 - 2r_2 - r_3)$$

$$SA_{16}^m = SA_{61}^m = P_{11}(3r_1 - r_2 - 2r_3) + P_{13}(14r_1 + 3r_2 + 3r_3)$$

$$SA_{22}^m = 3P_{22}(r_1 + 3r_2 + r_3)$$

$$SA_{23}^m = SA_{32}^m = -P_{23}(r_1 + 2r_2 + 2r_3)$$

$$SA_{24}^m = SA_{42}^m = P_{12}(3r_1 + 14r_2 + 3r_3) + P_{22}(-2r_1 + 3r_2 - r_3)$$

$$SA_{25}^m = SA_{52}^m = P_{22}(-r_1 + 3r_2 - 2r_3) + P_{23}(3r_1 + 14r_2 + 3r_3)$$

$$SA_{26}^m = SA_{62}^m = P_{12}(-r_1 + 3r_2 - 2r_3) + P_{23}(-2r_1 + 3r_2 - r_3)$$

$$SA_{33}^m = P_{33}(r_1 + r_2 + 3r_3)$$

$$SA_{34}^m = SA_{43}^m = P_{13}(-r_1 - 2r_2 + 3r_3) + P_{13}(-2r_1 - r_2 + 3r_3)$$

$$SA_{35}^m = SA_{53}^m = P_{23}(3r_1 + 3r_2 + 14r_3) + P_{33}(-r_1 - 2r_2 + 3r_3)$$

$$SA_{36}^m = SA_{63}^m = P_{13}(3r_1 + 3r_2 + 14r_3) + P_{33}(-r_1 - r_2 + 3r_3)$$

$$SA_{44}^m = 8(P_{11}(r_1 + 3r_2 + r_3) + P_{12}(2r_1 + 2r_2 + r_3)$$

$$+ P_{22}(3r_1 + r_2 + r_3))$$

$$SA_{45}^m = SA_{54}^m = 8P_{13}(r_1 + 3r_2 + r_3) - 4(P_{12}r_1 + P_{22}r_2 + P_{23}r_3)$$

$$SA_{46}^m = SA_{64}^m = 8P_{23}(3r_1 + r_2 + r_3) - 4(P_{11}r_1 + P_{12}r_2 + P_{13}r_3)$$

$$SA_{55}^m = 8(P_{22}(r_1 + r_2 + 3r_3) + P_{23}(r_1 + 2r_2 + 2r_3)$$

$$+ P_{23}(r_1 + 3r_2 + r_3))$$

$$SA_{56}^m = SA_{65}^m = 8P_{12}(r_1 + r_2 + 3r_3) - 4(P_{13}r_1 + P_{23}r_2 + P_{33}r_3)$$

$$SA_{66}^m = 8(P_{11}(r_1 + r_2 + 3r_3) + P_{13}(2r_1 + r_2 + 2r_3) + P_{33}(3r_1 + r_2 + r_3))$$

$$SAL_1^m = r_1 \left( \frac{\partial \phi^2}{\partial n} \ell_2 + \frac{\partial \phi^3}{\partial n} \ell_3 \right) / 6$$

$$SAL_2^m = r_2 \left( \frac{\partial \phi^3}{\partial n} \ell_3 + \frac{\partial \phi^1}{\partial n} \ell_1 \right) / 6$$

$$SAL_3^m = r_3 \left( \frac{\partial \phi^1}{\partial n} \ell_1 + \frac{\partial \phi^2}{\partial n} \ell_2 \right) / 6$$

$$SAL_4^m = (r_1 + r_2) \frac{\partial \phi^3}{\partial n} \ell_3 / 3$$

$$SAL_5^m = (r_2 + r_3) \frac{\partial \phi^1}{\partial n} \ell_1 / 3$$

$$SAL_6^m = (r_3 + r_1) \frac{\partial \phi^2}{\partial n} \ell_2 / 3$$

## APPENDIX 2

### COMPUTER PROGRAM AND CUBIC SPLINE INTERPOLATION

In this appendix the full computer program used to calculate the potential flow of an impinging jet and the resulting boundary layer is presented. A flow chart and a description of some of the important subroutines is given to aid in the understanding of this program. Also given is a description of the cubic spline interpolation technique used to calculate velocities and gradients of velocities on the impingement surface. The flow chart for the computer program is given in Figure A.1 and a description of the flow chart follows.

The first step is to read the input data required for the finite element and boundary layer analysis. As discussed in Chapter III only the nodal point data of the first six elements is required. Subroutine NGEN calculates the element node matrix for the remaining elements. Also formed are the matrices which consist of the nodes on various parts of the boundary. The X and Y or R and Z coordinates of the nodes on the boundary are read in and the coordinates of all other nodes are calculated in subroutine COORD. Every time a boundary node is moved, as in the adjustment of the free surface subroutine COORD must be called to recal-



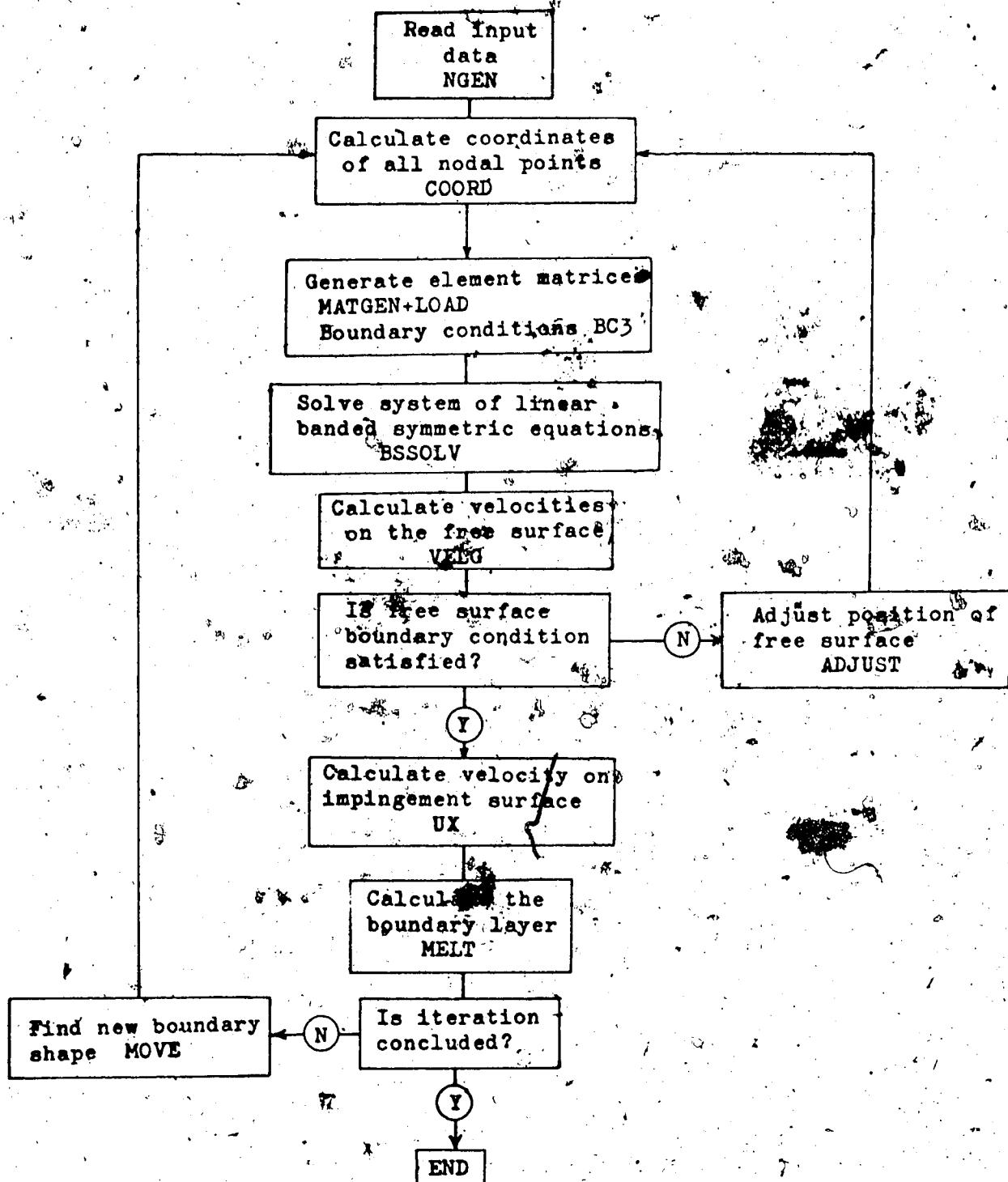


Figure A.1 Computer program flowchart

culate the coordinates of all the other nodes.

Next the element matrices are calculated in subroutines MATGEN and LOAD while specified boundary conditions are generated in BC3. The resulting set of linear, symmetric banded equations are solved by subroutine BSSOLV. Depending on the form chosen the output from BSSOLV is either the nodal point velocity potential or the nodal point stream function value. The velocities at each of the nodes are now calculated in subroutine VELG. Subroutine ADJUST checks the velocities on the free surface with the velocity at the tip of the nozzle and adjusts the coordinates of the free surface node in the manner described in Chapter III. If the free surface boundary condition is satisfied, the program carries on, if not then with the adjusted free surface the program recalculates the potential flow. This iteration procedure for finding the free surface is continued until the free surface boundary condition is satisfied.

Subroutine UX then obtains the tangential and normal velocity components at points on the impingement surface from the X and Y or R and Z components of velocity calculated by subroutine VELG. This is in preparation for the boundary layer calculation contained in subroutine MELT. In this subroutine the position of the melted surface is calculated and subroutine MOVE transforms the melted surface as described in Chapter VII. Now one iteration of the program has been completed. The option for continuing the melting process is available, and the computer program proceeds to

calculating the matrices for the potential flow on the adjusted melted surface and the process is repeated.

In order to understand the boundary layer calculation a brief description of subroutine MELT is given. The input to this subroutine are the coordinates of the points on the boundary and their tangential and normal velocities. First the coefficients required in the cubic spline interpolation of the velocities are calculated in subroutine BCS. The cubic spline interpolation routine is described in some detail by Ahlberg, Nielson and Walsh [55]. The parameters at the stagnation point are then evaluated.

Between each pair of nodal points the boundary layer parameters are calculated at ten equally spaced intervals. The velocity and gradient of velocity at these interior points are calculated by subroutine SPFUN using the cubic spline coefficients from subroutine BCS. Subroutine ROOT calculates the value of the new pressure gradient parameter  $\Lambda$  at each successive point on the boundary layer. The position of the melted surface is calculated at the nodes at the boundary as the solution procedure marches along the impingement surface.

The computer program follows.



```

NDEN= (NN-KE) / 7
NFS=NDEN/2
NEFN= (KE-7) / 7+1
NFAN=7
NBEE=3
NBNN=7
READ (7,902)  AMDA, EPS, XST, V0
READ (7,902)  PR, STE, R1, GAMMA
READ (7,902)  DT
902  FORMAT (4F20.6)
READ (7,901)  ((CHI (I, J), J=1, 3), I=1, 6)
901  FORMAT (3F20.6)
READ (7,900)  ((LEL (I, J), J=1, 6), I=1, 6)
CALL NGEN(NE, LEL, NN4, N4, NN, X, Y, NABN, NAB, NBCN, NBC, MCDN,
* NDE, NDEN, NDE, NEFN, NEF, NFAN, NFA, NBE, NBN)
DO 10 I=1, NABN, 2
NO=NAB(I)
READ (5,901)  X(NO), Y(NO)
10  CONTINUE
DO 11 I=1, NBN, 2
NO=NBC(I)
READ (7,901)  X(NO), Y(NO)
11  CONTINUE
DO 12 I=2, NDEN, 2
NO=NDE(I)
READ (5,901)  X(NO), Y(NO)
12  CONTINUE
DO 14 I=1, NEFN, 2
NO=NEF(I)
READ (5,901)  X(NO), Y(NO)
14  CONTINUE
CALL COORD(N4, NN4, NN, NE, LEL, Y, X)
CALL BAND(NBW, NN, NE, LEL)
IF (NBW.GT.KBW) GO TO 300

```

```

C
C
C
START MELTING ITERATIONS

```

```
DO 500 IJK=1,NT
```

```

C
C
C
START ITERATIONS TO FIND FREE SURFACE

```

```
DO 1 LL=1,NI
LMI=LL
```

```

C
C
C
C
CALCULATE ELEMENT MATRICES
INSERT BOUNDARY CONDITIONS

```

```
DO 17 M=1,NN
```

```

DO 17 N=1,NBW
17 GS(M,N)=0.0
DO 15 M=1,NN
15 GL(M)=0.0
LMM=0
DO 20 L=1,NE
CALL NODE(NN,NE,LEL,Y,X,IER)
IF(IER.EQ.1) GO TO 301
CALL MATGEN(GS,NN,NE,LEL,NA,NBW)
DO 20 I=1,NBEE
IF(L.EQ.NBE(I)) GO TO 22
GO TO 20
22 CALL LOAD(GL,NN,NE,LEL,NA,NBN,NBNN,VO)
20 CONTINUE
CALL BC3(GS,GL,NCD,NCDN,NN,NBW)

```

SOLVE LINEAR BANDED SYMMETRIC SYSTEM

```
CALL BSSOLV(NN,NBW,GS,GL)
```

CALCULATE NODAL POINT VELOCITIES

```

DO 29 I=1,NN
DO 29 J=1,4
GS(I,J)=0.0
IF(J.EQ.4) GS(I,J)=1.0
29 CONTINUE
DO 30 L=1,NE
CALL NODE(NN,NE,LEL,Y,X,IER)
IF(IER.EQ.1) GO TO 301
CALL VELG(NN,NBW,NE,LEL,GL,GS)
30 CONTINUE
KE6=KE-6
SUM=0.0
VIA=GS(KE,3)
UF=VIA/GS(KE6,3)
DO 60 M=1,NN
DO 60 I=1,3
60 GS(M,I)=GS(M,I)/VIA
VIA=1.0

```

ADJUST FREE SURFACE

```
CALL ADJUST(NDE,NDEN,VIA,Y,X,GS,NN,NBW,LMM,AMDA,EPS)
IF(LMM.EQ.NFS) GO TO 100
```

```

CALL COORD(N4, NN4, NN, NE, LEL, Y, X)
1 CONTINUE
GO TO 302
100 WRITE(6,800) LNI
800 FORMAT('0', 'FREE SURFACE LOCATED # OF ITERATIONS=', I4)
WRITE(6,904) UP
904 FORMAT('0', 'FREE SURFACE VELOCITY', F10.6)
WRITE(6,801)
801 FORMAT('0', 'NODE', 11X, 'VELOCITY', 20X, 'X', 22X, 'Y')
DO 70 J=2, NDE, 2
LJ=NDE(J)
70 WRITE(6,802) LJ, GS(LJ,3), X(LJ), Y(LJ)
802 FORMAT(' ', I3, 5X, F15.6, 9X, F15.6, 9X, F15.6)

```

PREPARE VELOCITIES FOR BOUNDARY LAYER

```
CALL SX(NBC, NBCN, X, Y, SX, SZ, SR, GS, NN, NBW, VT, VN, VIA)
```

CALCULATE BOUNDARY LAYER

```

CALL MELT(NBCN, VT, SX, SZ, SR, PB, STE, R1, GAMMA, NA, NDI,
*ZCOR, IER, UP, DT, NSS)
IF IER.GT.0) GO TO 999
WRITE(6,198)
198 FORMAT('0', 'POSITION OF MELTED SURFACE')
WRITE(6,199) (NBC(I), ZCOR(I), Y(NBC(I))), I=1, NBCN)
199 FORMAT('0', 3(I5, 2F15.6))
CALL MOVE(ZCOR, NBC, NBCN, X, Y, NN, NDE, NDE)
CALL COORD(N4, NN4, NN, NE, LEL, Y, X)
WRITE(6,200)
200 FORMAT('0', 'RELOCATED COORDINATES ON THE SURFACE')
WRITE(6,201) (NBC(I), X(NBC(I)), Y(NBC(I))), I=1, NBCN)
201 FORMAT('0', 3(I5, 2F15.6))
500 CONTINUE

```

```
GO TO 999
```

```

300 WRITE(6,400) NBW
400 FORMAT('1', 'BANDWIDTH TOO LARGE', I4)
GO TO 999
301 WRITE(6,401) IER
401 FORMAT('1', 'NEGATIVE AREA IER=', I3)
GO TO 999
302 WRITE(6,402) LNI
402 FORMAT('1', 'FREE SURFACE NOT FOUND WITHIN', I3, 2X,
*'ITERATIONS')
999 CONTINUE
DO 39 I=1, NBCN, 2

```

```
NO=NBC(I)  
39 WRITE(10,901) X(NO),Y(NO)  
DO 40 I=2,NDEN,2  
NI=NDE(I)  
40 WRITE(10,901) X(NI),Y(NI)  
STOP  
END
```



```

C*****
C
C          SUBROUTINES FOR FINITE ELEMENT PROGRAM
C
C*****
SUBROUTINE COORD(N4, NN4, NN, NE, LEL, Y, X)
REAL Y(NN), X(NN)
INTEGER N4(NN4, 4), LEL(NE, 6)
DO 300 N=1, NN4
  X(N4(N, 3)) = (X(N4(N, 1)) + 3.0*X(N4(N, 4))) * 0.25
  Y(N4(N, 3)) = (Y(N4(N, 1)) + 3.0*Y(N4(N, 4))) * 0.25
  X(N4(N, 2)) = (3.0*Y(N4(N, 1)) + Y(N4(N, 4))) * 0.25
  Y(N4(N, 2)) = (3.0*X(N4(N, 1)) + X(N4(N, 4))) * 0.25
300 CONTINUE
DO 301 L=1, NE
DO 301 I=1, 3
  J=I+1
  IF(J.EQ.4) J=1
  K=I+3
  LI=LEL(L, I)
  LJ=LEL(L, J)
  LK=LEL(L, K)
  Y(LK) = 0.5*(Y(LI) + Y(LJ))
  X(LK) = 0.5*(X(LI) + X(LJ))
301 CONTINUE
RETURN
END

C
C
SUBROUTINE BAND(NBW, NN, NE, LEL)
INTEGER LEL(NE, 6)
NBW=1
DO 1 L=1, NE
DO 1 I=1, 6
DO 1 J=1, 6
  LI=LEL(L, I)
  LJ=LEL(L, J)
  IF(LI.LT.LJ) GO TO 1
  NCOL=LI-LJ+1
  IF(NBW-NCOL.IT.0) NBW=NCOL
1 CONTINUE
RETURN
END

C
C
SUBROUTINE NCDE(NN, NE, LEL, Y, X, IER)
REAL Y(NN), X(NN), DY(3), DX(3)
INTEGER LEL(NE, 6)
COMMON /ELE/ L, DX, DY, YI, YJ, YK, XI, XJ, XK, AREA
YI=Y(LEL(L, 1))

```

```

YJ=Y (LEL (L, 2))
YK=Y (LEL (L, 3))
XI=X (LEL (L, 1))
XJ=X (LEL (L, 2))
XK=X (LEL (L, 3))
DX (1) =XK-XJ
DX (2) =XI-XK
DX (3) =XJ-XI
DY (1) =YJ-YK
DY (2) =YK-YI
DY (3) =YI-YJ
AREA=(DX (3) *DY (2) -DY (3) *DX (2)) /2.0
IF (AREA.LE.0.0) GO TO 7
RETURN
7 WRITE (6, 100) L, AREA
AREA=-AREA
IER=1
100 FORMAT ('0', 'ELEMENT', I10, ' NEG AREA', F16.3)
RETURN
END

```

```

SUBROUTINE MATGEN (GS, NM, NE, LEL, NA, NBW)
REAL S (3, 3), SA (6, 6), DX (3), DY (3), GS (NM, NBW)
INTEGER LEL (NE, 6)
COMMON /ELE/ L, DX, DY, YI, YJ, YK, XI, XJ, XK, AREA
RI=YI
RJ=YJ
RK=YK
IF (NA.EQ.0) GO TO 16
DO 13 I=1, 3
DO 13 J=1, 3
13 S (I, J) = (DX (I) *DX (J) +DY (I) *DY (J)) / (60.0*AREA)
SA (1, 1) =3*S (1, 1) * (3*RI+RJ+RK)
SA (1, 2) =-S (1, 2) * (2*RI+2*RJ+RK)
SA (1, 3) =-S (1, 3) * (2*RI+RJ+2*RK)
SA (1, 4) =S (1, 1) * (3*RI-2*RJ-RK) +S (1, 2) * (14*RI+3*RJ+3*RK)
SA (1, 5) =S (1, 2) * (3*RI-RJ-2*RK) +S (1, 3) * (3*RI-2*RJ-RK)
SA (1, 6) =S (1, 1) * (3*RI-RJ-2*RK) +S (1, 3) * (14*RI+3*RJ+3*RK)
SA (2, 2) =3*S (2, 2) * (RI+3*RJ+RK)
SA (2, 3) =-S (2, 3) * (RI+2*RJ+2*RK)
SA (2, 4) =S (1, 2) * (3*RI+14*RJ+3*RK) +S (2, 2) * (-2*RI+3*RJ-RK)
SA (2, 5) =S (2, 2) * (-RI+3*RJ-2*RK) +S (2, 3) * (3*RI+14*RJ+3*RK)
SA (2, 6) =S (1, 2) * (-RI+3*RJ-2*RK) +S (2, 3) * (-2*RI+3*RJ-RK)
SA (3, 3) =3*S (3, 3) * (RI+RJ+3*RK)
SA (3, 4) =S (1, 3) * (-RI-2*RJ+3*RK) +S (2, 3) * (-2*RI-RJ+3*RK)
SA (3, 5) =S (2, 3) * (3*RI+3*RJ+14*RK) +S (3, 3) * (-RI-2*RJ+3*RK)
SA (3, 6) =S (1, 3) * (3*RI+3*RJ+14*RK) +S (3, 3) * (-2*RI-RJ+3*RK)
SA (4, 4) =8*(S (1, 1) * (RI+3*RJ+RK) -SA (1, 2) +S (2, 2) *
* (3*RI+RJ+RK))

```

```

SA(4,5)=8*S(1,3)*(RI+3*RJ+RK)-4*(S(1,2)*RI+
*S(2,2)*RJ+S(2,3)*RK)
SA(4,6)=8*S(2,3)*(3*RI+RJ+RK)-4*(S(1,1)*RI+
*S(1,2)*RJ+S(1,3)*RK)
SA(5,5)=8*(S(2,2)*(RI+RJ+3*RK)-SA(2,3)+S(3,3)*
*(RI+3*RJ+RK))
SA(5,6)=8*S(1,2)*(RI+RJ+3*RK)-4*(S(1,3)*RI+
*S(2,3)*RJ+S(3,3)*RK)
SA(6,6)=8*(S(1,1)*(RI+RJ+3*RK)-SA(1,3)+S(3,3)*
*(3*RI+RJ+RK))
GO TO 17
16 CONTINUE
DO 20 I=1,3
DO 20 J=1,3
20 S(I,J)=(BX(I)*DX(J)+DY(I)*DY(J))/(12.0*AREA)
SA(1,1)=3.0*S(1,1)
SA(1,2)=-3.0*S(1,2)
SA(1,3)=3.0*S(1,3)
SA(1,4)=4.0*S(1,2)
SA(1,5)=0.0
SA(1,6)=4.0*S(1,3)
SA(2,2)=3.0*S(2,2)
SA(2,3)=-S(2,3)
SA(2,4)=4.0*S(2,3)
SA(2,5)=4.0*S(2,3)
SA(2,6)=0.0
SA(3,3)=3.0*S(3,3)
SA(3,4)=0.0
SA(3,5)=4.0*S(2,3)
SA(3,6)=4.0*S(1,3)
SA(4,4)=8.0*(S(3,3)-S(1,2))
SA(4,5)=8.0*S(1,3)
SA(4,6)=8.0*S(2,3)
SA(5,5)=8.0*(S(1,1)-S(2,3))
SA(5,6)=8.0*S(1,2)
SA(6,6)=8.0*(S(2,2)-S(1,3))
17 CONTINUE
DO 14 M=1,6
DO 14 N=1,6
14 SA(M,N)=SA(M,N)
DO 11 I=1,6
DO 11 J=1,6
LI=LEL(L,I)
LJ=LEL(L,J)
IF(LJ.LT.LI) GO TO 11
K=LJ-LI+1
GS(LI,K)=GS(LI,K)+SA(I,J)
11 CONTINUE
RETURN
END

```

C  
C

```

SUBROUTINE LCAD(GL, NN, NE, LEL, NA, NBN, NBNN, VO)
REAL GL(NN), DX(3), DY(3), SIDE(3), SL(6)
INTEGER LEL(NE,6), NBN(NBNN)
COMMON /ELE/ L, DX, DY, YI, YJ, YK, XI, XJ, XK, AREA
DO 38 I=1,3
38  SIDE(I)=SQRT(DX(I)**2+DY(I)**2)
    SIDE(1)=0.0
    SIDE(3)=0.0
    IF(NA.EQ.0) GO TO 40
    SL(1)=YI*VO*(SIDE(2)+SIDE(3))/6.0
    SL(2)=YJ*VO*(SIDE(3)+SIDE(1))/6.0
    SL(3)=YK*VO*(SIDE(1)+SIDE(2))/6.0
    SL(4)=(YI+YJ)*VO*SIDE(3)/3.0
    SL(5)=(YJ+YK)*VO*SIDE(1)/3.0
    SL(6)=(YI+YK)*VO*SIDE(2)/3.0
    GO TO 41
40  SL(1)=VO*(SIDE(2)+SIDE(3))/6.0
    SL(2)=VO*(SIDE(3)+SIDE(1))/6.0
    SL(3)=VO*(SIDE(1)+SIDE(2))/6.0
    SL(4)=2.0*VO*SIDE(3)/3.0
    SL(5)=2.0*VO*SIDE(1)/3.0
    SL(6)=2.0*VO*SIDE(2)/3.0
41  CONTINUE
    DO 42 M=1,6
    IF(L.LT.20) SL(M)=-SL(M)
42  CONTINUE
    DO 43 I=1,6
    DO 43 N=1, NBNN
    LI=LEL(L,I)
    NBB=NBN(N)
    IF(LI.EQ.NBB) GL(NBB)=GL(NBB)+SL(I)
43  CONTINUE
    RETURN
    END

```

C  
C

```

SUBROUTINE BSSOLV(NN, NBW, GS, GL)
REAL ST(18), GS(NN, NBW), GL(NN)
N=0
100 N=N+1
C   REDUCE PIVOT EQUATION
    GL(N)=GL(N)/GS(N,1)
    IF(N-NN) 150,300,150
150 DO 200 K=2, NBW
    ST(K)=GS(N,K)
200 GS(N,K)=GS(N,K)/GS(N,1)
C   REDUCE REMAINING EQUATIONS WITHIN SPAN
    DO 260 L=2, NBW

```

```

      I=N+L-1
      IF (NN-I) 260,240,240
240   J=0
      DO 250 K=L,NBW
      J=J+1
250   GS(I,J)=GS(I,J)-ST(L)*GS(N,K)
      GL(I)=GL(I)-ST(L)*GL(N)
260   CONTINUE
      GO TO 100
C     BACK SUBSTITUTION
300   N=N-1
      IF (N) 350,500,350
350   DO 400 K=2,NBW
      L=N+K-1
      IF (NN-L) 400,370,370
370   GL(N)=GL(N)-GS(N,K)*GL(L)
400   CONTINUE
      GO TO 300
500   CONTINUE
      WRITE(10,900)
900   FORMAT(' ','CALCULATED NODAL VALUES')
      DO 600 N=1,NN
      WRITE(10,901) N,GL(N)
901   FORMAT('0',I10,F20.6)
600   CONTINUE
      RETURN
      END
C
C
      SUBROUTINE VELG(NN,NBW,NE,LEL,GL,GS)
      REAL VELX(6),VELY(6),VEL(6),THETA(6),DX(3),DY(3),
      *T(6,6),TH(6,6),GS(NN,NBW),GL(NN),CHI(6,3)
      INTEGER LEL(NE,6)
      COMMON /SPEED/ CHI,VELX,VELY,VEL,THETA,T,TH,NB
      COMMON /ELE/ L,DX,DY,YI,YJ,YK,XI,XJ,YK,AREA
      PI=ARCOS(-1.E0)
      DO 2 I=1,6
      DO 2 J=1,3
      T(I,J)=(4.0*CHI(I,J)-1.0)*DY(J)/(2.0*AREA)
      TH(I,J)=(4.0*CHI(I,J)-1.0)*DX(J)/(2.0*AREA)
2     CONTINUE
      DO 3 I=1,6
      DO 3 J=1,3
      JJ=J+3
      K=J+1
      IF(K.EQ.4) K=1
      T(I,JJ)=2.0*(DY(J)*CHI(I,K)+DY(K)*CHI(I,J))/AREA
      TH(I,JJ)=2.0*(DX(J)*CHI(I,K)+DX(K)*CHI(I,J))/AREA
3     CONTINUE
      DO 4 I=1,6

```

```

SUMX=0.0
SUMY=0.0
DO 5 J=1,6
LJ=LEL(L,J)
SUMX=SUMX+GL(LJ)*T(I,J)
SUMY=SUMY+GL(LJ)*TH(I,J)
5 CONTINUE
VELX(I)=SUMX
VELY(I)=SUMY
IF(NB.EQ.0) VELX(I)=SUMY
IF(NB.EQ.0) VELY(I)=-SUMX
VEL(I)=SQRT(VELX(I)**2+VELY(I)**2)
THETA(I)=180.0*PI
LI=LEL(L,I)
IF(GS(LI,3).NE.0.0) GO TO 11
GS(LI,1)=VELX(I)
GS(LI,2)=VELY(I)
GS(LI,3)=VEL(I)
GO TO 4
11 GS(LI,4)=GS(LI,4)+1.0
VX=VELX(I)
VY=VELY(I)
VF=VEL(I)
GS(LI,1)=(VX+GS(LI,1)*(GS(LI,4)-1.0))/GS(LI,4)
GS(LI,2)=(VY+GS(LI,2)*(GS(LI,4)-1.0))/GS(LI,4)
GS(LI,3)=(VF+GS(LI,3)*(GS(LI,4)-1.0))/GS(LI,4)
4 CONTINUE
RETURN
END

```

C  
C

```

SUBROUTINE NGEN(NE,LEL,NN4,N4,NN,X,Y,NABN,NAB,NBCN,NBC,
* NCDN,NCD,NDEN,NDE,NEFN,NEP,NFAN,NFA,NBN,NBN)
REAL X(NN),Y(NN)
INTEGER LEL(NE,6),N4(NN4,4),NBE(3),NBN(7),NAB(NABN),
* NBC(NBCN),NCD(NCDN),NDE(NDEN),NEP(NEFN),NFA(NFAN)
COMMON /BOUND/ KS,KE,XST
NBN=3
NBN=7
DO 2 L=7,NE
J=L-6
DO 2 I=1,6
LJ=LEL(J,I)
2 LEL(L,I)=LJ+14
DO 3 I=1,NN4
J=(I-1)*14-1
DO 3 K=1,4
J=J+2
3 N4(I,K)=J
K=NE-6

```

```

DO 4 I=1,3
II=I*2
4 NBE(I)=II
K=NN-7
DO 5 I=1,7
NFA(I)=I
NBN(I)=I
K=K+1
5 NCD(I)=K
DO 6 I=1,NABN
K=(I-1)*7+1
Y(K)=0.0
6 NAB(I)=K
DO 7 I=1,NBCN
K=(I-1)*7+KS
7 NBC(I)=K
DO 8 I=1,NDEN
K=K+7*I
8 NDE(I)=K
DO 9 I=1,NEFN
K=7+7*(I-1)
Y(K)=0.5
9 NEF(I)=K
WRITE(10,800) ((LEL(I,J),J=1,6),I=1,NE)
800 FORMAT(6I15)
WRITE(10,800) ((M4(I,J),J=1,4),I=1,NN4)
WRITE(10,800) (NBE(I),I=1,NBEN)
WRITE(10,800) (NBN(I),I=1,NBNM)
WRITE(10,800) (NAB(I),I=1,NABN)
WRITE(10,800) (NBC(I),I=1,NBCN)
WRITE(10,800) (NCD(I),I=1,NCDN)
WRITE(10,800) (NDE(I),I=1,NDEN)
WRITE(10,800) (NEF(I),I=1,NEFN)
WRITE(10,800) (NFA(I),I=1,NFAN)
RETURN
END

```

C  
C

```

SUBROUTINE ADJUST(NDE,NDEN,VIA,Y,X,GS,NN,NBW,LMH,AMDA
*,EPS)

```

```

REAL Y(NN),X(NN),GS(NN,NBW)
INTEGER NDE(NDEN)
DO 1 J=2,NDEN,2
II=J-1
K=J+1
IF(J.EQ.NDEN) K=J
LI=NDE(II)
LJ=NDE(J)
LK=NDE(K)
WRITE(8,101) LJ,GS(LJ,3),VIA

```

```

101  FORMAT ('0', ' NODE', I5, ' VELOCITY', F12.5, ' ACTUAL VELOCITY'
      *, F12.5)
      YII=Y (LI)
      YJJ=Y (LJ)
      YKK=Y (LK)
      XII=X (LI)
      XJJ=X (LJ)
      XKK=X (LK)
      WRITE (8, 102)  LJ, XJJ, YJJ
102  FORMAT (I10, 2F20.8)
      IF (YII-YKK.EQ.0.0) GO TO 2
      SLOPE=(XII-XKK)/(YII-YKK)
      GO TO 3
2     SLOPE=1.0E10
3     CONTINUE
      IF (SLOPE.EQ.0.0) SLOPE=1.0E-10
      SLN=-1.0/SLOPE
      IF (ABS(GS(LJ,3)-VIA).LT.EPS) GO TO 4
      DIST=AMDA*((GS(LJ,3)/VIA)**2-1.0)
      D=DIST/SQRT(1.0+SLN**2)
      IF (SLN.GE.0.0) GO TO 9
      Y(LJ)=Y(LJ)+D
      X(LJ)=X(LJ)+D*SLN
      WRITE (8, 102)  LJ, X(LJ), Y(LJ)
      GO TO 1
9     CONTINUE
      Y(LJ)=Y(LJ)-D
      X(LJ)=X(LJ)-D*SLN
      WRITE (8, 102)  LJ, X(LJ), Y(LJ)
      GO TO 1
10   WRITE (8, 100)  LJ, GS(LJ,3)
100  FORMAT ('-', ' NO ADJUSTMENT NODE=', I5, ' VELOCITY=', F12.5)
      LHM=LHM+1
1     CONTINUE
      RETURN
      END

```

C  
C  
C  
C

```

SUBROUTINE BC3(GS, GL, NCD, NCDN, NN, NBW)
  POTENTIAL FLOW BOUNDARY CONDITIONS
  UNIFORM FLOW AT THE OUTLET
  SPECIFIED VELOCITY AT THE INPUT FROM SUBROUTINE LOAD
  REAL GS(NN, NBW), GL(NN)
  INTEGER NCD(NCDN)
  DO 1 I=1, NCDN
    K=NCD(I)
    K1=K
    GL(K)=0.0
    GS(K, 1)=1.0
  DO 1 J=2, NBW

```



```

K1=K1-1
GS(K1,J)=0.0
1 GS(K,J)=0.0
RETURN
END

```

C  
C

```

SUBROUTINE UX(NBC,NBCN,X,Y,SX,SZ,SR,GS,NN,NBW,VT,VN,VIA)
REAL X(NN),Y(NN),GS(NN,NBW),VT(NBCN),VN(NBCN),SUT(3),
*SUN(3),SX(NBCN),SZ(NBCN),SR(NBCN)
INTEGER NBC(NBCN)
DO 1 N=1,NBCN
VT(N)=0.0
1 VN(N)=0.0
DO 2 J=2,NBCN,2
I=J-1
K=J+1
II=NBC(I)
KK=NBC(K)
XI=X(II)
YI=Y(II)
XK=X(KK)
YK=Y(KK)
THE=ABS(ATAN((XK-XI)/(YK-YI)))
DO 2 M=1,3
JJ=J+M-2
NJJ=NBC(JJ)
SUT(M)=GS(NJJ,2)*COS(THE)-GS(NJJ,1)*SIN(THE)
SUN(M)=- (GS(NJJ,2)*SIN(THE)+GS(NJJ,1)*COS(THE))
IF(VT(JJ).EQ.0.0) GO TO 4
VT(JJ)=(VT(JJ)+SUT(M))/2.0
VN(JJ)=(VN(JJ)+SUN(M))/2.0
GO TO 2
4 VT(JJ)=SUT(M)
VN(JJ)=SUN(M)
2 CONTINUE
SX(1)=0.0
SZ(1)=4.0
SR(1)=0.0
DO 5 K=2,NBCN
KI=NBC(K)
XK=X(KI)
YK=Y(KI)
J=K-1
JI=NBC(J)
YJ=Y(JI)
XJ=X(JI)
SZ(K)=X(KI)
SR(K)=Y(KI)
5 SX(K)=SX(J)+SQRT((XK-XJ)**2+(YK-YJ)**2)

```

```

WRITE(6,100)
100 FORMAT(' ', 'NODE', 21X, 'S', 11X, 'TANGANTIAL VELOCITY', 7X,
*'NORMAL VELOCITY')
DO 3 I=1, NBCN
NI=NBC(I)
WRITE(6,101) NI, SX(I), VT(I), VN(I)
101 FORMAT(' ', I4, 10X, F15.6, 2.(8X, F15.6))
3 CONTINUE
RETURN
END

```

```

C
C*****
C
C          BOUNDARY LAYER SUBROUTINE MELT
C          AND ASSOCIATED SUBROUTINES
C
C*****
C
C

```

```

SUBROUTINE MELT(NBCN, U, S, ZA, R, PR, ST, R1, GAMMA, NA, M, ZCOR,
*IER, UP, DT, NSS)
REAL S(NBCN), U(NBCN), H(123), R(NBCN), GG(41), DG(41),
*ZA(NBCN), ZCOR(NBCN)
DO 10 I=1, NBCN
GG(I)=S(I)
U(I)=U(I)*UP
10 ZCOR(I)=ZA(I)
G=GAMMA
IER=0
PRP=SQRT(0.25+ST/3.0)-0.5
N=NBCN
NOP=N
P=PRP/PR
PP=P/R1
WRITE(6,200) ST, PR, P, R1
200 FORMAT('0', 'STEPAN NUMBER', F6.2, /, 'PRANDTL NUMBER', F6.2,
* /, 'MELTING PARAMETER', F10.6, /, 'BOUNDARY THICKNESS RATIO'
*, F10.6)
H(1)=0.0
ZS=0.0
DZ1=0.0
WS=0.0
DW1=0.0
CALL BCS(U, S, N, NOP, GG, DG, H, IER)
JJ=2
X=0.0
CALL SPFUN(H, U, S, N, X, JJ, V, DV)
CALL FUN(PR, ST, R1, G, PG, GGG, GK, GL, D1, D2, D3)
Z0=GK/DV
W0=D3*D3*R1*R1*Z0/(D2*D2)

```

```

IP(NA.EQ.0) ZS=Z0
IP(NA.EQ.0) WS=W0
IF (Z0.LT.0.0.CR.W0.LT.0.0) GO TO 300
THK2=SQRT(Z0)
THK3=SQRT(W0)
BL=THK2/D2
BLE=THK3/D3
VW=6.0*P/BLE
VW1=6.0*P/(R1*BL)
DUUDY=(2.0+G/6.0)/(BL+BL*PP)
DTDY=2.0/(BLE+BLE*PRP)
CTSR=V*DUUDY
WRITE(8,212) VW,VW1
212 FORMAT('0',' VW,VW1',2F20.6)
DWZ=VW*DT+CTSR*DT*WSS
ZA(1)=ZA(1)+DWZ
ZCOR(1)=ZA(1)
WRITE(6,207) ZCOR(1)
WRITE(8,800)
800 FORMAT('0',' STAGNATION FUNCTIONS')
WRITE(8,801)
801 FORMAT('0',' V,DV,G//D1,D2,D3//BL,BLE,Y(1)//DUUDY,DTDY
*,CTSR')
WRITE(8,207) V,DV,G
WRITE(8,207) D1,D2,D3
WRITE(8,207) BL,BLE,ZA(1)
WRITE(8,207) DUUDY,DTDY,CTSR
207 FORMAT(6F20.6)
DO 1 J=2,N
DEL=H(J)/H
THETA=ABS(ATAN((ZA(J)-ZA(J-1))/(R(J)-R(J-1))))
SIT=SIN(THETA)
CT=COS(THETA)
JJ=J
WRITE(8,205)
205 FORMAT('*****')
WRITE(8,202) JJ,X,S(JJ)
202 FORMAT('0',' NEW ELEMENT',I5,2F20.6)
DO 1 I=1,N
X=X+DEL
2 CONTINUE
CALL FUN(PB,ST,R1,G,PG,GGG,GK,GL,D1,D2,D3)
WRITE(8,208) X
208 FORMAT('0',40X,'***** X=',F20.6)
CALL SPFUN(H,U,S,N,X,JJ,V,DV)
RR=R(JJ-1)+DEL*I*(R(JJ)-R(JJ-1))/(S(JJ)-S(JJ-1))
SRR=RR
IF(NA.EQ.0) RR=1.0
ZZ=ZA(JJ-1)+I*(ZA(JJ)-ZA(JJ-1))/H
DZ2=RR*RR*PG/V

```

```

DW2=RR*RR*GGG/V
ZS=ZS+(DZ1+DZ2)*DEL/2.0
WS=WS+(DW1+DW2)*DEL/2.0
Z=ZS/(RR*RR)
W=WS/(RR*RR)
GK1=Z*DV
GL1=W*DV
IF(I.NE.N) GC TO 50
WRITE(8,204)
204 FORMAT('0', 'GK1,Z,ZS//GL1,W,WS//RM1')
WRITE(8,207) GK1,Z,ZS
WRITE(8,207) GL1,W,WS
IF(Z.LT.0.0.OR.W.LT.0.0) GO TO 301
RM1=SQRT(D2*D2*W/(D3*D3*Z))
WRITE(8,207) RM1
50 CONTINUE
IF(JJ.EQ.2) GO TO 3
CALL ROOT(PR,ST,R1,G,GK1,IFLAG,JJ)
IF(IFLAG.EQ.2) GO TO 500
3 CONTINUE
CALL FUN(PR,ST,R1,G,FG,GGG,GK,GL,D1,D2,D3)
DZ1=RR*RR*FG/V
DW1=RR*RR*GGG/V
C EVALUATE PARAMETERS
THK2=SQRT(Z)
THK3=SQRT(W)
BL=THK2/D2
BLE=THK3/D3
VW=6.0*P/BLE
VW1=6.0*P/(R1*BL)
DUUDY=(2.0+G/6.0)/(BL+BL*FP)
DTDY=2.0/(BLE+BLE*PRP)
CTSR=DUUDY*V
IF(I.NE.N) GC TO 51
WRITE(8,802)
802 FORMAT('0', 'V,DV,G//D1,D2,D3//BL,BLE//DUUDY,DTDY,CTSR')
WRITE(8,207) V,DV,G
WRITE(8,207) D1,D2,D3
WRITE(8,207) BL,BLE
WRITE(8,207) DUUDY,DTDY,CTSR
WRITE(8,212) VW,VW1
51 CONTINUE
DWZ=VW*CT*DT+NSS*CTSR*CT*DT
DWR=VW*SIT*DT+NSS*CTSR*SIT*DT
DWZN=VW*DT/CT+NSS*CTSR*DT/CT
ZN=ZZ+DWZ
RN=SRR+DWR
ZNN=ZZ+DWZN
IF(I.NE.N) GC TO 52
WRITE(8,209) VW,RN,ZN,ZNN

```

```

209  FORMAT('0','VN,RN,ZN,ZNN',4F20.6)
52   CONTINUE
    IF (I.EQ.M) ZCOR(J)=ZNN
1    CONTINUE
500  CONTINUE
    RETURN
300  IER=1
    WRITE(6,206) IER
206  FORMAT('0','ERROR',I4)
    WRITE(6,207) X,G,R1,V,DV
    WRITE(6,207) GK,GL,D1,D2,D3
    WRITE(6,207) ZO,W0
    RETURN
301  IER=2
    WRITE(6,206) IER
    WRITE(6,207) X,G,R1,V,DV
    WRITE(6,207) GK,GL,D1,D2,D3
    WRITE(6,207) Z,W,GK1,GL1
    RETURN
    END

```

C  
C

```

SUBROUTINE BCS (F,X,N,M,GG,DG,H,IER)
IMPLICIT REAL*4 (A-H,O-Z)
DIMENSION F(1),X(1),H(1),GG(1),DG(1)
WRITE(6,100)
IER=0
DO 1 J=2,M
H(J)=X(J)-X(J-1)
1  CONTINUE
DO 3 J=1,M
B=2.0
IF(J.EQ.1) GO TO 4
IF(J.EQ.M) GO TO 4
C=H(J+1)/(H(J)+H(J+1))
A=1.0-C
D=6.0*((F(J+1)-F(J))/H(J+1)-(F(J)-F(J-1))/H(J))
*/(H(J)+H(J+1))
GO TO 5
4  A=0.0
   C=0.0
   D=0.0
5  CONTINUE
CCC      Q(J)=H(N+J)      U(J)=H(2*N+J)
P=A*H(N+J-1)+B
10  IF(ABS(P).LT.1.E-40) GO TO 10
    H(N+J)=-C/P
    H(2*N+J)=(D-A*H(2*N+J-1))/P
    GO TO 3
10  IER=130

```

```

WRITE(6,301) IER
GO TO 18
3 CONTINUE
DO 11 K=2,N
J=N+1-K
11 H(2*N+J)=H(N+J)*H(2*N+J+1)+H(2*N+J)
DO 12 I=1,M
IF(GG(I).LT.X(1)) GO TO 13
IF(GG(I).GT.X(N)) GO TO 14
DO 15 J=2,N
JJ=J
IF(GG(I).LE.X(J)) GO TO 17
15 CONTINUE
13 JJ=2
IER=131
WRITE(6,302) IER,I
GO TO 17
14 JJ=N
IER=132
WRITE(6,302) IER,I
17 CONTINUE
A=X(JJ)-GG(I)
B=GG(I)-X(JJ-1)
C=H(JJ)
GG(I)=(H(2*N+JJ-1)*A*A*A+H(2*N+JJ)*B*B*B
**+(6.0*F(JJ-1)-H(2*N+JJ-1)*C*C)*A
2+(6.0*F(JJ)-H(2*N+JJ)*C*C)*B)/(6.0*C)
DG(I)=-1.0*H(2*N+JJ-1)*A*A/(2.0*C)
**+H(2*N+JJ)*B*B/(2.0*C)+(F(JJ)-F(JJ-1))/C
**-(H(2*N+JJ)-H(2*N+JJ-1))*C/6.0
12 CONTINUE
WRITE(6,101) (GG(I),I=1,M)
WRITE(6,101) (DG(I),I=1,M)
18 CONTINUE
100 FORMAT('0','OUTPUT FROM CUBIC SPLINE INTERPOLATION')
101 FORMAT(10F9.5)
301 FORMAT('0',///,T10,'ERROR',I3,///,T10,'NO SOLUTION')
302 FORMAT('0',///,T10,'ERROR',I3,'AT I=',I3,///,T10,
*' SOLUTION TRIED')
RETURN
END

```

C  
C

```

SUBROUTINE SEFUN(H,P,S,N,I, JJ,SPP,DSF)
DIMENSION H(1),S(1),F(1)
A=S(JJ)-X
B=X-S(JJ-1)
C=H(JJ)
NJJ=N*2+JJ
NJJ1=NJJ-1

```

```

SPP=(H(NJJ1)*A*A*A+H(NJJ)*B*B*B+(6.0*F(JJ-1)-
*H(NJJ1)*C*C)*A+(6.0*F(JJ)-H(NJJ)*C*C)*B)/(6.0*C)
DSP=-1.0*H(NJJ1)*A*A/(2.0*C)+H(NJJ)*B*B/(2.0*C)
*+(F(JJ)-F(JJ-1))/C-(H(NJJ)-H(NJJ1))*C/6.0
RETURN
END

```

```

SUBROUTINE FUN(PR,ST,R1,G,FG,GGG,GK,GL,D1,D2,D3)
PRP=SQRT(0.25+ST/3.0)-0.5
P=PRP/PR
PP=P/R1
R2=B1*R1
R3=R2*R1
R4=R3*R1
D1=(0.3-G/120.0+0.4*PP)/(1.0+PP)
D2=(7.4-G/15.0-G*G/144.0+G*PP/10.0+15.6*PP+7.2*PP*PP)
*/(63.0*(1.0+PP)**2)
GK=D2*D2*G
FG=2.0*D2*((2.0+G/6.0)/(1.0+PP)+6.0*PP)-2.0*GK*
*(2.0+D1/D2)
B1=R1-R3/2.0+R4/5.0
B2=R1/12.0-R2/6.0+R3/8.0-R4/30.0
B3=R2*2.0-2.0*R3+3.0*R4/5.0
A1=13.0*R1/15.0-67.0*R3/140.0+7.0*R4/36.0
A2=0.8*R1-13.0*R3/28.0+4.0*R4/21.0
A3=13.0*R1/30.0-13.0*R2/14.0+201.0*R3/280.0-7.0*R4/36.0
A4=0.4*R1-31.0*R2/35.0+39.0*R3/56.0-4.0*R4/21.0
A5=13.0*R2/7.0-67.0*R3/35.0+7.0*R4/12.0
A6=62.0*R2/35.0-13.0*R3/7.0+4.0*R4/7.0
UI=(B1+G*B2+FF*B3)/(1.0+PP)
UTI=(A1+PRP*A2+G*A3/6.0+G*PRP*A4/6.0+PP*A5+PP*PRP*A6)/
*(1.0+PP)*(1.0+PRP)
D3=UI-UTI
GL=D3*D3*R2*G
GGG=2.0*D3*(2.0/(PR+PR*PRP)+6.0*P)-2.0*GL
RETURN
END

```

```

SUBROUTINE ROOT(PR,ST,R1,G,GK1,IFLAG,JJ)
X1=12.0
X2=8.0
J=0
G=X1
CALL FUN(PR,ST,R1,G,FG,GGG,GK,GL,D1,D2,D3)
FUNC1=GK-GK1
5 G=X2
CALL FUN(PR,ST,R1,G,FG,GGG,GK,GL,D1,D2,D3)
FUNC2=GK-GK1

```

```

      IF (FUNC1*FUNC2) 1,2,3
3    FUNC1=FUNC2
      X1=X2
      X2=X2-4.0
      IF (X2.LT.-12.0) GO TO 40
      GO TO 5
1    WRITE (8,101) X1,X2,FUNC1,FUNC2,
101  FORMAT ('0', 'ROOT IS BETWEEN', F10.6, 'AND', F10.6,
* 'FUNCTION VALUES', 2F10.6)
6    XI=(FUNC2*X1-FUNC1*X2)/(FUNC2-FUNC1)
      G=XI
      J=J+1
      IF (ABS (XI-X1).LT.1.0E-4) GO TO 7
      IF (ABS (XI-X2).LT.1.0E-4) GO TO 7
      IF (ABS (FUNC1-FUNC2).GT.1.0E-20) GO TO 8
7    WRITE (8,102) X1,X2,FUNC1,FUNC2
102  FORMAT ('0', 'ROOT IS', 2F10.6, 'FUNCTION VALUE', 2F10.6)
      WRITE (8,104) J
104  FORMAT ('0', 'NUMBER OF ITERATIONS=', I6)
      RETURN
8    CALL FUN (PR,ST,R1,G,PG,GGG,GK,GL,D1,D2,D3)
      FUNC1=GK-GK1
      IF (J.GT.30) GO TO 50
      IF (FUNC1*FUNC1) 11,12,13
13   FUNC1=FUNC1
      X1=XI
      GO TO 6
11   FUNC2=FUNC1
      X2=XI
      GO TO 6
2    G=X1
      IF (FUNC2.EQ.0.0) G=X2
      IFLAG=0
      WRITE (8,103) G,X1,X2,IFLAG,FUNC1,FUNC2
103  FORMAT ('0', 'ROOT IS', 3F10.6, ' IFLAG=', I4,
* ' FUNCTION ', 2F10.6)
      WRITE (8,104) J
      RETURN
12   G=XI
      IF (FUNC1.EQ.0.0) G=X1
      IFLAG=1
      WRITE (8,103) G,X1,X2,IFLAG,FUNC1,FUNC2
      WRITE (8,104) J
      RETURN
40   WRITE (6,100) JJ
100  FORMAT ('0', 'NO ROOT BETWEEN -12.0 AND 12.0', I4)
      IF (GK1.GT.0.0) G=12.0
      IF (GK1.LT.0.0) G=-7.0
      WRITE (6,105) G
105  FORMAT ('0', 'ASSUME ROOT=', F10.2)

```



```
RETURN
50  IFLAG=2
    WRITE(6,106)
106 FORMAT('0','NUMBER OF ITERATIONS >30')
STOP
END
SUBROUTINE MOVE(ZCOR,NBC,NBCN,X,Y,NN,NDE,NDEN)
REAL ZCOR(NBCN),X(NN),Y(NN)
INTEGER NBC(NBCN),NDE(NDEN)
DIST=ZCOR(1)-4.0
DO 1 I=1,NBCN,2
ZCOR(I)=ZCOR(I)-DIST
NI=NBC(I)
1  X(NI)=ZCOR(I)
DO 2 J=2,NDEN,2
NJ=NDE(J)
IF (Y(NJ).LT.1.15) GO TO 2
X(NJ)=X(NJ)-DIST
2  CONTINUE
RETURN
END
```